**FRIEDRICH-ALEXANDER-UNIVERSITÄT**
**ERLANGEN-NÜRNBERG**
TECHNISCHE FAKULTÄT • DEPARTMENT INFORMATIK

**Lehrstuhl für Informatik 10 (Systemsimulation)**

# Energy Corrected Finite Elements for Elliptic PDEs and Linear Elasticity

Paras Kumar

Master-Thesis

# Energy Corrected Finite Elements for Elliptic PDEs and Linear Elasticity

Paras Kumar

Master-Thesis

| | |
|---|---|
| Aufgabensteller: | Prof. Dr. Ulrich Rüde |
| Betreuer: | Dominik Thönnes, M. Sc. |
| Bearbeitungszeitraum: | 01.03.2018 – 03.09.2018 |

**Erklärung:**

Ich versichere, dass ich die Arbeit ohne fremde Hilfe und ohne Benutzung anderer als der angegebenen Quellen angefertigt habe und dass die Arbeit in gleicher oder ähnlicher Form noch keiner anderen Prüfungsbehörde vorgelegen hat und von dieser als Teil einer Prüfungsleistung angenommen wurde. Alle Ausführungen, die wörtlich oder sinngemäß übernommen wurden, sind als solche gekennzeichnet.

Der Universität Erlangen-Nürnberg, vertreten durch den Lehrstuhl für Systemsimulation (Informatik 10), wird für Zwecke der Forschung und Lehre ein einfaches, kostenloses, zeitlich und örtlich unbeschränktes Nutzungsrecht an den Arbeitsergebnissen der Master-Thesis einschließlich etwaiger Schutzrechte und Urheberrechte eingeräumt.

Erlangen, den 1. September 2018 .....

# Acknowledgement

First and Foremost, I would like to convey my heartfelt thanks to Prof. Ulrich Rüde for providing me the opportunity to work on this interesting and challenging topic of energy corrected finite elements. This thesis would not have been possible without the continual encouragement, guidance and support he offered throughout the duration of the master thesis. It was indeed an enlightening experience working under his supervision, considering the mathematical insight I developed on the topic of finite elements.

A special thanks goes to LSS group members, Dominik Thönnes and Nils Kohl for their help during the writing of the thesis. I would also like to thank the administrative staff at the LSS for their help and support during the master thesis.

# Abstract

Finite element approximation to the solution of elliptic PDEs on domains with re-entrant corners yields sub-optimal convergence rates when using quasi-uniform meshes. Reduced regularity or the *singular* behaviour of the solution caused by the presence of re-entrant corners induces the decrease in convergence rates or the so-called *pollution effect*. In this thesis, the Energy Corrected Finite Element Method (ECFEM) which provides a computationally efficient alternative to tackle the pollution effect by means of local modifications to the stiffness matrix in the vicinity of the singular point is thoroughly examined and successfully applied to scalar elliptic problems. A simple modification of the ECFEM leading to optimal $\mathcal{O}\left(h^{p+1}\right)$ convergence rates in the $L^2$-norm for the region far away from the singularity when using higher polynomials of order $p$ is presented. An extension of this energy correction idea, based on exhaustive numerical investigation, to *planar linear elasticity* problems, particularly the problems of planar Linear Elastic Fracture Mechanics (LEFM) is proposed.

# List of Abbreviations

**BVP** Boundary Value Problem

**DOF** degree of freedom

**DSFM** Dual Singular Function Method

**ECFEM** Energy Corrected Finite Element Method

**eoc** estimated order of convergence

**FEM** Finite Element Method

**LEFM** Linear Elastic Fracture Mechanics

**PDE** Partial Differential Equation

**SFM** Singular Function Method

**SLE** System of Linear Equations

# List of Figures

# List of Tables

# Contents

# Chapter 1

# Introduction

Elliptic Partial Differential Equations (PDEs) play a vital role in modeling of several phenomena of practical interest in both natural and engineering sciences. Some of the most common examples include elasticity, (steady state) heat transfer, fluid mechanics and electrostatics. For almost all cases of practical interest, *closed form solutions* to these differential equations are not possible and *numerical methods* provide the only viable alternative to get approximate solutions with the desired accuracy, depending on the method chosen. Development of *fast* and *accurate* numerical solution techniques for different types of PDEs has been the primary goal in applied mathematics for past several decades.

Finite Element Methods (FEMs) are undoubtedly the most common choice for solving elliptic differential equations. In order to achieve optimal convergence rates in the error norms with finite element discretisations, a certain minimal *regularity* of the true solution is required. Quite often, there arise *singularities*, resulting in reduced regularity of the true solution and consequently *sub-optimal convergence rates* for the finite element approximation on quasi-uniform meshes. Some of the common causes of singularities include non-smooth domain boundary, discontinuous coefficients and singular forcing functions. In this thesis, we will focus on domains with a non-smooth boundary, in particular, polygonal domains having a *re-entrant corner*. Domains with re-entrant corners, especially those with a *crack* are of great importance in engineering applications such as *Fracture Mechanics*. The topic of *corner singularities* has therefore garnered a great deal of attention from applied mathematicians and engineers alike. Consequently there have been various research publications studying how the presence of a re-entrant corner affects the regularity of the true solution and proposing possible remedies to this problem of reduced convergence, also referred to as the *pollution effect*. Perhaps one of the fundamental and early works is that of Kondrat'ev [14], where it was shown that the solution to the Poisson problem on a domain having a re-entrant corner with an interior angle $\omega$, comprises of singular functions of the form

$$s_n = r^{\frac{n\pi}{\omega}} \sin\left(\frac{n\pi\theta}{\omega}\right)$$

in the vicinity of the re-entrant corner with $(r, \theta)$ representing the polar coordinates of a point. This fact has been used by several researchers in developing methods to overcome the pollution effect. Grading the mesh towards the singular point or enriching the finite element function spaces with appropriate singular functions are amongst the most widely used solution strategies presented in the literature (see Section 3.1 for a short review of these and other relevant methods).

Most of these approaches suffer from the drawback that they require substantial modification of the existing finite element code, which for instance may arise from the use of adaptive meshes or the extension of the finite element spaces. In this work, we will examine the *energy correction* technique which only involves local modification of the weak form in the vicinity of the singular point, thereby requiring minimal code modification and computational effort. The fundamental basis of this approach is that the finite element approximation can only be as accurate as the approximation of the energy $a(u, u)$.

The rest of the thesis is organized as follows: We begin by reviewing in Chapter 2, some common a priori error estimates for the Poisson problem on domains with smooth boundaries and analyse how these estimates change in the presence of a re-entrant corner. In Chapter 3, we delve deep into the theoretical details of energy corrected finite elements, followed by numerical examples describing the implementation aspects and applicability of this method to scalar elliptic problems in Chapter 4. We then explore the possibility of extending this idea of energy correction to planar linear elasticity problems in Chapter 5. Finally, in Chapter 6, we summarise the findings of this thesis and discuss the way forward.

# Chapter 2

# Finite Elements and Corner Singularities

In this chapter, we first present a few important results pertaining to how the finite element approximation to the solution of an elliptic PDE converges with subsequent mesh refinement. Another objective here is to develop an understanding of how the presence of a *re-entrant corner* affects *regularity* of the solution and therefore the convergence of the finite element approximation. This chapter also serves to lay down the notation and terminologies to be used in the remainder of this thesis. As is done in this and the following chapters, we only consider problems in $2D$. Also, unless explicitly specified, we will only consider *Dirichlet* boundary conditions for the Boundary Value Problems (BVPs) studied in this work.

## 2.1 Finite Elements: Recapitulation

In this section we describe briefly, the procedure of solving an elliptic BVP using *continuous Galerkin finite elements*. For a detailed description of the procedure, including the derivation of the weak form, we refer the reader to [13, Chapter 2]. For the sake of simplicity, we consider *steady state heat equation* in two dimensions.

The *strong form* of the problem is stated as follows: Given $\kappa : \Omega \to \mathbb{R}$ and $f : \Omega \to \mathbb{R}$, find $u : \Omega \to \mathbb{R}$, s.t.

$$\begin{aligned} -\nabla \cdot (\kappa \nabla u) &= f \text{ in } \Omega \\ u &= g \text{ on } \partial\Omega. \end{aligned} \tag{2.1}$$

As a first step towards the *weak form* of the BVP given in (2.1), we define appropriate functional spaces:

$$\begin{aligned} \mathcal{U} &\coloneqq \left\{ u \in H^1(\Omega) : u|_{\partial\Omega} = g \right\}, \\ \mathcal{V} &\coloneqq \left\{ u \in H^1(\Omega) : u|_{\partial\Omega} = 0 \right\}, \end{aligned}$$

where $H^1(\Omega)$ is the standard *Sobolev* space. Here, $\mathcal{U}$ and $\mathcal{V}$ represent the *trial* and the *test* function spaces respectively. The weak form of the above BVP reads: Given $f \in L^2(\Omega)$, find $u \in \mathcal{U}(\Omega)$, s.t.

$$a(u, v) = b(v) \;\; \forall \; v \in \mathcal{V}, \tag{2.2}$$

where, $a(u,v) = \int_\Omega \kappa \nabla u \cdot \nabla v \, dv$ and $b(v) = (f,v) = \int_\Omega f v \, dv$ represent the *bilinear form* and the *linear form* respectively. It is stated without proof that for the problem (2.2), the *Lax-Milgram Theorem* [13, Theorem 3.1] is satisfied and thus there exists a *unique* solution $u$ to the weak form defined above.

The next step involves replacing the functional spaces $\mathcal{U}$ and $\mathcal{V}$ by their *finite dimensional* counter-parts $\mathcal{U}^h$ and $\mathcal{V}^h$ respectively. This entails partitioning the domain $\Omega$ into finite elements $K \in \mathcal{T}_h$ where $\mathcal{T}_h$ is a *conforming triangulation* of $\Omega$. The triangulation $\mathcal{T}_h$ is characterized by its *mesh size* $h$ which is defined as

$$h \coloneqq \max\left\{\operatorname{diam}(K) \;\middle|\; K \in \mathcal{T}_h\right\},$$

where, $\operatorname{diam}(K) \coloneqq \sup\{|x-y| \colon x, y \in K\}$ denotes the diameter of $K$. The finite dimensional functional spaces comprise of basis functions which are *piecewise continuous polynomials*. The functional spaces $\mathcal{U}^h$ and $\mathcal{V}^h$ can thus be defined as

$$\mathcal{U}^h \coloneqq \{u \in \mathcal{U} \colon u|_K = \mathcal{P}_p(K) \;\forall\; K \in \mathcal{T}_h\},$$
$$\mathcal{V}^h \coloneqq \{v \in \mathcal{V} \colon v|_K = \mathcal{P}_p(K) \;\forall\; K \in \mathcal{T}_h\},$$

where, $\mathcal{P}_p(K)$ represents the space of polynomials of order $p$ defined on the element $K$. Thus, the *finite dimensional weak form* for the problem (2.2) is given as: Find $u^h \in \mathcal{U}^h$ s.t.

$$a\left(u^h, v^h\right) = b\left(v^h\right) \;\forall\; v^h \in \mathcal{V}^h, \tag{2.3}$$

where, $u_h$ is the finite element approximation to the analytical solution $u$. The finite dimensional weak form of (2.3) leads to a System of Linear Equations (SLE) of the form

$$AU^h = F,$$

which can be solved to find $U^h$, the *nodal finite element solution vector*. Here, $A$ represents the *finite element stiffness matrix* and $F$ is the *load vector*.

## 2.2 Error Estimates

Having seen how an elliptic BVP can be discretized using finite elements, an extremely important question to be answered is how well the subspace $\mathcal{U}^h$ approximates the full admissible space $\mathcal{U}$. This can be estimated by the *finite element error* $u - u^h$ which is usually measured in terms of suitable *Sobolev* norms.

The weak form of (2.2) can be alternatively written in its *minimization* form: Find

$$u = \underset{v \in \mathcal{U}}{\mathbf{arg\,min}}\; I(v),$$

where, $I(v) = a(v,v) - 2(f,v)$ represents the *energy functional* and the term $a(u,u)$ represents *energy* of the function $u$. Consequently, the term $a\left(u - u^h, u - u^h\right)$ is referred to as the *energy of the error*.

The finite element solution $u^h$ is the one which minimizes the energy of the error or in other words the error in the *energy norm*. This can be shown as follows. Inserting $v^h$ in (2.2) and subtracting (2.3) from it yields the *Galerkin Orthogonality* condition:

$$a\left(u - u^h, v^h\right) = 0 \quad \forall\ v^h \in \mathcal{V}^h, \tag{2.4}$$

which means that the error is *orthogonal* to the space $\mathcal{V}^h$. This also leads us to another important fact: *The energy of the error equals the error in the energy.* This can be shown by inserting the above orthogonality condition in the definition of the energy of the error term, i.e.

$$\begin{aligned} a\left(u - u^h, u - u^h\right) &= a\left(u - u^h, u\right) - \cancelto{0}{a\left(u - u^h, u^h\right)} \\ &= a\left(u, u\right) - a\left(u^h, u\right) \\ &= a\left(u, u\right) - a\left(u, u^h\right), \quad \text{yielding,} \\ a\left(u - u^h, u - u^h\right) &= a\left(u, u\right) - a\left(u^h, u^h\right) \end{aligned}$$

which is the required result. Next, we consider the following term for some $x^h \in \mathcal{V}^h$:

$$\begin{aligned} a\left(u - u^h - x^h, u - u^h - x^h\right) &= a\left(u - u^h - x^h, u - u^h\right) - a\left(u - u^h - x^h, x^h\right) \\ &= a\left(u - u^h, u - u^h\right) - a\left(x^h, u - u^h\right) - a\left(u - u^h, x^h\right) + a\left(x^h, x^h\right) \\ &= a\left(u - u^h, u - u^h\right) - 2a\left(u - u^h, x^h\right) + a\left(x^h, x^h\right) \\ &= a\left(u - u^h, u - u^h\right) - 2\,\cancelto{0}{a\left(u - u^h, x^h\right)} + a\left(x^h, x^h\right) \\ &= a\left(u - u^h, u - u^h\right) + a\left(x^h, x^h\right) \\ \implies a\left(u - u^h, u - u^h\right) &\leq a\left(u - u^h - x^h, u - u^h - x^h\right) \end{aligned}$$

where, equality occurs only if $x^h = 0$. This could be alternatively stated in terms of the energy norm:

$$\left\|u - u^h\right\|_E \leq \min_{v \in \mathcal{V}^h} \left\|u - v\right\|_E \tag{2.5}$$

where, $\left\|\cdot\right\|_E$ represents the energy norm (see Appendix A.1 for details on definition and notation of norms). Thus, the finite element solution is optimal in sense of the energy norm. It is noteworthy that the conditions (2.3), (2.4) and (2.5) are equivalent.

Another important point to note here is that, in case of domains with smooth boundary, the so called *shift theorem* [9] holds. For second order elliptic BVPs, this means that the order of the Sobolev space is shifted from $k$ to $k+2$ by the inverse of considered differential operator, i.e if $f \in H^k(\Omega)$, then $u \in H^{k+2}(\Omega)$. Thus, the solution $u$ depends continuously on the right hand side $f$.

### 2.2.1 Error Estimates in Mean Square Sense

As shown above, the finite element solution process basically involves minimizing the difference between the derivatives of the solution and its finite element approximation in a mean squared sense. Hence, the use of error estimates in Sobolev norms is quite common. For an elliptic BVP

of order $2m$, assuming the domain boundary and the coefficient $\kappa$ is smooth and that the bilinear form satisfies the *V-ellipticity* condition, the finite element approximation $u^h$ differs from the true solution $u$ by [25, Theorem 3.7]:

$$\begin{aligned} \|u - u^h\|_s &\leq Ch^{p+1-s} \|u\|_{p+1} \qquad \text{if } s \geq 2m - (p+1), \\ \|u - u^h\|_s &\leq Ch^{2(p+1-m)} \|u\|_{p+1} \qquad \text{if } s \leq 2m - (p+1), \end{aligned} \tag{2.6}$$

where, $\|\cdot\|_s$ represents some Sobolev norm (see Appendix A.1 for notation and definitions). Considering the particular case of *second order* elliptic BVPs i.e., inserting $m = 1$ in (2.6) we obtain

$$\begin{aligned} \|u - u^h\|_s &\leq Ch^{p+1-s} \|u\|_{p+1} \qquad \text{if } s \geq 1 - p, \\ \|u - u^h\|_s &\leq Ch^{2p} \|u\|_{p+1} \qquad \text{if } s \leq 1 - p. \end{aligned}$$

More specifically, inserting $s = 0$ in the above equations, we obtain the error estimate in the $L^2$-norm:

$$\|u - u^h\|_0 \leq Ch^{p+1} \|u\|_{p+1}. \tag{2.7}$$

In similar fashion, inserting $s = 1$ yields the estimate in the $H^1$-norm:

$$\|u - u^h\|_1 \leq Ch^{p} \|u\|_{p+1}. \tag{2.8}$$

A noteworthy point here is that for the above error estimates to hold, the condition $u \in H^{p+1}$ must be satisfied, which eventually happens once the smoothness requirements mentioned above are fulfilled.

### 2.2.2 Error Estimates in $L^\infty$ norm

The error estimates in the $L^\infty$-norm for *irregular* meshes on domains with smooth boundaries are given as [24, Theorem 1]:

$$\|u - u^h\|_{L^\infty} \leq C \left\{ \begin{array}{ll} h^2 |\log h| & \text{if } \ p = 1 \\ h^{p+1} & \text{if } \ p > 1 \end{array} \right\} |u|^{p+1}_\infty \tag{2.9}$$

where, $C$ is a constant independent of the mesh size $h$.

Numerical examples demonstrating the validity of these error estimates will be presented in Section 4.2. These error estimates are of critical importance in understanding the how exactly the presence of singularities deteriorates the convergence rates obtained with quasi-uniform finite element meshes.

## 2.3 Corner Singularities

Presence of sufficient regularity is a requisite for achieving optimal convergence rates as mentioned in the previous section. The regularity of solution $u$ to elliptic BVPs such as the one given in (2.2) is governed by smoothness of the domain boundary $\partial\Omega$, the right hand side function $f$ and the coefficient $\kappa$. Non-fulfillment of any of these smoothness requirements results in appearance of singularities in the solution, whereby the solution could have unbounded derivatives (or may even be itself unbounded) in the neighbourhood of certain points in $\Omega$. These situations are commonly observed in many practical applications. Such singular behaviour could emerge because of the following reasons:

- non-smooth domain boundary: re-entrant corners,
- discontinuous coefficients,
- forcing terms with singularities, e.g. point loads,
- boundary conditions involving singular functions.

In this work, we will focus only on the singularities caused by non-smooth domain boundaries, in particular, *re-entrant* corners. Figure 2.1 depicts a domain with a re-entrant corner having an interior angle $\omega$ formed by the two straight edges $\Gamma_1$ and $\Gamma_2$. The co-ordinate system has been setup such that the re-entrant corner is located at the origin and one of the edges forming the re-entrant corner , i.e. $\Gamma_1$ coincides with the positive x-axis.

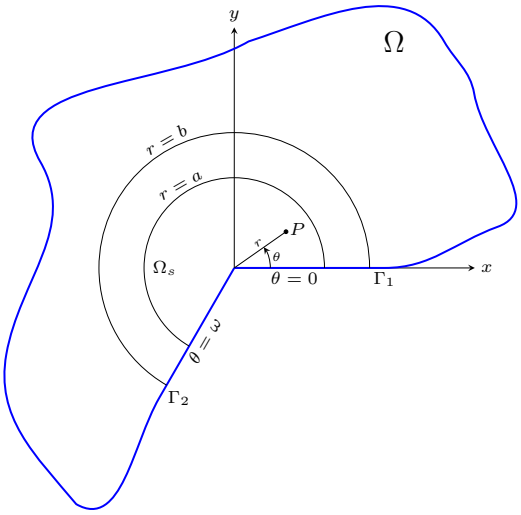


Figure 2.1: A two-dimensional domain with a re-entrant corner located at the origin, having an interior angle $\omega$ with $\pi < \omega \leq 2\pi$.

### 2.3.1 Regularity of solution in Presence of Re-entrant Corner

It was first shown by Kondrat'ev [14] and then by several other authors (see for e.g. [4] or [6]) that, for a domain with a re-entrant corner (see Figure 2.1), the true solution can be split into a singular components and a smooth remainder, provided some additional regularity condition is assumed on the right hand side $f$. Let $f \in H^0_\beta$ with some $\beta < 0$, then the solution $u$ to the BVP given in (2.2), admits an expansion of the form

$$u(r,\theta) = \sum_{0<n<N} k_n \, s_n + U, \tag{2.10}$$

where the *singular functions* $s_n$ and the singular terms $\tilde{s}_n$ are given as

$$s_n(r,\theta) = \tau(r) \; \tilde{s}_n(r,\theta)$$

$$\tilde{s}_n(r,\theta) = r^{\nu_n} \sin(\nu_n \theta); \quad \nu_n = \frac{n\pi}{\omega},$$

with a smooth *cutoff function* $\tau$ having the property

$$\tau(r) = \begin{cases} 1 & \text{for } 0 \le r \le a \\ 0 & \text{for } b \le r \end{cases}, \quad 0 < a < b.$$

Here, $U$ represents the smooth component of the solution while the coefficients $k_n$ are referred to as the *stress intensity factors*.

A note on the assumed regularity of $f$ is in order. It is noteworthy that unlike (2.2), where we required $f \in H^0$, here we need the right hand side to be a bit more regular in the vicinity of the singular point. The reasoning behind this is that we wish to avoid additional singularities which could have been caused if $f$ for e.g. was unbounded at the re-entrant corner (which is possible for $L^\infty$ functions). It appears that the sufficient regularity requirement to fulfill this condition is : Let $\beta < 0$, then

$$\|r^\beta f\|_{L^2(\Omega)} < \infty,$$

which can be alternatively described by using *weighted Sobolev spaces* denoted by $H^m_\beta(\Omega)$. For further details on the definition of these spaces, see Appendix A.2.

**Remark 2.1.** *Our review of the arguments presented in [6] reveals that there could be a possible typing error in their Lemma 2.1 where it is mentioned that $\beta < 1$. On the other hand, our arguments from above require $\beta < 0$.*

The regularity of the solution $u$ is dominated by that of the constituent singular functions, in particular the first singular function $s_1$, because it comprises of singular terms of the from $r^\nu$ with $0 < \nu < 1$. The strength of the singularity increases with increase in interior angle. For the case of domain with a slit, i.e. $\omega = 2\pi$, it can be easily verified that $s_1 \in H^1(\Omega_s)$ but $s_1 \notin H^2(\Omega_s)$. It can further shown that [25, Chapter 8],

$$s_1 \in H^\sigma(\Omega); \quad \sigma = 1 + \nu - \epsilon,$$

for some $\epsilon > 0$. Here, $\Omega_s = \left\{(r,\theta) \,\middle|\, 0 < r < a,\, 0 < \theta < \omega\right\}$ is a region in the neighborhood of the re-entrant corner where the singular effect is pre-dominant. Presence of these singular components ultimately results in reduced regularity of the solution $u$, i.e. $u \in H^\sigma(\Omega)$, irrespective of the smoothness of the right hand side $f$. The shift theorem mentioned above does not hold any more due to the presence of the re-entrant corner.

**Remark** In line with the notation employed in the literature, we shall use polar coordinate system for the purpose of analyzing the singular parts of the solution .

### 2.3.2 Error Estimates in Presence of Singularities

The error estimates mentioned in the previous section are no longer valid because of the reduced regularity of the solution $u$ resulting from the presence of re-entrant corner as explained above. This necessitates the need for modified error estimates accounting for the reduced regularity of the solution.

**Error Estimates in $L^2$-Norm**

For an elliptic PDE of order $2m$ on a domain with re-entrant corner, the following error estimate holds in the $L^2$ norm [25, Section 8.3]:

$$\|u - u^h\|_0 \leq C \left[h^{r+\sigma-2m} + h^{2(p+1-m)}\right] \|u\|_r \; ; \quad r = \min\{p+1, \sigma\}. \tag{2.11}$$

As has been already shown above, $\sigma < 2$ for the dominant singular component $s_1$. For a second order BVP ($m = 1$), this yields,

$$\|u - u^h\|_0 \leq C \left[h^{2(\sigma-1)} + h^{2p}\right] \|u\|_\sigma .$$

Neglecting the higher order term, we obtain

$$\|u - u^h\|_0 \leq C h^{\frac{2\pi}{\omega}-\epsilon} \|u\|_\sigma, \tag{2.12}$$

which is the error estimate describing the reduced convergence rates occurring due to presence of re-entrant corners. Comparing the estimate in (2.12) with that in (2.7), we find that deterioration of the convergence rate happens irrespective of the order of polynomial basis functions employed for finite element discretization.

**Error Estimates in $H^1$-Norm**

It is clear from the above analysis that $s_1$ dominates the regularity of the true solution $u$. Employing the result of [4, Theorem 3.1], we obtain

$$\|u - u^h\|_1 \leq C h^{\frac{\pi}{\omega}-\epsilon} \|u\|_\sigma, \tag{2.13}$$

which seems to be in accordance with the usual relationship amongst the error estimates in the $L^2$ and $H^1$-norms. We get a convergence rate of the form $h^\alpha$ in the $H^1$-norm and that of the form $h^{(\alpha+\alpha)}$ for the $L^2$-norm.

**Error Estimates in $L^\infty$-Norm**

Error estimates in the $L^\infty$ norm for Poisson's equation on domain with multiple re-entrant corners have been presented in [23]. The results for non uniform meshes read

$$\begin{aligned}
\|u - u^h\|_{L^\infty(\Omega)} &\leq C h^{\min(p+1,\beta_M)-\epsilon}, \\
\|u - u^h\|_{L^\infty(\Omega_s)} &\leq C h^{\min(p+1,\beta,2\beta_M)-\epsilon}, \\
\|u - u^h\|_{L^\infty(\Omega\setminus\Omega_s)} &\leq C h^{\min(p+1,2\beta_M)-\epsilon},
\end{aligned}$$

where, $\beta = \frac{\pi}{\omega}$ and $\beta_M = \max \beta$ considered over all the re-entrant corners. Considering the case of a single re-entrant corner, the we obtain the following error estimates,

$$\begin{aligned}
\|u - u^h\|_{L^\infty(\Omega)} &\leq C h^{\frac{\pi}{\omega}-\epsilon}, \\
\|u - u^h\|_{L^\infty(\Omega_s)} &\leq C h^{\frac{\pi}{\omega}-\epsilon}, \\
\|u - u^h\|_{L^\infty(\Omega\setminus\Omega_s)} &\leq C h^{\frac{2\pi}{\omega}-\epsilon}.
\end{aligned} \tag{2.14}$$

A significant implication of (2.14) is that the degradation of the convergence rate happens, although to a relatively smaller extent, even in the region away from the re-entrant corner.

**Remark** In all of the above mentioned error estimates, $C$ is a constant independent of the mesh size $h$.

This phenomenon of reduced convergence rates with quasi-uniform finite element meshes is referred to as the *pollution effect*. A noteworthy point here is that, despite of the singularity being local in nature (as depicted by (2.10)), the deterioration in the convergence rate is global in case of all of the error estimates presented above.

# Chapter 3

# Energy Corrected Finite Elements

This chapter is dedicated to a comprehensive study of energy corrected finite elements, a computationally efficient technique for mitigating the pollution effect. We introduce the *energy correction* technique and examine the theoretical aspects of its functioning.

## 3.1 Mitigating the Pollution Effect

In the previous chapter, we saw, how the presence of a re-entrant corner can lead to reduced convergence rates with quasi-uniform finite elements, the so called *pollution effect*. Here, we have a look at some of the approaches presented in the literature for mitigating the pollution effect. A commonly used strategy comprises of graded refinement of the finite element mesh with higher mesh resolution towards the re-entrant corner [1]. A variation of this strategy is the $hp-$FEM [2], where not just reduced mesh sizes, but also higher order polynomials for the finite element basis functions are employed, in order to have more degrees of freedom (DOFs) near the singular point. Another approach consists of enriching the finite element spaces by appropriate *singular functions* defined in (2.10), also called as the Singular Function Method (SFM), so as to capture the singular behaviour accurately [25, Section 8.4]. In [4], the Dual Singular Function Method (DSFM), another technique based on similar ideas is presented and compared with the SFM. Yet another remedy for the pollution effect is proposed in [5], where an *extrapolation* procedure comprising of linear combination of finite element solutions on different refinement levels have been employed. A detailed survey on various other techniques for tackling the pollution effect can be found in [17].

Some of the methods mentioned above offer the flexibility of handling different kind of singularities. However, they typically suffer from substantial implementation overheads or modifications to be made to the existing finite element code. The use of locally adapted unstructured meshes in case of graded mesh refinement; extension of the finite element spaces or use of nonstandard quadrature rules for accurate integration of singular functions, lead to nontrivial, global modifications in the stiffness matrix. This inevitably affects the performance of linear solvers employed for solving the resulting SLE. The energy correction technique, which is being considered in this work only entails local modifications in the vicinity of the re-entrant corner thereby leaving the approximation spaces and the sparsity pattern of the stiffness matrix unaltered. This local nature of modifications permits easy integration into existing finite element codes.

The idea of performing local modifications on the discrete problem to attenuate the pollution effect was first introduced by Zenger & Gietl [27] in the context of finite differences. This was later extended to finite element discretizations [19, 20]. A complete convergence analysis in weighted Sobolev norms, of this approach, hereafter referred to as the Energy Corrected Finite Element Method (ECFEM), has been presented in [6]. Generalization of this technique to the Stokes systems was carried out in [12]. In what follows, we follow the presentation of [6] to explain the working of ECFEM and summarize the mathematical theory behind it without going deep into the proofs. Particular attention has been paid to the aspects which are critical to successful practical implementation of the technique.

## 3.2 Introduction to ECFEM

In order to explain the idea, we consider Poisson's equation with homogeneous Dirichlet boundary conditions as the model problem. The strong form of the problem reads: Given $f : \Omega \to \mathbb{R}$, find $u : \Omega \to \mathbb{R}$, s.t.

$$\begin{aligned} -\Delta u &= f \qquad \text{in } \Omega, \\ u &= 0 \qquad \text{on } \partial\Omega, \end{aligned} \tag{3.1}$$

where, $\Omega \subset \mathbb{R}^2$ is a bounded polygonal domain containing a single re-entrant corner with an interior angle $\pi < \omega \leq 2\pi$. The origin is assumed to be located at the re-entrant corner and one edge of the boundary touching the re-entrant corner lies along the positive x-axis (see Figure 3.1a for details). Following the steps enumerated in Section 2.1, we restate the procedure for solving this model problem, describing the modifications entailed by the energy correction technique.

The weak form for the BVP given in (3.1) reads as follows: Given $f \in H^0_\beta(\Omega)$ for some $\beta < 0$, find $u \in H^1_0(\Omega)$, s.t.

$$a(u, v) = b(v) \quad \forall\ v \in H^1_0(\Omega), \tag{3.2}$$

where, $a(u, v) = \int_\Omega \kappa \nabla u \cdot \nabla v \, dv$ and $b(v) = (f, v) = \int_\Omega f v \, dv$ represent the *bilinear form* and the *linear form* respectively.

As usual, the next step involves setting up the finite dimensional weak form. By

$$\mathcal{V}^h := \left\{ v \in H^1_0(\Omega) : v|_K = \mathcal{P}_1(K) \ \forall\ K \in \mathcal{T}_h \right\},$$

we denote the standard finite element space of continuous piecewise linear functions. The symbols have their meanings as defined in Section 2.1. Now comes the point of digression from the standard procedure. In ECFEM, a modified finite dimensional weak form, also referred to as the *energy corrected weak form* is considered. The energy corrected weak form reads: Find $R^m_h u \in \mathcal{V}^h$, s.t.

$$a_h\left(R^m_h u, v^h\right) = b\left(v^h\right) \quad \forall\ v^h \in \mathcal{V}^h, \tag{3.3}$$

where, $R^m(\gamma) =: R^m_h : H^1(\Omega) \mapsto \mathcal{V}^h$ represents the Ritz projector of the modified Galerkin approximation to the analytical solution $u$. The linear form remains unaltered, i.e. $b(v) = \int_\Omega f\, v \, d\Omega$ and $a(u, v) = \int_\Omega \nabla u \cdot \nabla v \, d\Omega$ as usual. The mesh dependent bilinear form $a_h(u, v)$ is given as

$$a_h(u, v) = a(u, v) - c_h(u, v),$$

with, the *correction term*

$$c_h(u,v) = \gamma\, d_h(u,v) = \gamma \int_{\mathcal{S}_h} \nabla u \cdot \nabla v \, d\Omega. \tag{3.4}$$

The constant $\gamma$ is referred to as the *correction parameter* and the region

$$\mathcal{S}_h := \{K \in \mathcal{T}_h : \, O \in \partial K\}$$

represents one element neighbourhood of the singular point, i.e. the layer of elements having the re-entrant corner $O$ as one of the vertices (see Figure 3.1b).

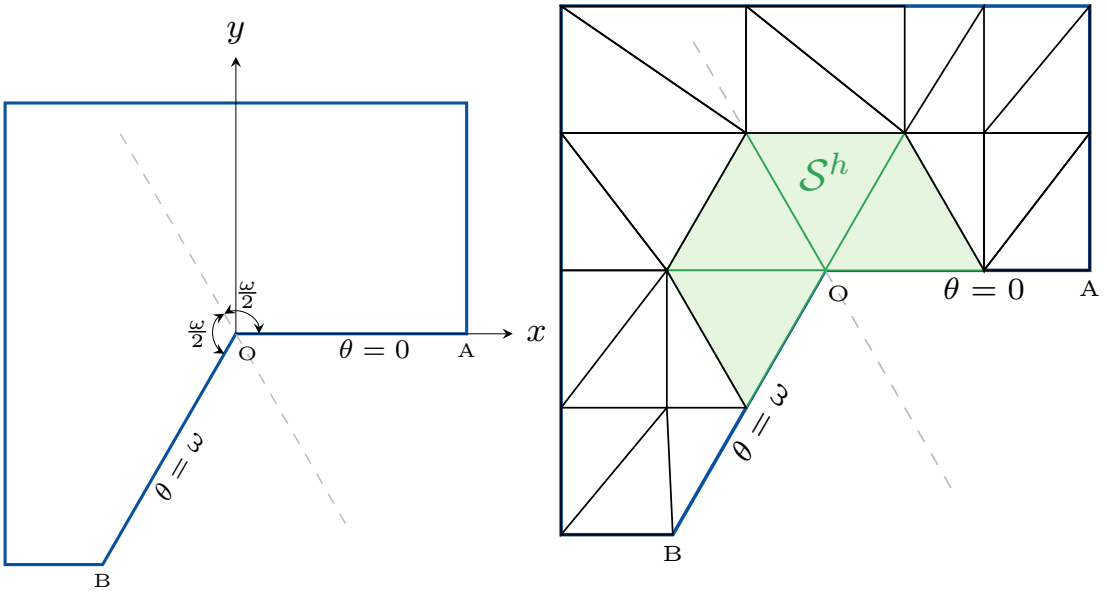


(a) A polygonal domain in two-dimensions.

(b) Symmetric mesh about the angle bisector, forming the region $S^h$.

Figure 3.1: Two-dimensional polygonal domain with a re-entrant corner having an interior angle $\angle AOB = \omega$ with $\pi < \omega \leq 2\pi$. The dashed line represents the angle bisector of the interior angle.

Let us have a closer look at the energy corrected weak form, so as to understand what exactly changes at the implementation level. We have,

$$\begin{aligned} a_h\left(R_h^m u, v^h\right) &= a\left(R_h^m u, v^h\right) - \gamma\, d_h\left(R_h^m u, v^h\right) \\ &= \int_{\Omega} \nabla R_h^m u \cdot \nabla v^h \, d\Omega \; - \; \gamma \int_{\mathcal{S}_h} \nabla R_h^m u \cdot \nabla v^h \, d\Omega, \end{aligned}$$

$$\text{i.e.} \quad a_h\left(R_h^m u, v^h\right) = \int_{\Omega \setminus \mathcal{S}_h} \nabla R_h^m u \cdot \nabla v^h \, d\Omega \; + \; (1-\gamma) \int_{\mathcal{S}_h} \nabla R_h^m u \cdot \nabla v^h \, d\Omega,$$

which means that this local modification only requires the stiffness values corresponding to the elements $K \in \mathcal{S}_h$, to be scaled by a factor of $1-\gamma$. How can this local modification can lead us to optimal convergence rates? How do we get the optimal correction parameter? The following sections are dedicated to answering these questions.

## 3.3 ECFEM: Working Principle

The basic working principle behind this technique is that, sufficiently accurate approximation of the energy is not only *necessary*, but also *sufficient* for attaining low errors in the weighted $L^2$-norms. In order to achieve this, we consider a modified bilinear form or the modified energy term $a_h(\cdot,\cdot)$ with a suitable correction as defined above.

**Symmetry Requirement** In order for the technique to work, there is a symmetry requirement on the finite element mesh $\mathcal{T}_h$ which is to be fulfilled when $\frac{3\pi}{2} < \omega < 2\pi$ [6, Section 2.2]. It is required that the mesh is locally symmetric about the angle bisector of the interior angle (see Figure 3.1b). This is essential to ensure that combinations of the form $(s_1, s_2)$ and $(s_2, s_1)$ cancel out as will be explained later. It must be noted that not only the elements in $S^h$, but also sufficient layers of elements in the vicinity of the singular point should depict this symmetry. In case, the mesh $\mathcal{T}_h$ is obtained through a systematic uniform refinement of a coarse mesh $\mathcal{T}_H$, symmetry of only the elements in $S^h$ would be sufficient as this would lead to layers of elements with the necessary symmetry.

It is further assumed that the modification satisfies the following conditions:

(C1) $a_h(u,u) > C\|u\|_1^2$ for all $u \in H_0^1(\Omega)$,

(C2) $c_h(u,v) < C\|\nabla u\|_{0,\mathcal{S}_h}\|\nabla v\|_{0,\mathcal{S}_h}$ for all $u, v \in H_0^1(\Omega)$,

(C3) $c_h(u,v) = c_h(v,u)$ for all $u, v \in H_0^1(\Omega)$.

Now, we present the theorem (based on [6, Theorem 2.2]) stating the necessity of an accurate energy computation for achieving optimal convergence rates.

**Theorem 3.1** (Necessary Condition)**.** *If $f \in H^0_{-\alpha}$ for some $\alpha > 0$ and the modified Galerkin approximation satisfies*

$$\|u - R_h^m u\|_{0,\alpha} = \mathcal{O}\left(h^2\right),$$

*Then, it must hold that,*

$$|a(u,u) - a_h(R_h^m u, R_h^m u)| = \mathcal{O}\left(h^2\right).$$

*Proof.* According to the arguements given previously, there exist unique solutions $u, R_h^m u$ to the continuous and the discrete problems in the space $H_0^1(\Omega)$. Applying the definition of the modified Galerkin approximation yields,

$$\begin{aligned}
|a(u,u) - a_h(R_h^m u, R_h^m u)| &= |(f,u) - (f, R_h^m u)| \\
&= |r^{-\alpha} f\, r^{\alpha}\,(u - R_h^m u)| \\
&\leq \|r^{-\alpha} f\|_0 \|r^{\alpha}\,(u - R_h^m u)\|_0 = \|f\|_{0,-\alpha}\|(u - R_h^m u)\|_{0,\alpha},
\end{aligned}$$

which proves the assertion of this theorem. □

The above theorem also implies that the pollution effect persists in the weighted $L^2$-norms as well, i.e. the mere usage of these weighted Sobolev norms does not help in achieving convergence rates with optimal order. This can be shown by utilizing the result of the above theorem and employing the fact that without the local correction, i.e. putting $c_h(\cdot,\cdot) = 0$, we have $a_h(\cdot,\cdot) = a(\cdot,\cdot)$, which means,

$$\|(u - R_h^m u)\|_{0,\alpha} \geq |a\,(u,u) - a\,(R_h^m u, R_h^m u)|.$$

Now, utilizing the fact that, the energy of the error equals the error in energy for the original Galerkin approximation yields,

$$\|(u - R_h^m u)\|_{0,\alpha} \geq |a\,(u - R_h^m u, u - R_h^m u)| = \|\nabla\,(u - R_h^m u)\|_0^2.$$

Further, inserting the results of [4, Theorem 3.1], i.e. $\|\nabla\,(u - R_h^m u)\|_0 \geq C h^{\frac{\pi}{\omega}}$ gives the following desired result

$$\|(u - R_h^m u)\|_{0,\alpha} \geq \|\nabla\,(u - R_h^m u)\|_0^2 \geq C h^{\frac{2\pi}{\omega}}.$$

Thus, we see that the conventional Galerkin approximation is sub-optimal even if the errors are measured in the weighted norms. It is noteworthy that the above result is independent of the behaviour of $f$ near the re-entrant corner and thus the pollution effect is a global phenomenon.

The modified Galerkin approximation also satisfies an orthogonality condition, provided the assumptions (C1) and (C2) hold. Inserting $v = v^h$ in (3.2) and subtracting from (3.3) results in

$$a\left(u - R_h^m u, v^h\right) + c_h\left(R_h^m u, v^h\right) = 0 \quad \forall\ v^h \in \mathcal{V}^h, \tag{3.5}$$

which is the *modified Galerking orthogonality condition*. Further, if (C3) is satisfied, the minimization property analogous to (2.5) is valid, i.e.

$$a\,(u - R_h^m u, u - R_h^m u) - c_h\,(R_h^m u, R_h^m u) \leq a\left(u - v^h, u - v^h\right) - c_h\left(v^h, v^h\right) \quad \forall\ v^h \in \mathcal{V}^h. \tag{3.6}$$

Alike the standard Galerkin case, the conditions (3.3), (3.5) and (3.6) are equivalent.

The next important step is to show that the modified Galerkin approximation is sufficient to eliminate the pollution effect in the weighted $L^2$-norm, i.e. using a suitable energy correction $c_h(\cdot,\cdot)$, we can achieve optimal convergence rate even with quasi-linear finite elements. This is stated in the following theorem.

**Theorem 3.2** (Sufficient Condition)**.** *Let $f \in H^0_{-\alpha}(\Omega)$ for some $1 - \pi/\omega < \alpha < 1$, and assume that (C1)-(C3) hold and also the symmetry requirement is met if $\frac{3\pi}{2} < \omega < 2\pi$. Additionally, If the modification satisfies*

$$a\,(s_1 - R_h^m s_1, s_1 - R_h^m s_1) - c_h\,(R_h^m s_1, R_h^m s_1) = \mathcal{O}\left(h^2\right), \tag{3.7}$$

*then, optimal order convergence in weighted norms is obtained, i.e.*

$$\|\nabla\,(u - R_h^m u)\|_{0,\alpha} \leq C\,h\,\|f\|_{0,-\alpha} \qquad \textit{and} \qquad \|u - R_h^m u\|_{0,\alpha} \leq C\,h^2\,\|f\|_{0,-\alpha}.$$

For the detailed proof of this theorem, we refer the reader to [6]. Here, we try to summarize the ideas and steps involved in the proof. We begin by considering an auxiliary problem based on Nitsche's *duality arguement* [25, Section 1.6]: Find $z$, s.t.

$$-\Delta z = r^{2\alpha}\left(u - R_h^m u\right) \quad \text{in } \Omega,$$
$$z = 0 \quad \text{on } \partial\Omega,$$

so that the corresponding weak form reads: Find $z$, s.t.

$$a\left(z, v^h\right) = \left(r^{2\alpha}\left(u - R_h^m u\right), v^h\right) \quad \forall\ v^h \in \mathcal{V}^h, \tag{3.8}$$

and by $R_h^m z \in \mathcal{V}^h$, we denote the modified Galerkin approximation to $z$. Inserting $u - R_h^m u$ in place of $v^h$ in (3.8) yields

$$a\left(z, u - R_h^m u\right) = \left(r^{2\alpha}\left(u - R_h^m u\right), u - R_h^m u\right) = \|u - R_h^m u\|_{0,\alpha}^2.$$

Also, using the modified Galerkin orthogonality of (3.5), we obtain

$$\begin{aligned} a\left(u - R_h^m u, z\right) &= a\left(u - R_h^m u, z\right) - \left[a\left(u - R_h^m u, R_h^m z\right) + c_h\left(R_h^m u, R_h^m z\right)\right] \\ &= a\left(u - R_h^m u, z - R_h^m z\right) - c_h\left(R_h^m u, R_h^m z\right), \end{aligned}$$

which on combining with the above relation yields

$$\|u - R_h^m u\|_{0,\alpha}^2 = a\left(z, u - R_h^m u\right) = a\left(u - R_h^m u, z - R_h^m z\right) - c_h\left(R_h^m u, R_h^m z\right). \tag{3.9}$$

The next task is to decide how many singular functions $s_i$ should be considered. It can be easily shown that the first singular function $s_1 \notin H^2(\Omega)$ for all permissible values of the interior angle. Higher order singular functions $s_k$ for $k \geq 2$ posses regularity at least better than $H^2(\Omega)$ and therefore require no treatment (See Appendix B for detailed calculations). However, the combinations of the form $(s_1, s_2)$ could contribute to the singular nature and thus need attention. Using (2.10) with $\beta = -\alpha$, the solutions $u, z$ to the primary and the auxiliary problems respectively, can be expanded as

$$u = \sum_{i=1}^{2} \lambda_i\, s_i + U \qquad \text{and} \qquad z = \sum_{j=1}^{2} \mu_j\, s_j + Z,$$

where, $U, Z \in H^2_{-\alpha}$ represent the smooth remainder part of the solution. Inserting these expansions in (3.9) and considering above arguements about number of singular functions, we arrive at

$$\begin{aligned} \|u - R_h^m u\|_{0,\alpha}^2 = {} & \lambda_1\,\mu_1\left[a\left(s_1 - R_h^m s_1, s_1 - R_h^m s_1\right) - c_h\left(R_h^m s_1, R_h^m s_1\right)\right] \\ & + \lambda_1\,\mu_2\left[a\left(s_1 - R_h^m s_1, s_2 - R_h^m s_2\right) - c_h\left(R_h^m s_1, R_h^m s_2\right)\right] \\ & + \lambda_2\,\mu_1\left[a\left(s_2 - R_h^m s_2, s_1 - R_h^m s_1\right) - c_h\left(R_h^m s_2, R_h^m s_1\right)\right] \\ & + \mu_1\left[a\left(U - R_h^m U, s_1 - R_h^m s_1\right) - c_h\left(R_h^m U, R_h^m s_1\right)\right] \\ & + \lambda_1\left[a\left(s_1 - R_h^m s_1, Z - R_h^m Z\right) - c_h\left(R_h^m s_1, R_h^m Z\right)\right] \\ & + a\left(U - R_h^m U, Z - R_h^m Z\right) - c_h\left(R_h^m U, R_h^m Z\right). \end{aligned}$$

Now, it remains to show that each of these terms on the right hand side can be bounded from the above by $C\,h^2\,\|u - R_h^m u\|_{0,\alpha}$, thereby giving the desired result even when combinations of the form $a\left(s_1 - R_h^m s_1, s_2 - R_h^m s_2\right)$ are considered. This can be simplified by assuming that the

symmetry condition holds, so that the cross terms cancel out. Moreover, the condition (3.7) can be generalized to

$$a\left(u - R_h^m u, u - R_h^m u\right) - c_h\left(R_h^m u, R_h^m u\right) = \mathcal{O}\left(h^2\right),$$

which upon utilization of (3.5) and some algebraic manipulation can be simplified as

$$\begin{aligned} a\left(u - R_h^m u, u - R_h^m u\right) - c_h\left(R_h^m u, R_h^m u\right) &= a\left(u - R_h^m u, u\right) - \left[a\left(u - R_h^m u, R_h^m u\right) + c_h\left(R_h^m u, R_h^m u\right)\right] \\ &= a\left(u, u\right) - a\left(R_h^m u, u\right) \\ &= a\left(u, u\right) - \left[a\left(R_h^m u, R_h^m u\right) - c_h\left(R_h^m u, R_h^m u\right)\right] \\ &= a\left(u, u\right) - a_h\left(R_h^m u, R_h^m u\right), \end{aligned}$$

resulting in the estimate

$$a\left(u, u\right) - a_h\left(R_h^m u, R_h^m u\right) = \mathcal{O}\left(h^2\right)$$

for the energy defect.

It is noteworthy that the above theorems describing the necessity and sufficiency of the local modification given in (3.3), are valid for any correction $c_h(\cdot,\cdot)$ satisfying the conditions (C1)-(C3) and the symmetry requirement. It can be shown that the correction defined by (3.4), with $0 \leq \gamma \leq \frac{1}{2}$ fulfills all these requirements.

**Remark 3.3.** *In accordance with Remark 2.1, we use the condition $\alpha > 0$ for Theorem 3.1.*

## 3.4 Determining Optimal Correction Parameter

The ECFEM essentially intends to minimise the *energy defect* functional

$$\begin{aligned} g_h\left(\gamma_h\right) &\coloneqq a\left(u, u\right) - a_h\left(R_h^m u, R_h^m u\right) \\ &= a\left(u, u\right) - a_h\left(R_h^m u, R_h^m u\right) + \gamma_h\, d_h\left(R_h^m u, R_h^m u\right), \end{aligned} \tag{3.10}$$

in order to achieve optimal convergence rates in the weighted norms. The level dependent correction parameter $\gamma_h$ which serves this purpose can be thus determined as the root of the *nonlinear* equation

$$g_h\left(\gamma\right) = 0.$$

It can be further shown that these level dependent correction parameters converge to

$$\gamma_\infty = \gamma_h + c\, h^{2 - \frac{2\pi}{\omega}}, \tag{3.11}$$

which is a level independent value of the correction parameter and gives reasonably good results for all mesh levels [6]. A numerical procedure based on *Richardson's extrapolation*, which can be used to determine the value of $\gamma_\infty$, will be described in the next chapter.

Computation of the energy defect in its current formulation involves calculation of the analytical energy $a\left(u, u\right)$, which is only feasible for very simple domains. A work around to this problem is to consider the following definition of the energy defect

$$g_h\left(\gamma_h\right) = a\left(u - R_h^m u, u - R_h^m u\right) - \gamma_h\, c_h\left(R_h^m u, R_h^m u\right), \tag{3.12}$$

which, as shown in the previous section is equivalent to the one in (3.10). However, as determined from experience with numerical experiments, this method suffers from loss of accuracy due to the numerical errors creeping in from the computation of the finite element error terms having singular behaviour. Moreover, both of the above mentioned approaches require prior knowledge of the true solution, which hinders the practical applicability of this technique. In order to circumvent this problem, an alternative definition of the energy defect as given in [3] will be considered in this work. This approach is based on the idea that sufficiently accurate computation of the energy $a_h(\cdot,\cdot)$ and consequently the finite element solution $R_h^m u$ can be realized when the difference in the energies for two consecutive mesh refinement levels vanishes. The *two-level* energy defect functional is defined as

$$g_h^{TL}(\gamma_h) \coloneqq a_h\left(R_h^m u, R_h^m u\right) - a_{2h}\left(R_{2h}^m u, R_{2h}^m u\right) \tag{3.13}$$

where $a_{2h}(\cdot,\cdot)$ is the energy computed at the coarser mesh level. Thus, determination of the energy defect involves solving two finite element problems with mesh sizes $h$ and $2h$ leading to approximate solutions $R_h^m u$ and $R_{2h}^m u$ respectively. The energy for each problem is then computed through numerical integration, thereby giving the value of the energy defect. A suitable nonlinear equation solving technique, such as *bisection* method, can then be applied to determine the optimal correction parameter for the mesh size $h$. Another possibility for determining the optimal correction parameter by *nested-Newton* type approach has been explored in [21].

A noteworthy feature of the energy correction technique is that the value of the correction parameter computed on a given mesh for a given type of PDE, say Poisson's equation or elasticity equation can be used for another problem (of the same type and on the same mesh), say different right hand side or boundary conditions. For example, the value of $\gamma$ computed for the problem in (4.3) will also result in optimal convergence rates for non-zero, but sufficiently smooth right hand side.

# Chapter 4

# ECFEM for Scalar Elliptic Problems

In this chapter, we present some numerical examples to demonstrate the working of ECFEM in context of scalar problems.

## 4.1 A Brief on Implementation

In order to carry out the numerical tests presented in this chapter and also in Section 5.3, a MATLAB code based on [8] has been developed. This code is capable of solving Poisson's equation as well as the elasticity equation on arbitrary two-dimensional domains using continuous Galerkin finite elements. The only element type supported is *Lagrange* triangles. The code has provisions to allow the use of general $p$-order polynomials for finite element basis functions. Currently, Gaussian quadrature rules with degree of precision up to 20 are supported, thereby restricting the degree of polynomials to $p = 11$ for the elliptic problems considered in this work. The MATLAB *backslash* operator is used to solve the SLE arising from the finite element discretisation.

Since, we will primarily focus on computation of the finite element error, considered in different aforementioned norms, a note on the methodology adopted for computing these error norms is in order. The mean square type error norms have been computed through numerical integration of the error integral using quadrature rules of sufficient accuracy. For the computation of the max error norm, a simplified approach has been adopted in order to avoid the complexities which would arise otherwise. The finite element error in the max norm is computed as max norm of the vector obtained as the difference between the finite element nodal solution vector $U_h$ and the vector $U$ comprising of the true solution computed at the corresponding nodes, i.e.

$$\|u - u^h\|_{L^2(\Omega)} \approx |U - U^h|_\infty$$

where, $|V|_\infty$ represents the max norm of $V \in \mathbb{R}^n$.

In order to the study the rates of convergence, we solve the considered BVPs on a family of meshes $\{\mathcal{T}_h\}_{h \leq H}$ obtained by a systematic *uniform* refinement of a coarse mesh $\mathcal{T}_H$. During the refinement process, each edge of the triangle is divided at its midpoint, thereby resulting in

formation of four new triangular elements. The coarse mesh is constructed in such a way that it results in the least possible number of DOFs (see for e.g. Figure 4.1a). For presenting the results of the convergence studies, we will use the notion of the mesh refinement level $l$. Assuming, the level $l = 1$ corresponds to the coarsest mesh considered in the study, the mesh size for the finite element mesh at level $l$ is

$$h = \frac{H}{2^{l-1}},$$

where, $H$ denotes mesh size for the level $l = 1$ or the coarsest mesh considered.

The error estimates presented in Section 2.2 and Section 2.3.2 imply that the finite element error in any of the three norms considered, varies with the mesh size $h$ as

$$\|u - u^h\| = \mathcal{O}\left(h^\alpha\right)$$

where, $\alpha$ is the order of convergence. The estimated order of convergence (eoc) or the numerically determined order of convergence, can be computed by considering the error norms for two consecutive mesh refinement levels, having mesh sizes $2h$ and $h$ respectively. The eoc is then determined by

$$\frac{\|u - u^h\|}{\|u - u^{2h}\|} = \frac{h^\alpha}{(2h)^\alpha} = \frac{1}{2^\alpha},$$

resulting in

$$\alpha = \frac{\log\left(\frac{\|u-u^h\|}{\|u-u^{2h}\|}\right)}{\log\left(\frac{1}{2}\right)} \tag{4.1}$$

which is the expression for the eoc.

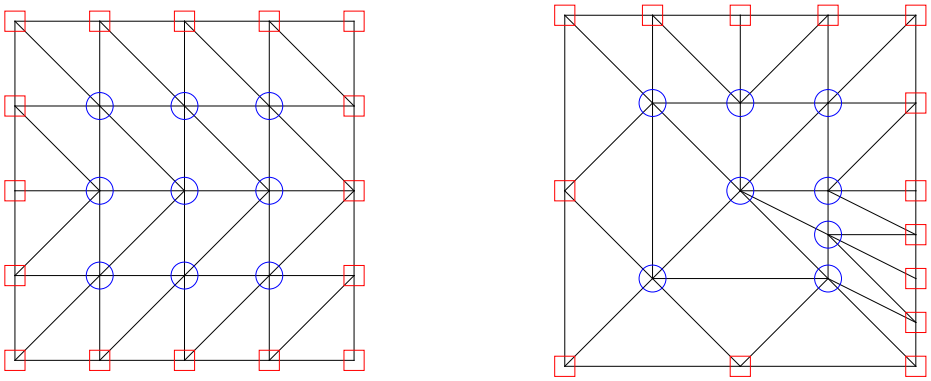

(a) Uniform mesh $\mathcal{T}_H$ with $H = 0.5$.

(b) Non-uniform mesh $\mathcal{T}_H$ with $H = 1.0$.

Figure 4.1: Different types of coarse linear finite element meshes used for solving the BVP (4.2). The interior nodes (or the free DOFs) have been denoted by a blue circle, while those on the boundary (the constrained DOFs) have been marked by a red square.

## 4.2 Case of Smooth Boundary

We begin by considering the example of a domain with smooth boundary, so as to exemplify the validity of the error estimates presented in Section 2.2. This example also serves to setup certain methodologies to be employed later on in the singular cases. We consider the following BVP: Find $u\colon \Omega \to \mathbb{R}$, s.t.

$$\begin{aligned} -\Delta u &= f \quad \text{in } \Omega, \\ u &= g \quad \text{on } \partial\Omega, \end{aligned} \tag{4.2}$$

where, $\Omega$ is a square domain, centered about the origin, i.e. $\Omega = (-1,1)^2$. The right hand side function $f$ has been chosen such that the exact solution is given by

$$u = \cos\frac{\pi\, x}{2}\ \cos\frac{\pi\, y}{2}.$$

We solve this problem on two different kinds of meshes, once on a *uniformly* sized mesh (see Figure 4.1a) and also on a *non-uniformly* sized mesh(see Figure 4.1b).

The manner in which the finite element error reduces with increasing mesh refinement levels for both the initial mesh types considered (see Figures 4.3a − 4.3f), seems to be in good agreement with the error estimates of (2.7), (2.8) and (2.9). Such a behaviour is expected considering the smoothness of the true solution $u$ and hence it's finite element approximation. As is depicted in Figure 4.2, the solution is quite smooth, in-fact $u \in C^\infty$ for this particular problem. Consequently the requirement $u \in H^{p+1}$ is fulfilled for all the considered values of $p$, thereby resulting in optimal convergence rates. However, a slight deviation is observed for $p = 4$ in $L^2$-norm (cf. Figure 4.3a) and $L^\infty$-norm (cf. Figure 4.3e). This can be attributed to the fact that in these cases, the error is already smaller than $10^{-10}$ and working with such small values could lead to numerical errors. Another observation is that, when using linear finite elements, the graph for $\|u - u^h\|_{L^\infty}$ is not exactly quadratic, especially for the non-uniform mesh. This is due to the fact that the expected behaviour when using linear finite elements is $\mathcal{O}\left(h^2 \log h\right)$, which approaches the quadratic behaviour as $h$ decreases with subsequent mesh refinement.

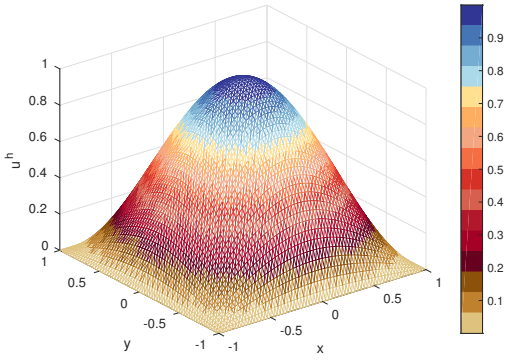


Figure 4.2: The finite element solution $u^h$ for the BVP (4.2) computed using linear finite elements on a uniform mesh with mesh size $h = 0.03125$, corresponding to the $5^{th}$ mesh refinement level.

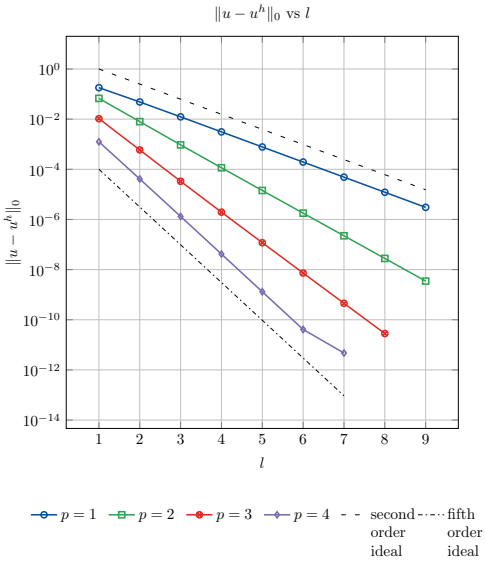


(a) Error in $L^2$-norm for uniform mesh.

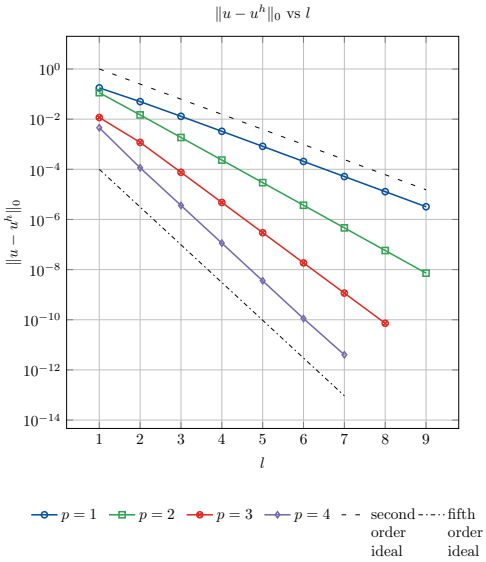


(b) Error in $L^2$-norm for non-uniform mesh.

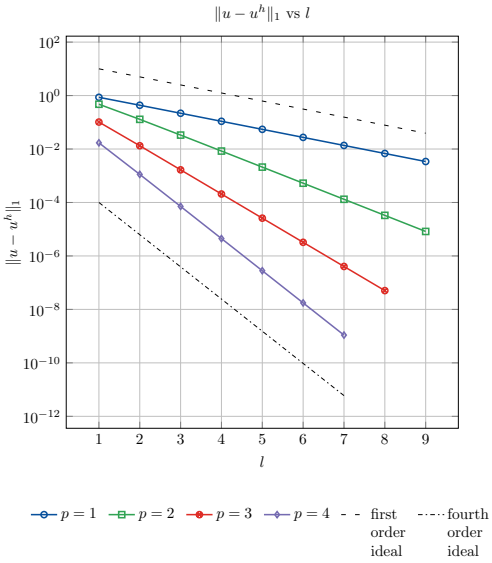


(c) Error in $H^1$-norm for uniform Mesh.

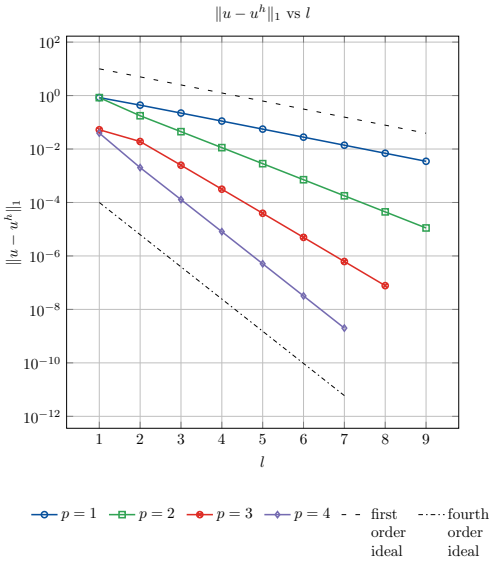


(d) Error in $H^1$-norm for non-uniform mesh.

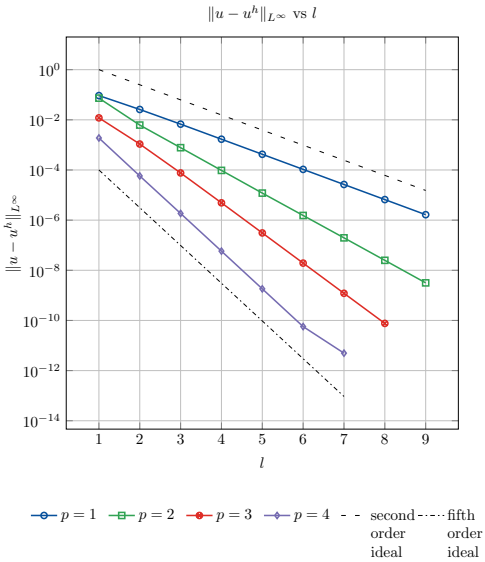


(e) Error in $L^\infty$-norm.

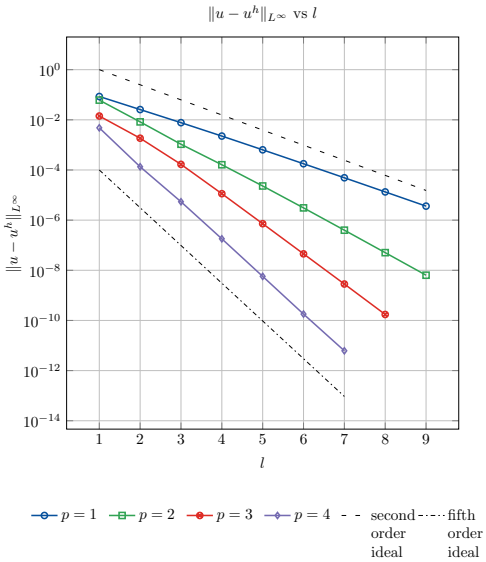


(f) Error in $L^\infty$-norm for non-uniform mesh.

Figure 4.3: Variation of the finite element error $u - u^h$ in different norms, with the mesh refinement level $l$ for the BVP (4.2) on the two types of finite element meshes considered. The error norms have been plotted for different polynomial orders used for the finite element basis functions.

## 4.3 Case of Slit Domain

In order to explain the working of ECFEM in context of scalar elliptic BVPs, we consider the case of a domain with slit, corresponding to an interior angle $\omega = 2\pi$ in Figure 3.1, leading to: $\Omega = (-1,1)^2 \setminus [0,1] \times \{0\}$. We choose

$$u = \tilde{s}_1 = r^{\frac{1}{2}} \sin\frac{\theta}{2}$$

as the exact solution for this model problem. The BVP to be solved thus reads: Find $u$, s.t.

$$\begin{aligned} -\Delta u &= 0 \quad \text{in } \Omega, \\ u &= \tilde{s}_1 \quad \text{on } \partial\Omega. \end{aligned} \tag{4.3}$$

### Symmetric Mesh

We first solve this problem on a family of meshes $\{\mathcal{T}_h\}_{h \leq H}$ obtained through uniform refinement(as explained in Section 4.1) of the coarse mesh $\mathcal{T}_H$ shown in Figure 4.4a. It has been ensured that the mesh is symmetric about the angle bisector of the interior angle, which in this case is the x-axis. This is important for the assertion of Theorem 3.2 to hold. Moreover, because of this uniform refinement process, it is sufficient to have $S^h$ as the one element neighbourhood of the singular point. Additionally, we choose a region $\Omega_s = (-0.2, 0.2)^2$ in the vicinity of the re-entrant corner, where the effect of the singular behaviour is prominent (see Figure 4.5). The region $\Omega_s$ will be referred to as the *singular* region in this work. The choice of the dimensions of the singular region are arbitrary as long as we are dealing with domains having only one re-entrant corner, with the only requirement that $\Omega_s$ is sufficiently large to capture the singular behaviour of the solution, and thus should not effect the results.

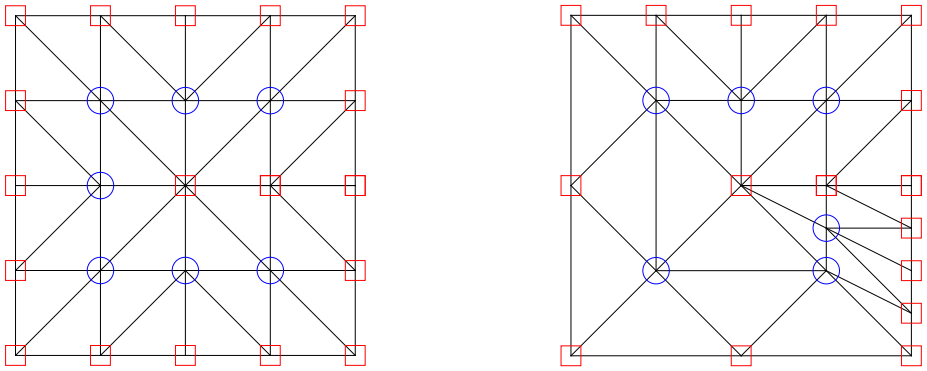

(a) Symmetric mesh $\mathcal{T}_H$ with $H = 0.5$.

(b) Non-uniform mesh $\mathcal{T}_H$ with $H = 2.0$.

Figure 4.4: Different types of coarse linear finite element meshes used for solving the BVP (4.3). The interior nodes (or the free DOFs) have been denoted by a blue circle, while those on the boundary (the constrained DOFs) have been marked by a red square.

In order to have an understanding of the nature of the singularity caused due to the presence of the re-entrant corner, we first solve the BVP by using the standard Galerkin approximation

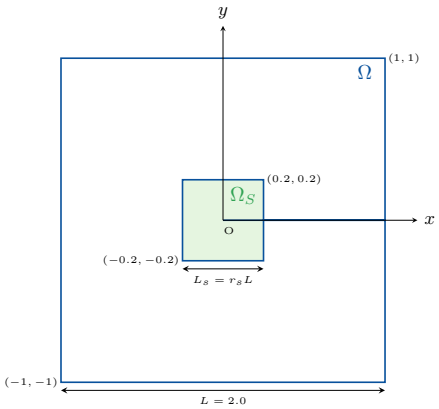


Figure 4.5: The location of the singular region $\Omega_s$ within the domain $\Omega$ for the slit domain. For this study, we choose $r_s = 0.2$, resulting in the coordinates marked here.

which means $\gamma = 0$ or no local modification. As is depicted in Figure 4.8, the plot of the finite element approximation $R_h^m u$ exhibits singular behaviour of the form $r^{1/2}$ as is expected from the theory presented in Section 2.3.1. The eocs for different error norms computed for a range of refinement levels have been presented in Table 4.1. The numerical results are in accordance with the estimates presented in (2.12), (2.13) and (2.14) respectively. Sub-optimal convergence rates for the error are exhibited in both the $L^2$-norm as well as the *weighted* $L^2$-norm globally. This can be also observed in the error plot presented in Figure 4.9. The pollution effect is global in the sense that sub-optimal convergence rates are observed not just for the singular region $\Omega_s$, but also in the outside region $\Omega \backslash \Omega_s$. It is noteworthy that the error in the $H^1$-norm computed for the outside region, i.e. $\|u - R_h^m u\|_{\Omega \backslash \Omega_s}$ exhibits an eoc of $\mathcal{O}(h)$, which coincidently matches with optimal convergence rate, since linear finite elements have been considered. This, however seems to be an exception as we observed the same $\mathcal{O}(h)$ convergence even with higher order elements (see Section 4.4), thereby validating the existence of pollution effect. A possible reason for this could be that the error term probably has the form

$$\|u - R_h^m u\|_{H^1(\Omega \backslash \Omega_s)} = \mathcal{O}\left(h^{\min\{1, f(p,\omega)\}}\right), \tag{4.4}$$

where, $f(p, \omega)$ is some function of the polynomial order $p$ and the interior angle $\omega$. As a consequence of this, the singular region has much larger contribution to $\|u - R_h^m u\|_{H^1(\Omega)}$ than the outside region.

Moving towards the optimally corrected Galerkin approximation, the first step is to determine the optimal correction parameter $\gamma_\infty$ which leads to optimal convergence rates for all of the mesh refinement levels. This is probably the most critical part of the entire ECFEM procedure. As mentioned in Section 3.4, this can be done by computing the root of the energy defect functional. In order to study how the two level energy defect functional (3.13) behaves with variation of the correction parameter $\gamma$, we plot this variation in Figure 4.6, where the energy defect has been scaled by a suitable factor to get straight lines. It is clear that with subsequent mesh refinement, the different $g_h$ curves converge to the one corresponding to the finest mesh. Consequently, the points at which these curves meet the 0-value mark (which represents $\gamma_h$) also converge as the mesh is refined. The level dependent correction parameters $\gamma_h$ have been computed by employing the *bisection method* to find the root of the energy defect functional. Suitable stopping criterion

has been applied for the bisection method, ensuring sufficiently small value of the target function $g_h$ as the algorithm stops. The level independent correction paramater is then computed by using the *Richardson* extrapolation procedure which works as follows: Let $\gamma_h$ and $\gamma_{2h}$ be the optimal correction parameters corresponding to wo consecutive meshes having sizes $h$ and $2h$ respectively. Then we have,

$$\gamma_\infty = \gamma_h + C\, h^\beta \qquad \text{and} \qquad \gamma_\infty = \gamma_{2h} + C\, (2h)^\beta\,,$$

which leads to

$$\frac{\gamma_\infty - \gamma_h}{\gamma_\infty - \gamma_{2h}} = \frac{h^\beta}{(2h)^\beta},$$

resulting in

$$\gamma_\infty = \frac{2^\beta\, \gamma_h - \gamma_{2h}}{2^\beta - 1}, \tag{4.5}$$

which is the required expression for computing $\gamma_\infty$. The exponent $\beta = 2 - \frac{2\pi}{\omega}$ in case of linear finite elements according to (3.11). The values of $\gamma_h$ and its Richardson extrapolant for different mesh levels have been plotted in Figure 4.7.

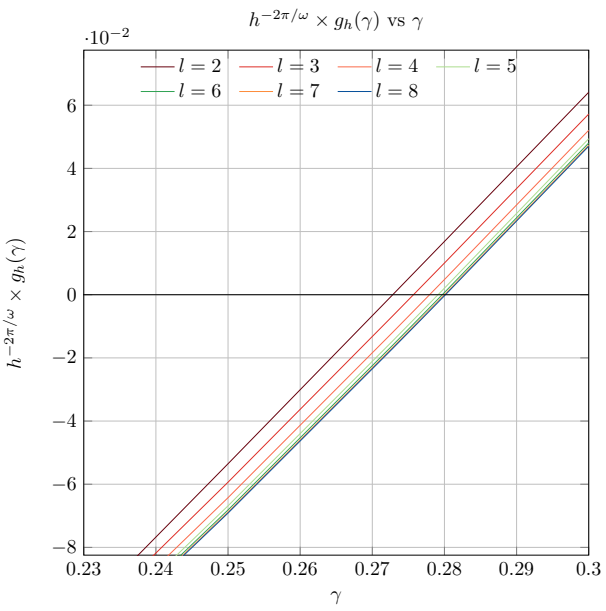


Figure 4.6: Variation of the energy defect $g_h$ with the correction parameter $\gamma$ for different mesh refinement levels; corresponds to linear finite elements on symmetric mesh for the BVP (4.3).

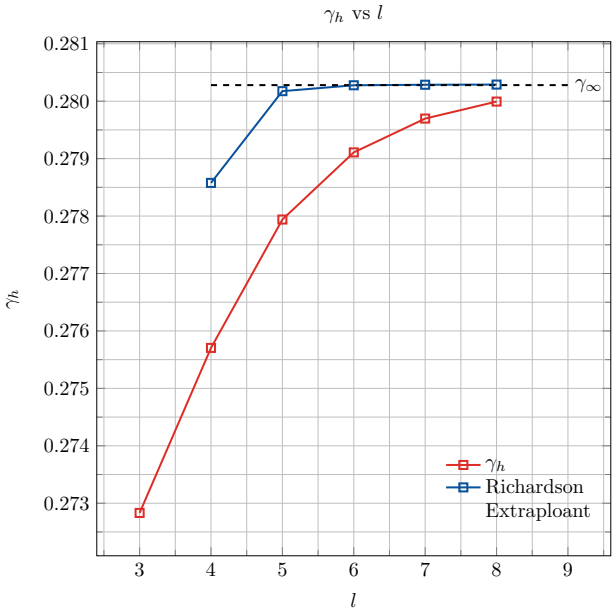


Figure 4.7: The level dependent optimal correction parameter $\gamma_h$ and its Richardson extrapolant; corresponds to linear finite elements on symmetric mesh for the BVP (4.3).

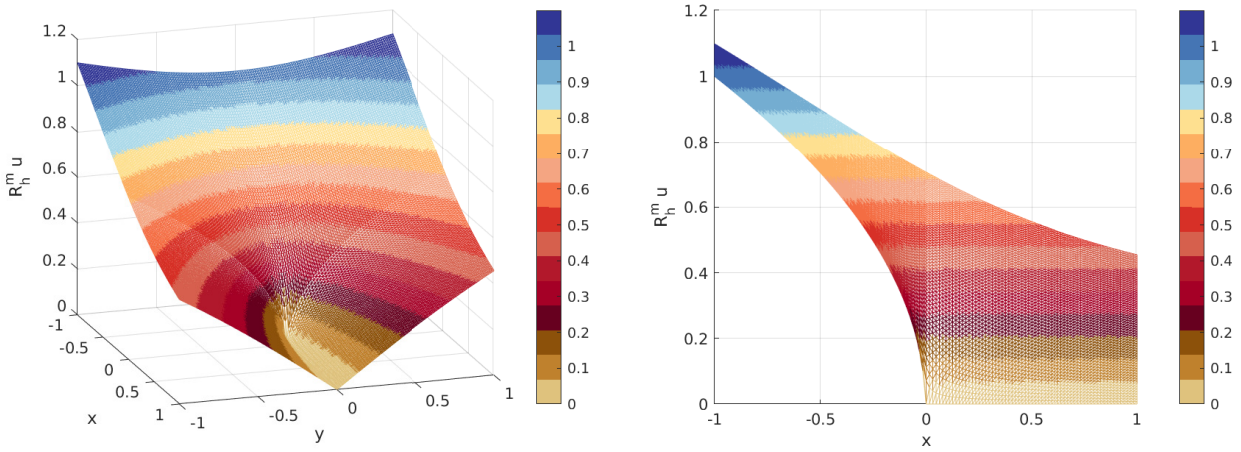


Figure 4.8: Plot of the finite element approximation $R_h^m u$ obtained using linear finite elements for the BVP (4.3) for the $6^{th}$ mesh refinement level.

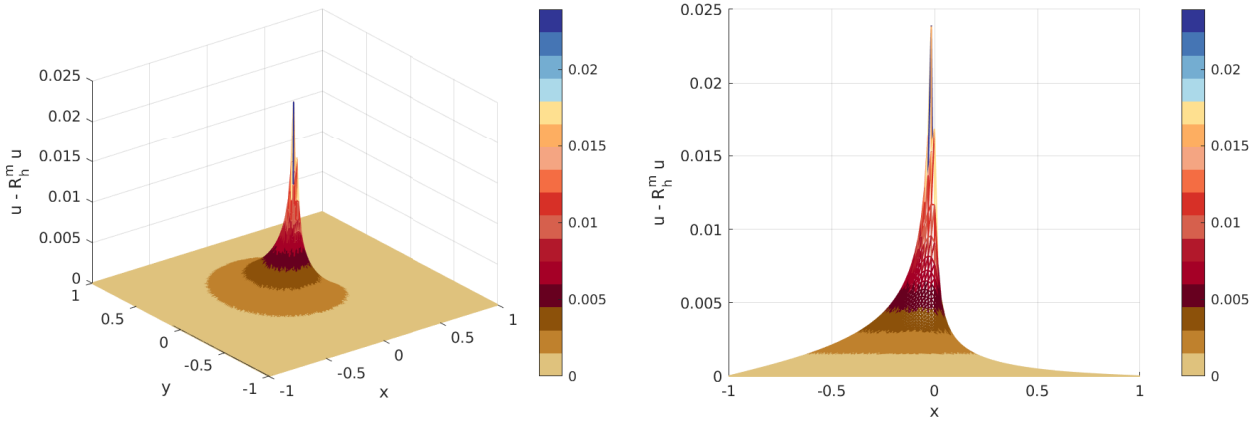


Figure 4.9: Plot of the finite element error $u - R_h^m u$ obtained using linear finite elements with $\gamma = 0.0$, i.e. no correction for the BVP (4.3) for the $6^{th}$ mesh refinement level.

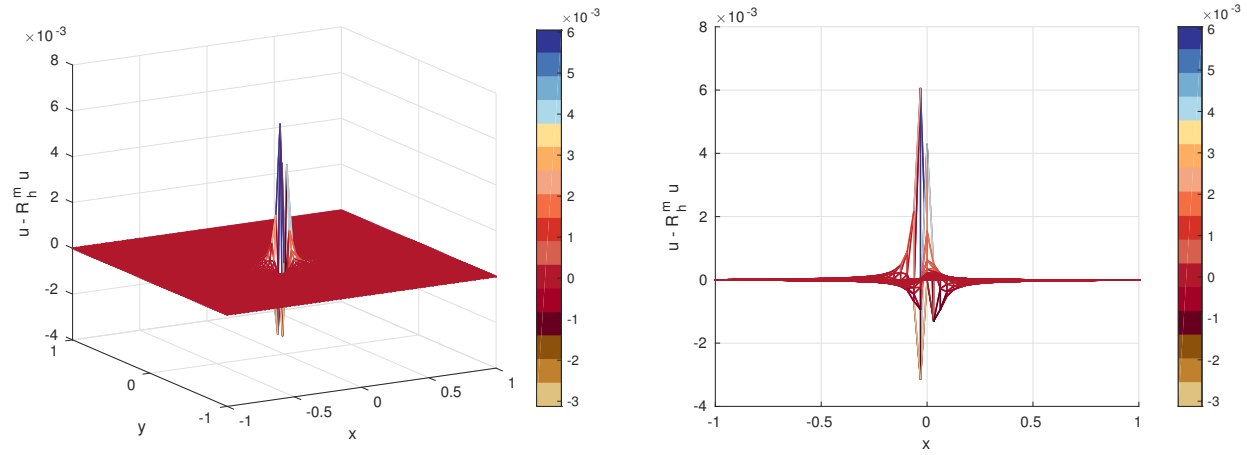


Figure 4.10: Plot of the finite element error $u - R_h^m u$ obtained using linear finite elements with $\gamma = 0.28028$, i.e. with optimal correction for the BVP (4.3) for the $6^{th}$ mesh refinement level.

Table 4.1: Error using linear finite elements on symmetric mesh, for the BVP (4.3) with no correction applied, i.e. $\gamma = 0.0$.

| $l$ | $h/\sqrt{2}$ | $\|u - R_h^m u\|_{0,1/2;\Omega}$ | eoc | $\|u - R_h^m u\|_{L^2(\Omega)}$ | eoc | $\|u - R_h^m u\|_{L^2(\Omega_s)}$ | eoc | $\|u - R_h^m u\|_{L^2(\Omega\setminus\Omega_s)}$ | eoc | $\|u - R_h^m u\|_{H^1(\Omega)}$ | eoc |
|---|---|---|---|---|---|---|---|---|---|---|---|
| 1 | 0.50000000 | 6.437135e-02 | - | 1.084520e-01 | - | - | - | 1.282595e-02 | - | 4.850518e-01 | - |
| 2 | 0.25000000 | 2.859099e-02 | 1.1709 | 5.256207e-02 | 1.0450 | - | - | 1.692831e-02 | - | 3.345537e-01 | 0.5359 |
| 3 | 0.12500000 | 1.325092e-02 | 1.1095 | 2.538735e-02 | 1.0499 | 1.472758e-02 | - | 8.024789e-03 | 1.0769 | 2.343286e-01 | 0.5137 |
| 4 | 0.06250000 | 6.360660e-03 | 1.0588 | 1.234246e-02 | 1.0405 | 8.666192e-03 | 0.7651 | 3.917947e-03 | 1.0344 | 1.650167e-01 | 0.5059 |
| 5 | 0.03125000 | 3.117016e-03 | 1.0290 | 6.052658e-03 | 1.0280 | 4.239981e-03 | 1.0313 | 2.213533e-03 | 0.8237 | 1.164666e-01 | 0.5027 |
| 6 | 0.01562500 | 1.543483e-03 | 1.0140 | 2.989289e-03 | 1.0178 | 2.084819e-03 | 1.0241 | 1.175311e-03 | 0.9133 | 8.228190e-02 | 0.5013 |
| 7 | 0.00781250 | 7.681396e-04 | 1.0067 | 1.483596e-03 | 1.0107 | 1.047177e-03 | 0.9934 | 5.860099e-04 | 1.0040 | 5.815740e-02 | 0.5006 |
| 8 | 0.00390625 | 3.831949e-04 | 1.0033 | 7.385996e-04 | 1.0062 | 5.240435e-04 | 0.9987 | 2.925955e-04 | 1.0020 | 4.111494e-02 | 0.5003 |

| $l$ | $h/\sqrt{2}$ | $\|u - R_h^m u\|_{H^1(\Omega_s)}$ | eoc | $\|u - R_h^m u\|_{H^1(\Omega\setminus\Omega_s)}$ | eoc | $\|u - R_h^m u\|_{L^\infty(\Omega)}$ | eoc | $\|u - R_h^m u\|_{L^\infty(\Omega_s)}$ | eoc | $\|u - R_h^m u\|_{L^\infty(\Omega\setminus\Omega_s)}$ | eoc |
|---|---|---|---|---|---|---|---|---|---|---|---|
| 1 | 0.50000000 | - | - | 8.976362e-02 | - | 8.282490e-02 | - | - | - | 8.282490e-02 | - |
| 2 | 0.25000000 | - | - | 9.521775e-02 | - | 7.921331e-02 | 0.0643 | - | - | 7.921331e-02 | 0.0643 |
| 3 | 0.12500000 | 1.965099e-01 | - | 4.630998e-02 | 1.0399 | 6.237629e-02 | 0.3447 | 6.237629e-02 | - | 3.824805e-02 | 1.0504 |
| 4 | 0.06250000 | 1.573251e-01 | 0.3209 | 2.264303e-02 | 1.0323 | 4.625298e-02 | 0.4315 | 4.625298e-02 | 0.4315 | 1.783138e-02 | 1.1010 |
| 5 | 0.03125000 | 1.137941e-01 | 0.4673 | 1.253761e-02 | 0.8528 | 3.344948e-02 | 0.4676 | 3.344948e-02 | 0.4676 | 9.636818e-03 | 0.8878 |
| 6 | 0.01562500 | 8.134338e-02 | 0.4843 | 6.607991e-03 | 0.9240 | 2.391284e-02 | 0.4842 | 2.391284e-02 | 0.4842 | 5.031518e-03 | 0.9376 |
| 7 | 0.00781250 | 5.784198e-02 | 0.4919 | 3.290856e-03 | 1.0057 | 1.700061e-02 | 0.4922 | 1.700061e-02 | 0.4922 | 2.500958e-03 | 1.0085 |
| 8 | 0.00390625 | 4.100614e-02 | 0.4963 | 1.642082e-03 | 1.0029 | 1.205359e-02 | 0.4961 | 1.205359e-02 | 0.4961 | 1.246954e-03 | 1.0041 |

Table 4.2: Error using linear finite elements on symmetric mesh, for the BVP (4.3) with the optimal correction applied, i.e. $\gamma = \gamma_\infty = 0.28028$.

| $l$ | $h/\sqrt{2}$ | $\|u - R_h^m u\|_{0,1/2;\Omega}$ | eoc | $\|u - R_h^m u\|_{L^2(\Omega)}$ | eoc | $\|u - R_h^m u\|_{L^2(\Omega_s)}$ | eoc | $\|u - R_h^m u\|_{L^2(\Omega\setminus\Omega_s)}$ | eoc | $\|u - R_h^m u\|_{H^1(\Omega)}$ | eoc |
|---|---|---|---|---|---|---|---|---|---|---|---|
| 1 | 0.50000000 | 4.111897e-02 | - | 8.209398e-02 | - | - | - | 2.128298e-03 | - | 5.075490e-01 | - |
| 2 | 0.25000000 | 1.060240e-02 | 1.9554 | 2.926814e-02 | 1.4879 | - | - | 1.522625e-03 | 0.4831 | 3.614409e-01 | 0.4898 |
| 3 | 0.12500000 | 2.700424e-03 | 1.9731 | 1.037377e-02 | 1.4964 | 1.013244e-02 | - | 3.895615e-04 | 1.9666 | 2.575291e-01 | 0.4890 |
| 4 | 0.06250000 | 6.860199e-04 | 1.9769 | 3.671309e-03 | 1.4986 | 3.659033e-03 | 1.4694 | 9.866550e-05 | 1.9812 | 1.829224e-01 | 0.4935 |
| 5 | 0.03125000 | 1.741346e-04 | 1.9780 | 1.298595e-03 | 1.4993 | 1.296588e-03 | 1.4967 | 2.774082e-05 | 1.8305 | 1.296574e-01 | 0.4965 |
| 6 | 0.01562500 | 4.418072e-05 | 1.9787 | 4.592240e-04 | 1.4997 | 4.588729e-04 | 1.4986 | 7.389209e-06 | 1.9085 | 9.179547e-02 | 0.4982 |
| 7 | 0.00781250 | 1.120585e-05 | 1.9792 | 1.623781e-04 | 1.4998 | 1.623190e-04 | 1.4993 | 1.852419e-06 | 1.9960 | 6.495007e-02 | 0.4991 |
| 8 | 0.00390625 | 2.841777e-06 | 1.9794 | 5.741256e-05 | 1.4999 | 5.740228e-05 | 1.4997 | 4.656646e-07 | 1.9920 | 4.594120e-02 | 0.4995 |
| 9 | 0.00195312 | 7.207487e-07 | 1.9792 | 2.029901e-05 | 1.5000 | 2.029715e-05 | 1.4998 | 1.186738e-07 | 1.9723 | 3.249050e-02 | 0.4998 |

| $l$ | $h/\sqrt{2}$ | $\|u - R_h^m u\|_{H^1(\Omega_s)}$ | eoc | $\|u - R_h^m u\|_{H^1(\Omega\setminus\Omega_s)}$ | eoc | $\|u - R_h^m u\|_{L^\infty(\Omega)}$ | eoc | $\|u - R_h^m u\|_{L^\infty(\Omega_s)}$ | eoc | $\|u - R_h^m u\|_{L^\infty(\Omega\setminus\Omega_s)}$ | eoc |
|---|---|---|---|---|---|---|---|---|---|---|---|
| 1 | 0.50000000 | - | - | 5.082065e-02 | - | 2.194003e-02 | - | - | - | 2.194003e-02 | - |
| 2 | 0.25000000 | - | - | 6.345118e-02 | - | 1.695697e-02 | 0.3717 | - | - | 1.695697e-02 | 0.3717 |
| 3 | 0.12500000 | 2.351235e-01 | - | 3.341382e-02 | 0.9252 | 1.207127e-02 | 0.4903 | 1.207127e-02 | - | 4.293529e-03 | 1.9816 |
| 4 | 0.06250000 | 1.787595e-01 | 0.3954 | 1.688411e-02 | 0.9848 | 8.546379e-03 | 0.4982 | 8.546379e-03 | 0.4982 | 6.540788e-04 | 2.7146 |
| 5 | 0.03125000 | 1.282057e-01 | 0.4796 | 9.494932e-03 | 0.8304 | 6.044999e-03 | 0.4996 | 6.044999e-03 | 0.4996 | 1.603015e-04 | 2.0287 |
| 6 | 0.01562500 | 9.128463e-02 | 0.4900 | 5.047778e-03 | 0.9115 | 4.274779e-03 | 0.4999 | 4.274779e-03 | 0.4999 | 4.231220e-05 | 1.9216 |
| 7 | 0.00781250 | 6.477874e-02 | 0.4949 | 2.524382e-03 | 0.9997 | 3.022783e-03 | 0.5000 | 3.022783e-03 | 0.5000 | 1.045799e-05 | 2.0165 |
| 8 | 0.00390625 | 4.588216e-02 | 0.4976 | 1.262252e-03 | 0.9999 | 2.137442e-03 | 0.5000 | 2.137442e-03 | 0.5000 | 2.627154e-06 | 1.9930 |
| 9 | 0.00195312 | 3.246964e-02 | 0.4988 | 6.360451e-04 | 0.9888 | 1.511402e-03 | 0.5000 | 1.511402e-03 | 0.5000 | 6.769820e-07 | 1.9563 |

Next, we utilise this optimal value of the correction parameter, i.e. $\gamma_\infty = 0.28028$ and compute the optimally corrected finite element solution and the error in different norms for different mesh levels. From Table 4.2, it is clear that using the optimal correction parameter, we can achieve $\mathcal{O}\left(h^2\right)$ convergence in the weighted $L^2$-norm. Optimal convergence rates are also observed in the outside region $\Omega \backslash \Omega_s$ for all of the three norms considered. Moreover, better convergence rates of the form $\mathcal{O}\left(h^{1+\frac{\pi}{\omega}}\right)$ are observed for the $L^2$-norm both globally as well as in the singular region. This behaviour is also depicted in the error plot (see Figure 4.10), where the error is much more concentrated in the immediate neighbourhood of the singular point with a much smaller spread than the one observed without correction (see Figure 4.9). Comparing the results in Table 4.2 with those in Table 4.1, we observe that the magnitude of the error is significantly smaller, especially for the finer meshes with the use of the optimal correction parameter. The improvement is much more prominent in the outside region, where the errors obtained with the modified Galerkin approach are three to four orders of magnitude smaller than the standard Galerkin approximation.

Table 4.4: Error norms using linear finite elements on non-uniform mesh, without and with optimal correction for the BVP (4.3) on non-uniform mesh.

(a) Results for $\gamma = 0.0$: no correction applied

| $l$ | $h$ | $\|u - R_h^m u\|_{0,1/2;\Omega}$ | eoc | $\|u - R_h^m u\|_{L^2(\Omega)}$ | eoc | $\|u - R_h^m u\|_{L^2(\Omega_s)}$ | eoc | $\|u - R_h^m u\|_{L^2(\Omega\backslash\Omega_s)}$ | eoc |
|---|---|---|---|---|---|---|---|---|---|
| 1 | 1.00000000 | 6.050239e-02 | - | 1.012908e-01 | 0.0000 | - | - | 1.308344e-02 | - |
| 2 | 0.50000000 | 3.032257e-02 | 0.9966 | 5.320187e-02 | 0.9290 | - | - | 1.555750e-02 | - |
| 3 | 0.25000000 | 1.552869e-02 | 0.9655 | 2.801471e-02 | 0.9253 | 1.449427e-02 | - | 8.689126e-03 | 0.8403 |
| 4 | 0.12500000 | 7.881576e-03 | 0.9784 | 1.453071e-02 | 0.9471 | 9.511364e-03 | 0.6078 | 4.672712e-03 | 0.8950 |
| 5 | 0.06250000 | 3.971576e-03 | 0.9888 | 7.436912e-03 | 0.9663 | 4.973885e-03 | 0.9353 | 2.761904e-03 | 0.7586 |
| 6 | 0.03125000 | 1.993535e-03 | 0.9944 | 3.771417e-03 | 0.9796 | 2.556215e-03 | 0.9604 | 1.500048e-03 | 0.8807 |
| 7 | 0.01562500 | 9.987021e-04 | 0.9972 | 1.901480e-03 | 0.9880 | 1.320803e-03 | 0.9526 | 7.572550e-04 | 0.9862 |
| 8 | 0.00781250 | 4.998342e-04 | 0.9986 | 9.553225e-04 | 0.9931 | 6.717239e-04 | 0.9755 | 3.805339e-04 | 0.9928 |
| 9 | 0.00390625 | 2.500379e-04 | 0.9993 | 4.789684e-04 | 0.9961 | 3.375912e-04 | 0.9926 | 1.922807e-04 | 0.9848 |

(b) Results for $\gamma = \gamma_\infty = 0.32938$: with optimal correction

| $l$ | $h$ | $\|u - R_h^m u\|_{0,1/2;\Omega}$ | eoc | $\|u - R_h^m u\|_{L^2(\Omega)}$ | eoc | $\|u - R_h^m u\|_{L^2(\Omega_s)}$ | eoc | $\|u - R_h^m u\|_{L^2(\Omega\backslash\Omega_s)}$ | eoc |
|---|---|---|---|---|---|---|---|---|---|
| 1 | 1.00000000 | 3.657416e-02 | - | 7.357878e-02 | - | - | - | 4.068099e-03 | - |
| 2 | 0.50000000 | 1.033156e-02 | 1.8238 | 2.663272e-02 | 1.4661 | - | - | 2.652486e-03 | 0.6170 |
| 3 | 0.25000000 | 2.894362e-03 | 1.8357 | 9.559516e-03 | 1.4782 | 8.846998e-03 | - | 8.271280e-04 | 1.6812 |
| 4 | 0.12500000 | 8.018981e-04 | 1.8518 | 3.409926e-03 | 1.4872 | 3.319176e-03 | 1.4144 | 2.323053e-04 | 1.8321 |
| 5 | 0.06250000 | 2.201462e-04 | 1.8650 | 1.211736e-03 | 1.4927 | 1.194146e-03 | 1.4748 | 7.002984e-05 | 1.7300 |
| 6 | 0.03125000 | 6.010183e-05 | 1.8730 | 4.296813e-04 | 1.4957 | 4.262590e-04 | 1.4862 | 1.975352e-05 | 1.8259 |
| 7 | 0.01562500 | 1.637565e-05 | 1.8759 | 1.521851e-04 | 1.4974 | 1.515369e-04 | 1.4921 | 5.269622e-06 | 1.9063 |
| 8 | 0.00781250 | 4.469894e-06 | 1.8732 | 5.386561e-05 | 1.4984 | 5.373501e-05 | 1.4957 | 1.437343e-06 | 1.8743 |
| 9 | 0.00390625 | 1.228042e-06 | 1.8639 | 1.905857e-05 | 1.4989 | 1.903024e-05 | 1.4976 | 4.099088e-07 | 1.8100 |

## Non-Uniform Mesh

Here, we solve the problem by considering as $\mathcal{T}_h$, a non-uniform mesh shown in Figure 4.4b. The target here is to study how the technique would perform if the mesh does not fulfill the *symmetry condition*. Following the procedure explained above, we determine the level independent optimal correction parameter, which in this case comes out to be $\gamma_\infty = 0.32938$. Studying the variation of the error with mesh refinement for the optimal correction case (see Table 4.4b), we observe that the eoc for the weighted $L^2$-norm and consequently for the $L^2$-norm in the outside region is not truly optimal, but is close to $\mathcal{O}\left(h^2\right)$, which is the optimal convergence rate. Nonetheless,

much improved convergence and consequently much smaller error norms (cf. Table 4.4a) have been achieved both globally as well as in the singular region.

## 4.4 Extension to Higher Order Finite Elements

The theory and ideas presented in the previous chapter, including the theorems on *necessity* and *sufficiency* are based on the use of linear finite elements for discretising the BVP. A detailed extension of the linear ECFEM theory to higher order finite elements has been presented in [11], where the use of multiple correction factors based on the order $p$ of the finite elements and the interior angle $\omega$ has been proposed. Multiple regions $\mathcal{S}_h^i$ of elements in the neighbourhood of the singular point are considered, leading to major changes in the energy corrected weak form. This results in a much more complicated procedure for determining the optimal correction parameters.

In this work, we try an approach entailing some simple modifications to the linear ECFEM theory, in order to allow the use of higher order finite elements. The modified Galerkin approximation of (3.3) and the energy defect functional of (3.13) have been left untouched. The motivation here is to achieve optimal convergence rates in the weighted $L^2$-norm as given by the estimate

$$\|u - R_h^m u\|_{0,\alpha} = \mathcal{O}\left(h^{p+1}\right), \tag{4.6}$$

which leads us to the first important question: what should be the appropriate value of the exponent $\alpha$ used in the calculation of the weighted norm. Scrutinising the above expression in light of (2.10), we find that

$$\|u - R_h^m u\|_{0,\alpha} = \|r^\alpha \underbrace{(u - R_h^m u)}_{\approx \nabla^p u \approx r^{\frac{\pi}{\omega}-p}} \|_0,$$

which leads us to

$$\alpha = p - \frac{\pi}{\omega}.$$

The next parameter to decide upon is the exponent $\beta$ as required in (4.5). Our numerical experiments show that

$$\beta = \begin{cases} 2 - \frac{2\pi}{\omega} & \text{for } p = 1 \\ 2 - \frac{2\pi}{\omega} + p & \text{for } p \geq 2 \end{cases} \tag{4.7}$$

works well for the different mesh sizes considered, even with third order finite elements.

We solve the BVP (4.3), using finite elements of various order on meshes satisfying the symmetry condition (see Figure 4.11). By

$$\mathcal{V}_p^h \coloneqq \left\{ v \in H_0^1(\Omega) : v|_K = \mathcal{P}_p(K) \ \forall\ K \in \mathcal{T}_h \right\}, \tag{4.8}$$

we denote the standard finite element space of continuous piecewise polynomial functions of highest order $p$. Thus, we seek the modified Galerkin approximation $R_h^m u \in \mathcal{V}_p^h$ to the given BVP. The optimal correction parameter $\gamma_\infty$ is computed following the same procedure as for the linear finite element case, with the modified value of $\beta$ for the Richardson extrapolation procedure as mentioned in (4.7).

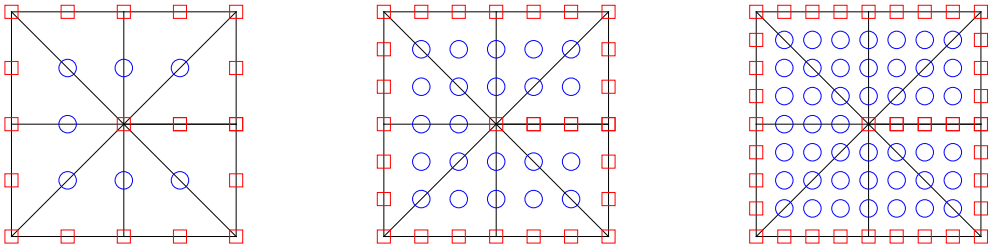

(a) Quadratic finite elements. ($p = 2$).

(b) Cubic finite elements. ($p = 3$)

(c) Quartic finite elements. ($p = 4$)

Figure 4.11: Symmetric coarse finite element meshes $\mathcal{T}_H$ of different orders used for solving the BVP (4.3). The interior nodes (or the free DOFs) have been denoted by a blue circle, while those on the boundary (the constrained DOFs) have been marked by a red square.

We first analyse the errors norms computed using quadratic finite elements. It is clear that the pollution effect indeed happens for the $H^1$-norm as well, since suboptimal convergence rates of $\mathcal{O}(h)$ are observed for the outside region when no correction is applied (cf. Table 4.6). This is in accordance with the assertion (4.4)). An optimal correction leads to full convergence rates of $\mathcal{O}\left(h^3\right)$ and $\mathcal{O}\left(h^2\right)$ in the weighted $L^2$-norm and the $H^1$-norm in the outside region $\omega \backslash \Omega_s$ respectively, along with close to optimal convergence rates for the $L^2$-norm as well as the $L^\infty$-norm in the outside region (cf. Table 4.7). Moreover, improved convergence rates of $\mathcal{O}\left(h^{1+\frac{\pi}{\omega}}\right)$ are observed for the $L^2$-norm globally as well as in the singular region. Thus, the proposed technique works reasonably well and in accordance with the estimate (4.6) for quadratic finite elements.

Table 4.5: Errors in weighted $L^2$-norm, with optimal correction for different higher order finite elements considered while solving the BVP (4.3) on symmetric mesh.

| $l$ | $\frac{h}{\sqrt{2}}$ | $p=2, \gamma=\gamma_\infty=0.08968$ | | $p=3, \gamma=\gamma_\infty=0.04660426$ | | $p=4, \gamma=\gamma_\infty=0.02843704$ | |
|---|---|---|---|---|---|---|---|
| | | $\|u-R_h^m u\|_{0,3/2;\Omega}$ | eoc | $\|u-R_h^m u\|_{0,5/2;\Omega}$ | eoc | $\|u-R_h^m u\|_{0,7/2;\Omega}$ | eoc |
| 1 | 1.00000000 | 2.150966e-02 | - | 8.536049e-03 | - | 5.280192e-03 | - |
| 2 | 0.50000000 | 2.840655e-03 | 2.9207 | 6.002460e-04 | 3.8299 | 1.942489e-04 | 4.7646 |
| 3 | 0.25000000 | 3.742238e-04 | 2.9243 | 3.983015e-05 | 3.9136 | 6.717233e-06 | 4.8539 |
| 4 | 0.12500000 | 4.864689e-05 | 2.9435 | 2.537008e-06 | 3.9727 | 2.286390e-07 | 4.8767 |
| 5 | 0.06250000 | 6.297173e-06 | 2.9496 | 1.604858e-07 | 3.9826 | 7.701237e-09 | 4.8918 |
| 6 | 0.03125000 | 8.130774e-07 | 2.9532 | 1.051087e-08 | 3.9325 | 6.575585e-10 | 3.5499 |
| 7 | 0.01562500 | 1.048849e-07 | 2.9546 | 1.533636e-09 | 2.7769 | 3.115180e-10 | 1.0778 |
| 8 | 0.00781250 | 1.373582e-08 | 2.9328 | 6.966942e-10 | 1.1384 | 1.529362e-10 | 1.0264 |

The eoc for the weighted $L^2$-norm, computed with cubic and quartic finite elements, however deviates from the optimal value of $\mathcal{O}\left(h^{p+1}\right)$, especially for the smaller mesh sizes (cf. Table 4.5). Considering the fact that the magnitude of the error norm is in the order of $10^{-10}$, this sub-optimal behaviour could be probably attributed to the errors creeping in due to lack of required numerical precision. Another possible reason could be that a stricter stopping criterion on the energy defect functional is required while computing the optimal correction parameter $\gamma_h$ using bisection method, so as to ensure more accurate value of the correction parameter.

Table 4.6: Error using quadratic finite elements($p = 2$) on symmetric mesh, for the BVP (4.3) with no correction applied, i.e. $\gamma = 0.0$.

| $l$ | $h/\sqrt{2}$ | $\|u - R_h^m u\|_{0,3/2;\Omega}$ | eoc | $\|u - R_h^m u\|_{L^2(\Omega)}$ | eoc | $\|u - R_h^m u\|_{L^2(\Omega_s)}$ | eoc | $\|u - R_h^m u\|_{L^2(\Omega\setminus\Omega_s)}$ | eoc | $\|u - R_h^m u\|_{H^1(\Omega)}$ | eoc |
|---|---|---|---|---|---|---|---|---|---|---|---|
| 1 | 1.00000000 | 2.150966e-02 | - | 8.245580e-02 | - | - | - | - | - | 3.543100e-01 | - |
| 2 | 0.50000000 | 7.034931e-03 | 1.6124 | 3.433292e-02 | 1.2640 | - | - | 3.203988e-03 | - | 2.425137e-01 | 0.5469 |
| 3 | 0.25000000 | 3.586665e-03 | 0.9719 | 1.555240e-02 | 1.1425 | - | - | 4.723479e-03 | - | 1.688136e-01 | 0.5226 |
| 4 | 0.12500000 | 1.792654e-03 | 1.0005 | 7.393018e-03 | 1.0729 | 4.669491e-03 | - | 2.306939e-03 | 1.0339 | 1.184726e-01 | 0.5109 |
| 5 | 0.06250000 | 8.942226e-04 | 1.0034 | 3.603496e-03 | 1.0368 | 2.547257e-03 | 0.8743 | 1.148665e-03 | 1.0060 | 8.346607e-02 | 0.5053 |
| 6 | 0.03125000 | 4.464645e-04 | 1.0021 | 1.778859e-03 | 1.0184 | 1.243047e-03 | 1.0351 | 6.552074e-04 | 0.8099 | 5.891296e-02 | 0.5026 |
| 7 | 0.01562500 | 2.230636e-04 | 1.0011 | 8.837537e-04 | 1.0092 | 6.138807e-04 | 1.0179 | 3.495584e-04 | 0.9064 | 4.162047e-02 | 0.5013 |
| 8 | 0.00781250 | 1.114893e-04 | 1.0006 | 4.404638e-04 | 1.0046 | 3.099047e-04 | 0.9861 | 1.747121e-04 | 1.0006 | 2.941700e-02 | 0.5006 |

| $l$ | $h/\sqrt{2}$ | $\|u - R_h^m u\|_{H^1(\Omega_s)}$ | eoc | $\|u - R_h^m u\|_{H^1(\Omega\setminus\Omega_s)}$ | eoc | $\|u - R_h^m u\|_{L^\infty(\Omega)}$ | eoc | $\|u - R_h^m u\|_{L^\infty(\Omega_s)}$ | eoc | $\|u - R_h^m u\|_{L^\infty(\Omega\setminus\Omega_s)}$ | eoc |
|---|---|---|---|---|---|---|---|---|---|---|---|
| 1 | 1.00000000 | - | - | - | - | 8.282490e-02 | - | - | - | 8.282490e-02 | - |
| 2 | 0.50000000 | - | - | 1.865286e-02 | - | 6.774688e-02 | 0.2899 | - | - | 6.774688e-02 | 0.2899 |
| 3 | 0.25000000 | - | - | 1.959045e-02 | - | 5.165685e-02 | 0.3912 | 5.165685e-02 | - | 1.789447e-02 | 1.9206 |
| 4 | 0.12500000 | 1.156347e-01 | - | 8.664166e-03 | 1.1770 | 3.784065e-02 | 0.4490 | 3.784065e-02 | 0.4490 | 9.797349e-03 | 0.8691 |
| 5 | 0.06250000 | 8.292818e-02 | 0.4796 | 4.236149e-03 | 1.0323 | 2.721796e-02 | 0.4754 | 2.721796e-02 | 0.4754 | 5.626121e-03 | 0.8003 |
| 6 | 0.03125000 | 5.872864e-02 | 0.4978 | 2.362729e-03 | 0.8423 | 1.940811e-02 | 0.4879 | 1.940811e-02 | 0.4879 | 2.976508e-03 | 0.9185 |
| 7 | 0.01562500 | 4.155589e-02 | 0.4990 | 1.250723e-03 | 0.9177 | 1.378079e-02 | 0.4940 | 1.378079e-02 | 0.4940 | 1.487516e-03 | 1.0007 |
| 8 | 0.00781250 | 2.939519e-02 | 0.4995 | 6.249139e-04 | 1.0010 | 9.764681e-03 | 0.4970 | 9.764681e-03 | 0.4970 | 7.435529e-04 | 1.0004 |

Table 4.7: Error using quadratic finite elements on symmetric mesh, for the BVP (4.3) with the optimal correction applied, i.e. $\gamma = \gamma_\infty = 0.08968$.

| $l$ | $h/\sqrt{2}$ | $\|u - R_h^m u\|_{0,3/2;\Omega}$ | eoc | $\|u - R_h^m u\|_{L^2(\Omega)}$ | eoc | $\|u - R_h^m u\|_{L^2(\Omega_s)}$ | eoc | $\|u - R_h^m u\|_{L^2(\Omega\setminus\Omega_s)}$ | eoc | $\|u - R_h^m u\|_{H^1(\Omega)}$ | eoc |
|---|---|---|---|---|---|---|---|---|---|---|---|
| 1 | 1.00000000 | 2.150966e-02 | - | 8.245580e-02 | - | - | - | - | - | 3.543100e-01 | - |
| 2 | 0.50000000 | 2.840655e-03 | 2.9207 | 2.904201e-02 | 1.5055 | - | - | 4.644151e-04 | - | 2.465241e-01 | 0.5233 |
| 3 | 0.25000000 | 3.742238e-04 | 2.9243 | 1.026680e-02 | 1.5002 | - | - | 2.092859e-04 | 1.1499 | 1.735348e-01 | 0.5065 |
| 4 | 0.12500000 | 4.864689e-05 | 2.9435 | 3.629861e-03 | 1.5000 | 3.622613e-03 | - | 2.320007e-05 | 3.1733 | 1.225578e-01 | 0.5018 |
| 5 | 0.06250000 | 6.297173e-06 | 2.9496 | 1.283351e-03 | 1.5000 | 1.283291e-03 | 1.4972 | 2.756230e-06 | 3.0734 | 8.663393e-02 | 0.5005 |
| 6 | 0.03125000 | 8.130774e-07 | 2.9532 | 4.537332e-04 | 1.5000 | 4.537307e-04 | 1.4999 | 4.222358e-07 | 2.7066 | 6.125448e-02 | 0.5001 |
| 7 | 0.01562500 | 1.048849e-07 | 2.9546 | 1.604189e-04 | 1.5000 | 1.604188e-04 | 1.5000 | 5.967678e-08 | 2.8228 | 4.331257e-02 | 0.5000 |
| 8 | 0.00781250 | 1.373582e-08 | 2.9328 | 5.671666e-05 | 1.5000 | 5.671666e-05 | 1.5000 | 8.496535e-09 | 2.8122 | 3.062646e-02 | 0.5000 |

| $l$ | $h/\sqrt{2}$ | $\|u - R_h^m u\|_{H^1(\Omega_s)}$ | eoc | $\|u - R_h^m u\|_{H^1(\Omega\setminus\Omega_s)}$ | eoc | $\|u - R_h^m u\|_{L^\infty(\Omega)}$ | eoc | $\|u - R_h^m u\|_{L^\infty(\Omega_s)}$ | eoc | $\|u - R_h^m u\|_{L^\infty(\Omega\setminus\Omega_s)}$ | eoc |
|---|---|---|---|---|---|---|---|---|---|---|---|
| 1 | 1.00000000 | - | - | - | - | 8.282490e-02 | - | - | - | 8.282490e-02 | - |
| 2 | 0.50000000 | - | - | 7.793989e-03 | - | 5.733030e-02 | 0.5308 | - | - | 5.733030e-02 | 0.5308 |
| 3 | 0.25000000 | - | - | 6.803883e-03 | - | 4.051307e-02 | 0.5009 | 4.051307e-02 | - | 3.309183e-03 | 4.1148 |
| 4 | 0.12500000 | 1.218870e-01 | - | 1.698892e-03 | 2.0018 | 2.864592e-02 | 0.5001 | 2.864592e-02 | 0.5001 | 3.204482e-04 | 3.3683 |
| 5 | 0.06250000 | 8.661372e-02 | 0.4929 | 4.246461e-04 | 2.0003 | 2.025568e-02 | 0.5000 | 2.025568e-02 | 0.5000 | 2.004845e-05 | 3.9985 |
| 6 | 0.03125000 | 6.125269e-02 | 0.4998 | 1.314831e-04 | 1.6914 | 1.432293e-02 | 0.5000 | 1.432293e-02 | 0.5000 | 1.983663e-06 | 3.3373 |
| 7 | 0.01562500 | 4.331242e-02 | 0.5000 | 3.694690e-05 | 1.8314 | 1.012784e-02 | 0.5000 | 1.012784e-02 | 0.5000 | 1.353938e-07 | 3.8729 |
| 8 | 0.00781250 | 3.062645e-02 | 0.5000 | 9.237481e-06 | 1.9999 | 7.161468e-03 | 0.5000 | 7.161468e-03 | 0.5000 | 1.949274e-08 | 2.7962 |

# Chapter 5

# ECFEM for Planar Linear Elasticity

In this chapter, we explore the possibility of applying the energy correction technique to planar linear elasticity problems. Domains with re-entrant corner(s), especially those consisting of *notches* or *cracks*, appear quite frequently in various *structural mechanics* applications and are therefore of great practical interest. In this thesis, we will focus on a domain with a crack, which essentially corresponds to a re-entrant corner having $\omega = 2\pi$ as the interior angle.

## 5.1 Governing Equations of Planar Linear Elasticity

Here, we summarize the governing equations for *plane strain* linear elasticity. Details of the tensor notation employed here can be found in Appendix C. The presentation is primarily based on [22].

Since, we consider planar problems, the *displacement* vector $\mathbf{u}$ is a function of the two coordinates $x_1$ and $x_2$, i.e.

$$\mathbf{u} = \mathbf{u}(x_1, x_2) \qquad \text{with} \quad [u_i] = \begin{bmatrix} u_1(x_1, x_2) \\ u_2(x_1, x_2) \end{bmatrix}$$

where, $u_1$ and $u_2$ represent the two components of the displacement vector.

The governing equations for the elasticity problem comprise of three major components: *Kinematics*, *Constitutive Relation* and *Balance Equations*.

#### Kinematics

The *kinematic equations* describe the geometry of deformation by means of the *strain tensor* $\boldsymbol{\epsilon} : \Omega \to \mathbb{R}^{2\times 2}$ and are therefore, also referred to as the *strain-displacement relations*. In case of linear elasticity, the strain tensor is defined as *symmetric gradient* of the displacement vector $u$, i.e.

$$\boldsymbol{\epsilon}_u \coloneqq \boldsymbol{\epsilon}(\mathbf{u}) = \frac{1}{2}\left[\nabla \mathbf{u} + (\nabla \mathbf{u})^t\right] \qquad \text{with} \quad [\epsilon_{ij}] = \frac{1}{2}\left[u_{i,j} + u_{j,i}\right],$$

which, in case of *plane strain* loading conditions means

$$[\epsilon_{ij}] = \begin{bmatrix} \frac{\partial u_1}{\partial x_1} & \frac{1}{2}\left(\frac{\partial u_1}{\partial x_2} + \frac{\partial u_2}{\partial x_1}\right) \\ \frac{1}{2}\left(\frac{\partial u_1}{\partial x_2} + \frac{\partial u_2}{\partial x_1}\right) & \frac{\partial u_2}{\partial x_2} \end{bmatrix},$$

showing that the strain tensor is *symmetric* by definition, i.e. $\boldsymbol{\epsilon} = \boldsymbol{\epsilon}^t$.

### Balance Equations

The balance of the *external*, *internal* and *inertial* loads is essential for the continuum body to be in *equilibrium*. Since, in this work, we only consider *statics*, the inertial forces are assumed to be zero. There are two types of balance equations: the *balance of linear momentum* and the *balance of angular momentum*. The balance of linear momentum states that the sum of all the *forces* acting on the body should vanish, i.e.

$$\operatorname{div} \boldsymbol{\sigma}^t + \mathbf{b} = \mathbf{0}$$

where, $\boldsymbol{\sigma} : \Omega \to \mathbb{R}^{2\times 2}$ is the stress tensor representing the internal resistance of the material to the external loadings and $\mathbf{b}$ denotes the body force vector acting on the elastic body. The other balance equation considers the balance of the various *moments* acting on the body and in case of linear elastostatics leads to

$$\boldsymbol{\sigma} = \boldsymbol{\sigma}^t,$$

which means that the stress tensor is symmetric.

### Constitutive Relation

The constitutive relation essentially serves to link the kinematics and the balance equations. Also, referred to as the *stress-strain relation*, it defines the deformation behavior of material as it is deformed under the prescribed stresses. Unlike, the above two components, the constitutive relation is unique to a material and is defined by certain material parameters. In this work, we consider *linear isotropic elasticity* and the corresponding constitutive relation or *Hook's law* reads

$$\boldsymbol{\sigma}_u \coloneqq \boldsymbol{\sigma}(\mathbf{u}) = 2\mu\, \boldsymbol{\epsilon}_u + \lambda \operatorname{tr} \boldsymbol{\epsilon}_u\, \boldsymbol{I}$$

where, $\lambda$ and $\mu$ denote Lamé's constant and the modulus of rigidity respectively. These are sometimes collectively referred to as *Lamé parameters*. In engineering literature, another set of parameters: the Young's modulus $E$ and the Poisson's ratio $\nu$ are more commonly used to describe the material behaviour and related to the Lamé parameters as

$$\mu = \frac{E}{2(1+\nu)} \qquad \text{and} \qquad \lambda = \frac{E\,\nu}{(1+\nu)(1-2\nu)}.$$

Here, it is important to note that a special case arises when $\nu = 0.5$, resulting in $\lambda \to \infty$. This case corresponds to the incompressibility limit and is not considered in this work.

Combining together the above components along with the *boundary conditions*, we put together the BVP for *plane strain linear elasticity* on an open and bounded domain $\Omega \subset \mathbb{R}^2$ and it reads: Given $\mathbf{f} : \Omega \to \mathbb{R}^2$, find $\mathbf{u} : \Omega \to \mathbb{R}^2$ s.t.

$$\begin{aligned} \operatorname{div} \boldsymbol{\sigma}^t + \mathbf{b} = \mathbf{0}, \quad \boldsymbol{\sigma} = 2\mu\, \boldsymbol{\epsilon} + \lambda \operatorname{tr} \epsilon\, \boldsymbol{I} \quad \text{and } \boldsymbol{\epsilon} = \frac{1}{2}\left[\nabla \mathbf{u} + (\nabla \mathbf{u})^t\right] \qquad & \text{in } \Omega, \\ \mathbf{u} = \mathbf{g} \qquad \text{on } \partial\Omega_D, & \\ \boldsymbol{\sigma} \cdot \mathbf{n} = \mathbf{h} \qquad \text{on } \partial\Omega_N, & \end{aligned} \tag{5.1}$$

where, $\partial\Omega_D$ and $\partial\Omega_N$ denote the *Dirichlet* and the *Neumann* parts of the domain boundary respectively, while, $\mathbf{n} = \mathbf{n}(x_1, x_2)$ is the outward normal vector to the boundary. Formulating everything in terms of the displacement and using the fact that

$$\operatorname{div} \boldsymbol{\epsilon} = \frac{1}{2}\left[\operatorname{div} \operatorname{grad} \mathbf{u} + \operatorname{grad} \operatorname{div} \mathbf{u}\right],$$

the governing equations transform to

$$\mu \operatorname{div} \operatorname{grad} \mathbf{u} + (\lambda + \mu) \operatorname{grad} \operatorname{div} \mathbf{u} + \mathbf{b} = 0,$$

which are also referred to as *Navier-Lamé* equations.

Alike the scalar case, the first step towards the finite element solution of the BVP (5.1) is the *weak form*. In this work, we only consider the *pure displacement formulation*. Owing to fact that the primary variable $\mathbf{u} \in \mathbb{R}^2$, we define appropriate function spaces

$$\boldsymbol{\mathcal{U}} = \left\{ \mathbf{u} \in \left[H^1(\Omega)\right]^2 \ : \ \mathbf{u}|_{\partial\Omega_D} = \mathbf{g} \right\}$$

$$\boldsymbol{\mathcal{V}} = \left\{ \mathbf{v} \in \left[H^1(\Omega)\right]^2 \ : \ \mathbf{v}|_{\partial\Omega_D} = \mathbf{0} \right\}$$

for the *trial* and the *test* functions respectively. Utilising the symmetry of $\boldsymbol{\sigma}$ and $\boldsymbol{\epsilon}$, we arrive at the weak form: Given $\mathbf{f} \in \left[L^2(\Omega)\right]^2$, find $\mathbf{u} \in \boldsymbol{\mathcal{U}}$, s.t.

$$a(\mathbf{u}, \mathbf{v}) = b(\mathbf{v}) \qquad \forall\ \mathbf{v} \in \boldsymbol{\mathcal{V}}, \tag{5.2}$$

with the *bilinear form*

$$a(\mathbf{u}, \mathbf{v}) \coloneqq \int_\Omega \boldsymbol{\sigma}_u : \boldsymbol{\epsilon}_v \, d\Omega = \int_\Omega 2\mu\, \boldsymbol{\epsilon}_u : \boldsymbol{\epsilon}_v \, d\Omega + \int_\Omega \lambda \operatorname{div} \mathbf{u} \operatorname{div} \mathbf{v} \, d\Omega$$

and the *linear form*

$$b(\mathbf{v}) \coloneqq \int_\Omega \mathbf{f} \cdot \mathbf{v} \, d\Omega + \int_{\partial\Omega_N} \mathbf{h} \cdot \mathbf{v} \, dA.$$

The weak form represents the *principle of virtual work* in case of elasticity problems.

It is stated without proof that unique solution to the weak form (5.2) indeed exists. A detailed explanation on the weak form and its well-posedness can be found in [7, Section 3.4].

## 5.2 Linear Elastic Fracture Mechanics (LEFM)

In this work, we consider the problem of a square plate with a crack subjected to *plane strain* loading conditions as the model problem. The plate with a crack corresponds to a polygonal domain with a re-entrant corner, having an interior angle of $2\pi$. The re-entrant corner in this case is also referred to as the *crack tip* and the pair of boundary edges forming this interior angle define the *crack plane*.

The field of *Fracture Mechanics* encompasses the study of what happens when a body containing a crack or a notch is subjected to different loading conditions. Whether and how a crack will grow under specified loads is of utmost interest in numerous engineering applications. In most of the practical cases, *plastic deformation* occurs in the vicinity of the crack tip, while the overall behavior is still elastic. In many cases, this local plastic behaviour can be neglected as it is prevalent in a much smaller region as compared to the component dimensions. LEFM is a sub-field, where in it is assumed that the material is *linear elastic*, i.e. it follows Hook's law globally. A concise introduction to this topic and description of finite element based techniques for solving fracture mechanics problems can be found in [16].

Restricting ourselves to planar problems, there are two possible ways in which an elastic body with a crack can deform :

- Mode-I: This is the crack *opening mode* and is caused by tensile loading. Here, the crack opens perpendicular to the crack plane (cf. Figure 5.1a).
- Mode-II: This is the mode of in-plane shear and in this case, the two crack faces are displaced in their plane (cf. Figure 5.1b).

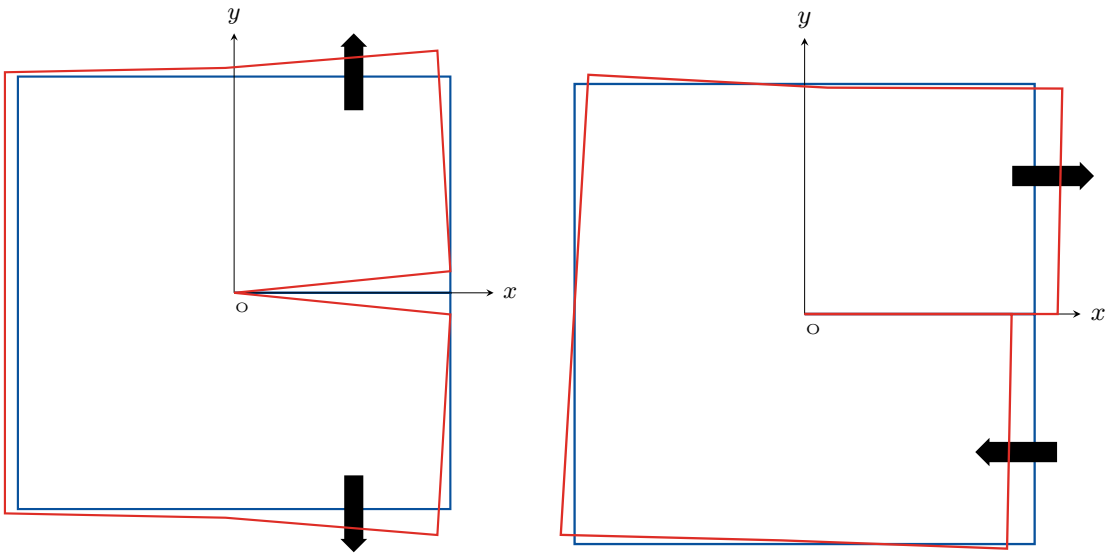


(a) Mode-I Fracture

(b) Mode-II Fracture.

Figure 5.1: The two types of fracture modes possible in case of planar deformations. The original shape is shown in blue, while the deformed shaped is depicted in red. The dark arrows show the loading direction.

Since, the crack is essentially a re-entrant corner, the solution $\mathbf{u}$ to the BVP (5.1) exhibits singular behaviour with leading term of the form $r^{1/2}$, but the nature of singularity is quite different from that observed for the scalar case. This will be discussed in more detail when we work with the numerical examples. The solution to a general planar LEFM problem in the vicinity of the crack tip can be expressed as a combination of $\mathbf{s}_I$ and $\mathbf{s}_{II}$, which represent the solutions to the Mode-I and Mode-II problems respectively. For the plane strain formulation, we have

$$\mathbf{s}_I = \frac{1}{4\mu}\sqrt{\frac{r}{2\pi}}\begin{bmatrix} -\left(2\kappa-1\right)\sin\frac{\theta}{2} - \sin\frac{3\theta}{2} \\ \left(2\kappa+1\right)\cos\frac{\theta}{2} + \cos\frac{3\theta}{2} \end{bmatrix} \quad \text{and} \quad \mathbf{s}_{II} = \frac{1}{4\mu}\sqrt{\frac{r}{2\pi}}\begin{bmatrix} \left(2\kappa+3\right)\cos\frac{\theta}{2} - \cos\frac{3\theta}{2} \\ \left(2\kappa-3\right)\sin\frac{\theta}{2} - \sin\frac{3\theta}{2} \end{bmatrix},$$

with, $\kappa = 3-4\nu$. A detailed analysis of the elasticity problem on domains with re-entrant corners along with the derivation of these singular solutions can be found in [26].

## 5.3 Applying ECFEM to LEFM Problems

In this work, we propose an extension of the energy correction idea explained in Chapter 3, to the planar linear elasticity problem. This formulation is based on the ideas used for the scalar case coupled with systematic numerical experimentation for the vector case. We begin by developing the *energy corrected weak formulation* for the BVP (5.1) and then present some numerical examples to describe the application of ECFEM to this type of elliptic PDE.

### 5.3.1 Energy Corrected Weak Form

The linear elasticity problem comprises of system of coupled PDEs and thus the nature of singularities is much different from those occurring for scalar elliptic problems, such as those considered in the previous chapter (cf. Figures 4.9 and 5.8 for instance). Moreover, the proposed correction needs to tackle the singularities arising for each of the components of the vector variable $\mathbf{u}$. This assertion along with experience from numerical tests leads us to the fact that a single correction parameter would no longer be sufficient to overcome the pollution effect. We consider an energy corrected formulation based on two correction parameters in this work. The finite dimensional functional space

$$\boldsymbol{\mathcal{V}}_p^h \coloneqq \left\{ \mathbf{v} \in \left[H^1\left(\Omega\right)\right]^2 : v_i|_K = \mathcal{P}_p\left(K\right) \ \forall\ K \in \mathcal{T}_h \text{ for } i = 1,2 \right\}$$

is simply an extension of the functional space (4.8) to vector valued functions. The *modified Galerkin approximation* for the BVP (5.1) then reads: Find $R_h^m\mathbf{u} \in \boldsymbol{\mathcal{V}}_1^h$, s.t.

$$a_h\left(R_h^m\mathbf{u}, \mathbf{v^h}\right) = b\left(v^h\right) \qquad \forall\ \mathbf{v}^h \in \boldsymbol{\mathcal{V}}_1^h, \tag{5.3}$$

where, $R^m\left(\gamma_1,\gamma_2\right) =: R_h^m : \left[H^1\left(\Omega\right)\right]^2 \mapsto \boldsymbol{\mathcal{V}}_1^h$ denotes the Ritz projection of the modified Galerkin approximation to the true solution $\mathbf{u}$. The terms $a\left(\mathbf{u},\mathbf{v}\right)$ and $b\left(\mathbf{v}\right)$ remain unaltered from (5.2). The mesh dependent bilinear form $a_h\left(\mathbf{u},\mathbf{v}\right)$ is given as

$$a_h\left(\mathbf{u},\mathbf{v}\right) = a\left(\mathbf{u},\mathbf{v}\right) - c_h\left(\mathbf{u},\mathbf{v}\right),$$

with the correction term

$$\begin{aligned} c_h\left(\mathbf{u},\mathbf{v}\right) &= \gamma_1\, d_h^1 + \gamma_2\, d_h^2 \\ &= \gamma_1 \int\limits_{\mathcal{S}_h^1} \boldsymbol{\sigma}_u : \boldsymbol{\epsilon}_v \ d\Omega \ + \ \gamma_2 \int\limits_{\mathcal{S}_h^2} \boldsymbol{\sigma}_u : \boldsymbol{\epsilon}_v \ d\Omega, \end{aligned} \tag{5.4}$$

with $\gamma_1$ and $\gamma_2$ being the two correction parameters corresponding to the regions $\mathcal{S}_h^1$ and $\mathcal{S}_h^2$, which represent the first and second layer of elements connected to singular point (see Figure 5.2). These regions are defined as

$$\bar{\mathcal{S}}_h^i := \cup \bar{K} \quad \forall K \in \mathcal{T}_h, \text{ s.t. } (i-1)\,h < \ dist\,(0,K) \leq i\,h.$$

The symmetry requirement on the mesh, described in Section 3.3 needs to be fulfilled. Further, it is assumed that the conditions of *continuity* and *coercivity* are satisfied, thereby ensuring that a unique solution to (5.3) indeed exists.

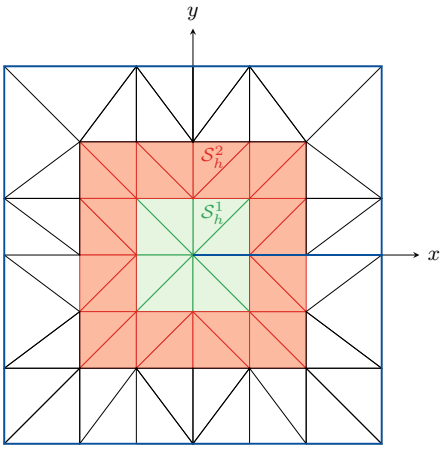


Figure 5.2: Locally symmetric mesh on a domain with a crack, depicting the regions $\mathcal{S}_h^1$ and $\mathcal{S}_h^2$ in the neighbourhood of the crack tip.

Taking a closer look at the energy corrected bilinear form, we find that

$$\begin{aligned} a_h\left(R_h^m\mathbf{u},\mathbf{v}^h\right) &= a\left(R_h^m\mathbf{u},\mathbf{v}^h\right) - \gamma_1\, d_h^1\left(R_h^m\mathbf{u},\mathbf{v}^h\right) - \gamma_2\, d_h^2\left(R_h^m\mathbf{u},\mathbf{v}^h\right) \\ &= \int_\Omega \boldsymbol{\sigma}_{R_h^m u} : \boldsymbol{\epsilon}_{v^h}\ d\Omega \ - \ \gamma_1 \int_{\mathcal{S}_h^1} \boldsymbol{\sigma}_{R_h^m u} : \boldsymbol{\epsilon}_{v^h}\ d\Omega \ - \ \gamma_2 \int_{\mathcal{S}_h^2} \boldsymbol{\sigma}_{R_h^m u} : \boldsymbol{\epsilon}_{v^h}\ d\Omega \end{aligned}$$

$$\text{i.e.} \quad a_h\left(R_h^m\mathbf{u},\mathbf{v}^h\right) = \int_{\Omega\setminus\left(\mathcal{S}_h^1\cup\mathcal{S}_h^2\right)} \boldsymbol{\sigma}_{R_h^m u} : \boldsymbol{\epsilon}_{v^h}\ d\Omega \ + \ (1-\gamma_1)\int_{\mathcal{S}_h^1} \boldsymbol{\sigma}_{R_h^m u} : \boldsymbol{\epsilon}_{v^h}\ d\Omega \ + \ (1-\gamma_2)\int_{\mathcal{S}_h^2} \boldsymbol{\sigma}_{R_h^m u} : \boldsymbol{\epsilon}_{v^h}\ d\Omega,$$

which means that this local modification is equivalent to relaxing or stiffening the material in the vicinity of the crack tip, depending on whether $\gamma_i$ is positive or negative. The procedure for determining the optimal correction parameters will be discussed when we do the numerical tests.

### 5.3.2 Numerical Example:Mode-I Problem

We consider the Mode-I problem formulated in terms of a pure Dirichlet problem as the first numerical example. We choose

$$\mathbf{u} = \tilde{\mathbf{s}}_I = \frac{K_I}{4\mu}\sqrt{\frac{r}{2\pi}} \begin{bmatrix} -(2\kappa-1)\sin\frac{\theta}{2} - \sin\frac{3\theta}{2} \\ (2\kappa+1)\cos\frac{\theta}{2} + \cos\frac{3\theta}{2} \end{bmatrix}$$

as the exact solution for this model problem. Here, $K_I$ represents the *stress intensity factor* for the Mode-I problem. The domain $\Omega = (-1,1)^2 \setminus [0,1] \times \{0\}$, is the same as the one considered in Section 4.3. The corresponding BVP then reads: Find $\mathbf{u}$, s.t.

$$\begin{aligned} \operatorname{div} \boldsymbol{\sigma}^t + \mathbf{b} = \mathbf{0}, \quad \boldsymbol{\sigma} = 2\mu\,\boldsymbol{\epsilon} + \lambda \operatorname{tr} \epsilon\, \boldsymbol{I} \quad \text{and } \boldsymbol{\epsilon} = \frac{1}{2}\left[\nabla \mathbf{u} + (\nabla \mathbf{u})^t\right] \qquad \text{in } \Omega, \\ \mathbf{u} = \tilde{\mathbf{s}}_I \qquad \text{on } \partial\Omega. \end{aligned} \tag{5.5}$$

with the material parameters

$$E = 2.1 \times 10^5 \quad \text{and} \quad \nu = 0.2$$

leading to

$$\lambda = 5.83 \times 10^4, \quad \mu = 87500, \quad \kappa = 2.20$$

and the stress intensity factor $K_I = 10^4$. We solve this BVP on the family of meshes $\{\mathcal{T}_h\}_{h \leq H}$ obtained from uniform refinement of the coarse mesh $\mathcal{T}_H$ shown in Figure 4.4a, so that the symmetry requirement is fulfilled.

In order to study the nature of the singularities in detail, we first solve this model problem putting $(\gamma_1, \gamma_2) = (0,0)$, i.e. without any correction. We choose the *singular region* $\Omega_s = (-0.4, 0.4)^2$ to have a quantitative measurement of the singular behaviour in the neighbourhood of the re-entrant corner (see Figure 4.5). Moreover, the singular behavour of both the dispalcement components has to be considered and rectified simultaneously. The tabulated values of the eocs for the error norms computed for different mesh refinement levels confirm the presence of the pollution effect globally (cf. Table 5.1a). Reduced convergence rates of $\mathcal{O}(h)$ are attained in the $L^2$-norm, not just globally, but also in the outside region. The nature of the singular function for $u_1$ appears to be quite similar to that for the Poisson problem studied earlier (cf. Figures 4.8 and 5.4). Consequently the the error plots also have similar shapes depicting the global nature of the singularity (cf. Figures 4.9 and 5.5). However, the the singularity occurring in case of $u_2$ has a quite different nature as is depicted in Figure 5.7 and Figure 5.8 respectively. The singularity is not so widespread as for $u_1$, but is almost equally strong in terms of magnitude of error.

Next comes the task of determining the optimal correction parameters $(\gamma_1, \gamma_2)$ so that the correction defined in (5.4) can overcome the pollution effect. Owing to the different nature of singularities for the two solution components, we need an approach which can deal with both singular components simultaneously. In this work, we propose the following: the optimal correction parameters are those which *minimise the error in the outside region*, i.e.

$$\left(\gamma_1^h, \gamma_2^h\right) = \underset{(\gamma_1, \gamma_2) \in (-1,1)^2}{\textbf{arg min}} \|\mathbf{u} - R_h^m \mathbf{u}\|_{L^2(\Omega \setminus \Omega_s)}, \tag{5.6}$$

where, $\left(\gamma_1^h, \gamma_2^h\right)$ are the level dependent optimal correction parameters. The initial search region $(\gamma_1, \gamma_2) \in (-1,1)^2$ has been selected based on numerical tests. It is clear that putting $\gamma_i \geq 1$ is equivalent to having negative stiffness and thus should be avoided. For the solution of the minimisation problem, we adopt a *golden section search* type algorithm applied recursively to each variable until convergence happens. The values of the optimal correction parameters $(\gamma_1, \gamma_2)$ are obtained by solving the minimisation problem (5.6) for different mesh sizes and have been plotted in Figure 5.3. It is clear that these level dependent values converge towards the level

independent values $\left(\gamma_1^\infty, \gamma_2^\infty\right)$ which works well for all mesh levels. We employ the Richardson extrapolation procedure of (4.5) on each parameter individually to obtain these values. For the current problem, we obtain

$$\left(\gamma_1^\infty, \gamma_2^\infty\right) = (0.814096, -0.887761)$$

as the optimal correction parameters.

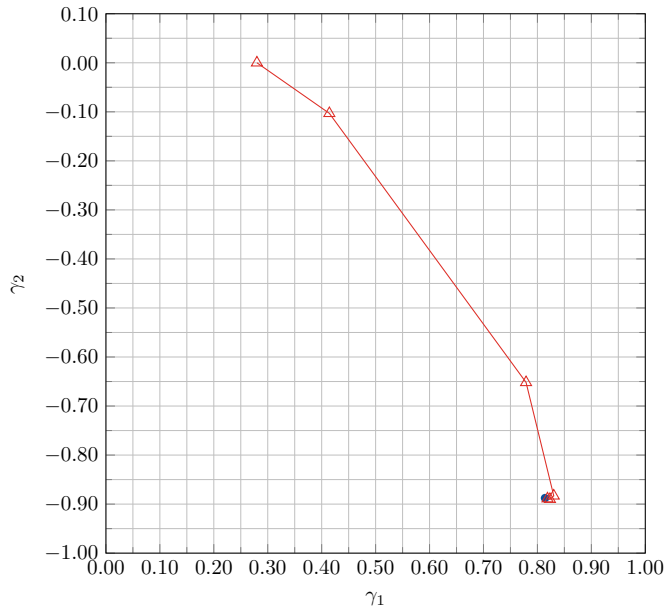


Figure 5.3: The level dependent correction parameters $(\gamma_1, \gamma_2)$ determined using the condition (5.6), for different mesh refinement levels for the BVP (5.5) with linear finite elements. The level independent optimal correction parameters $\left(\gamma_1^\infty, \gamma_2^\infty\right)$ have been marked by the blue dot.

Now, we solve the Mode-I problem with the optimal correction parameters determined above and analyse the results from the numerical test. The optimal correction helps us achieve close to the optimal convergence rate of $\mathcal{O}\left(h^2\right)$ for the weighted $L^2$-norm as the $L^2$-norm in the outside region (see Table 5.1b). Improved convergence rates of $\mathcal{O}\left(h^{1+\frac{\omega}{\pi}}\right)$ are attained for the $L^2$-norm both globally as well as in the singular region. Moreover improvement of one order of magnitude or better are observed in the error norms when compared with the finite element solution obtained without optimal correction. The proposed technique overcomes the pollution effect to a large extent especially for the $u_1$ component, where the spread of the error reduces significantly (cf. Figures 5.5 and 5.6). The improvement is relatively less for the $u_2$ component, where the peak error near the singularity slightly increases, but the error does get concentrated more towards the crack tip (cf. Figures 5.8 and 5.9). The correction however, still fulfills its purpose of eliminating the pollution effect in the far away region as desired.

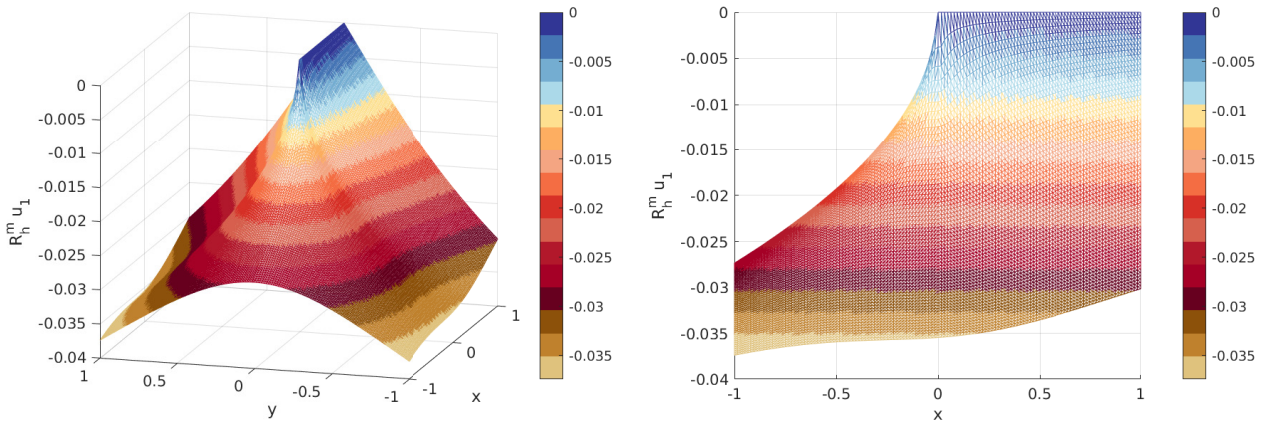


Figure 5.4: Plot of the finite element approximation for the displacement component $u_1$ obtained using linear finite elements for the BVP (5.5) for the $6^{th}$ mesh refinement level.

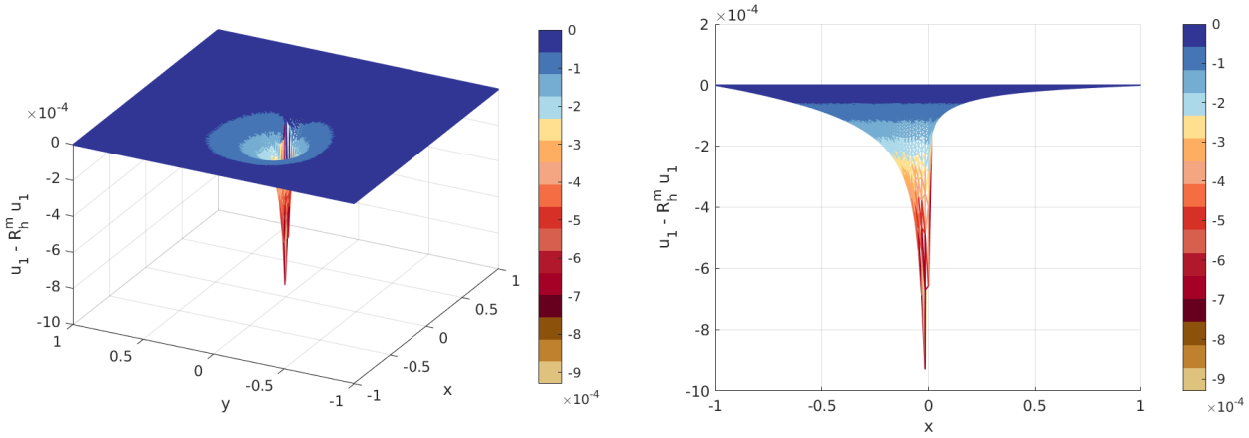


Figure 5.5: Plot of the finite element error for the displacement component $u_1$ obtained using linear finite elements with $(\gamma_1, \gamma_2) = (0, 0)$, i.e. no correction for the BVP (5.5) for the $6^{th}$ mesh refinement level.

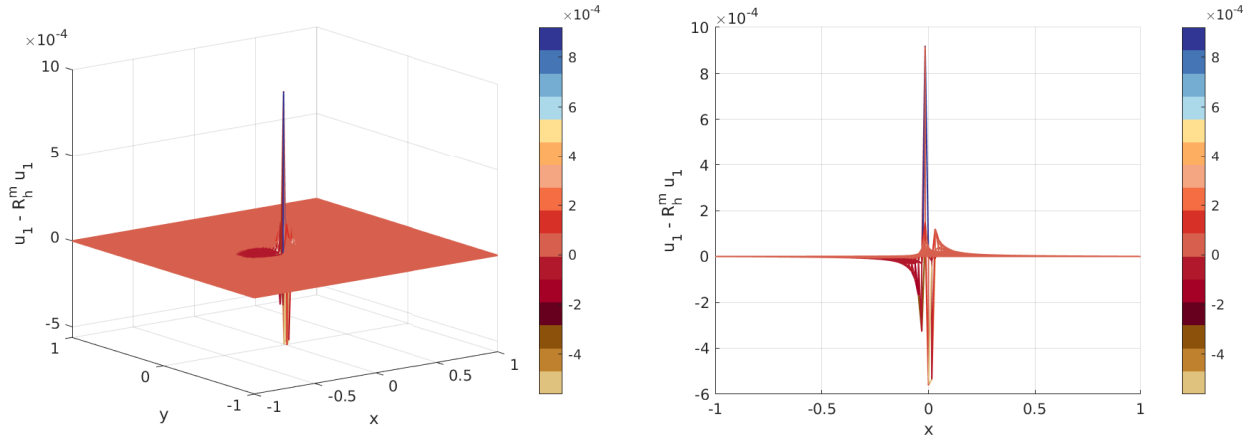


Figure 5.6: Plot of the finite element error for the displacement component $u_1$ obtained using linear finite elements with $(\gamma_1, \gamma_2) = (0.814096, -0.887761)$, i.e. with optimal correction for the BVP (5.5) for the $6^{th}$ mesh refinement level.

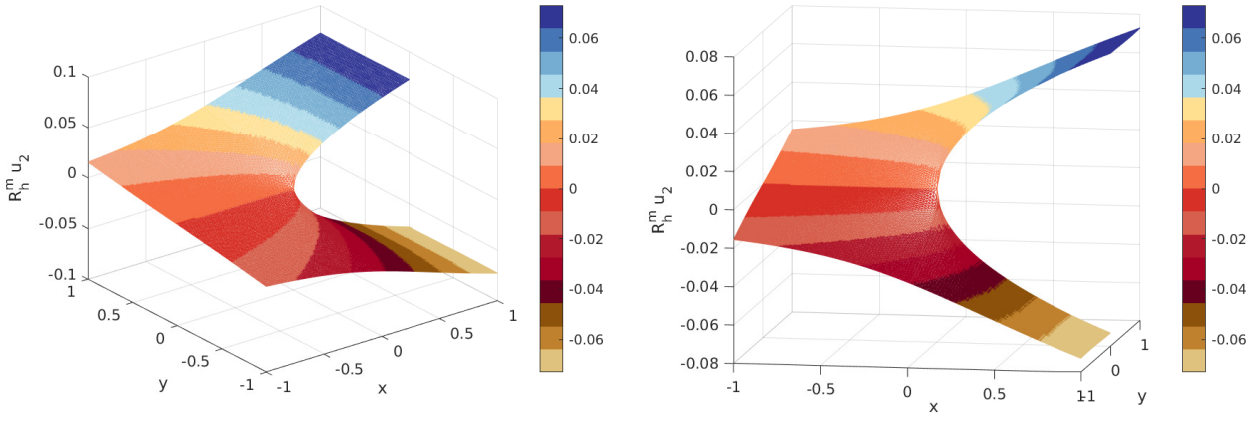


Figure 5.7: Plot of the finite element approximation for the displacement component $u_2$ obtained using linear finite elements for the BVP (5.5) for the $6^{th}$ mesh refinement level.

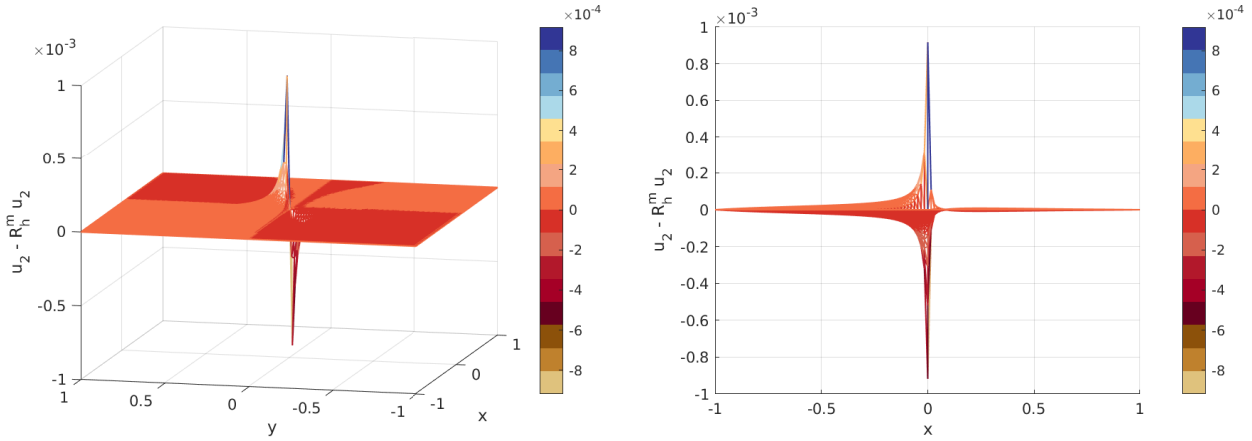


Figure 5.8: Plot of the finite element error for the displacement component $u_2$ obtained using linear finite elements with $(\gamma_1, \gamma_2) = (0, 0)$, i.e. no correction for the BVP (5.5) for the $6^{th}$ mesh refinement level.

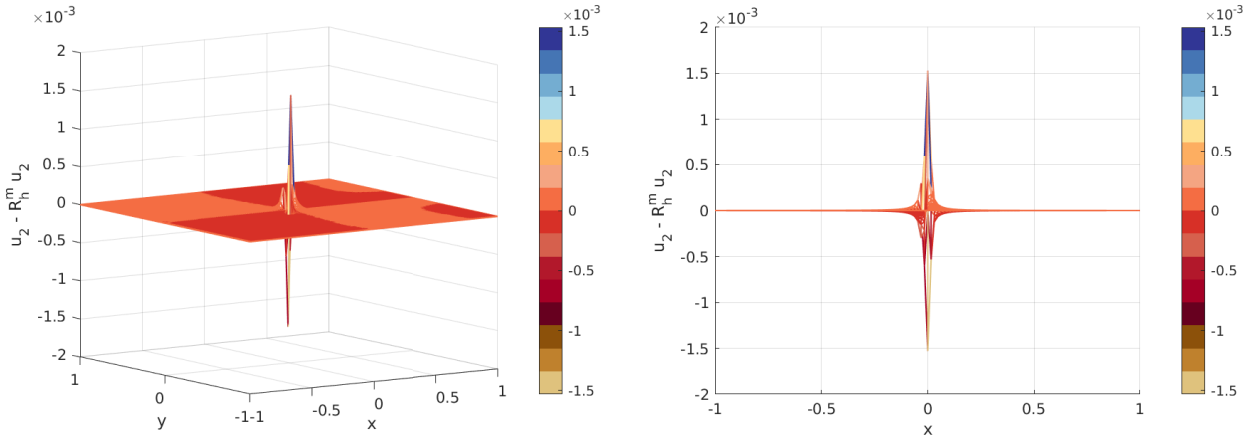


Figure 5.9: Plot of the finite element error for the displacement component $u_2$ obtained using linear finite elements with $(\gamma_1, \gamma_2) = (0.814096, -0.887761)$, i.e. with optimal correction for the BVP (5.5) for the $6^{th}$ mesh refinement level.

Table 5.1: Error norms using linear finite elements on non-uniform mesh, without and with optimal correction for the BVP (5.5) on non-uniform mesh.

(a) Results for $(\gamma_1, \gamma_2) = (0, 0)$: no correction applied

| $l$ | $h/\sqrt{2}$ | $\|\mathbf{u} - R_h^m \mathbf{u}\|_{0,1/2;\Omega}$ | eoc | $\|\mathbf{u} - R_h^m \mathbf{u}\|_{L^2(\Omega)}$ | eoc | $\|\mathbf{u} - R_h^m \mathbf{u}\|_{L^2(\Omega_s)}$ | eoc | $\|\mathbf{u} - R_h^m \mathbf{u}\|_{L^2(\Omega \setminus \Omega_s)}$ | eoc |
|---|---|---|---|---|---|---|---|---|---|
| 1 | 0.50000000 | 4.134198e-03 | - | 7.293539e-03 | - | - | - | 7.477156e-04 | - |
| 2 | 0.25000000 | 1.523834e-03 | 1.4399 | 3.096075e-03 | 1.2362 | - | - | 7.900607e-04 | - |
| 3 | 0.12500000 | 5.952052e-04 | 1.3562 | 1.309867e-03 | 1.2410 | 9.311890e-04 | - | 3.431020e-04 | 1.2033 |
| 4 | 0.06250000 | 2.509413e-04 | 1.2460 | 5.629933e-04 | 1.2182 | 4.529859e-04 | 1.0396 | 1.526527e-04 | 1.1684 |
| 5 | 0.03125000 | 1.135709e-04 | 1.1438 | 2.496505e-04 | 1.1732 | 1.966117e-04 | 1.2041 | 8.045156e-05 | 0.9241 |
| 6 | 0.01562500 | 5.388409e-05 | 1.0757 | 1.146405e-04 | 1.1228 | 8.770397e-05 | 1.1646 | 4.107964e-05 | 0.9697 |
| 7 | 0.00781250 | 2.625238e-05 | 1.0374 | 5.426792e-05 | 1.0789 | 4.096386e-05 | 1.0983 | 2.006208e-05 | 1.0340 |
| 8 | 0.00390625 | 1.296611e-05 | 1.0177 | 2.626691e-05 | 1.0469 | 1.959838e-05 | 1.0636 | 9.905710e-06 | 1.0181 |

(b) Results for $(\gamma_1, \gamma_2) = (\gamma_1^\infty, \gamma_2^\infty) = (0.814096, -0.887761)$: with optimal correction

| $l$ | $h/\sqrt{2}$ | $\|\mathbf{u} - R_h^m \mathbf{u}\|_{0,1/2;\Omega}$ | eoc | $\|\mathbf{u} - R_h^m \mathbf{u}\|_{L^2(\Omega)}$ | eoc | $\|\mathbf{u} - R_h^m \mathbf{u}\|_{L^2(\Omega_s)}$ | eoc | $\|\mathbf{u} - R_h^m \mathbf{u}\|_{L^2(\Omega \setminus \Omega_s)}$ | eoc |
|---|---|---|---|---|---|---|---|---|---|
| 1 | 0.50000000 | 5.298461e-03 | - | 7.962363e-03 | - | - | - | 1.702320e-03 | - |
| 2 | 0.25000000 | 1.499446e-03 | 1.8211 | 3.020249e-03 | 1.3985 | - | - | 6.799750e-04 | 1.3239 |
| 3 | 0.12500000 | 4.080110e-04 | 1.8777 | 1.097474e-03 | 1.4605 | 8.077280e-04 | - | 1.433342e-04 | 2.2461 |
| 4 | 0.06250000 | 1.072669e-04 | 1.9274 | 3.919276e-04 | 1.4855 | 3.835256e-04 | 1.0745 | 2.422459e-05 | 2.5648 |
| 5 | 0.03125000 | 2.773936e-05 | 1.9512 | 1.390761e-04 | 1.4947 | 1.381220e-04 | 1.4734 | 6.000396e-06 | 2.0133 |
| 6 | 0.01562500 | 7.150233e-06 | 1.9559 | 4.925474e-05 | 1.4975 | 4.911464e-05 | 1.4917 | 1.483702e-06 | 2.0159 |
| 7 | 0.00781250 | 1.853939e-06 | 1.9474 | 1.743277e-05 | 1.4985 | 1.740646e-05 | 1.4965 | 3.749246e-07 | 1.9845 |
| 8 | 0.00390625 | 4.902170e-07 | 1.9191 | 6.168983e-06 | 1.4987 | 6.162145e-06 | 1.4981 | 1.113911e-07 | 1.7510 |

### 5.3.3 Numerical Example:Mode-II Problem

Here, we solve the Mode-II problem to further test the proposed method. We choose as the exact solution for this model problem

$$\mathbf{u} = \tilde{\mathbf{s}}_{II} = \frac{K_{II}}{4\mu}\sqrt{\frac{r}{2\pi}}\begin{bmatrix}(2\kappa+3)\cos\frac{\theta}{2} - \cos\frac{3\theta}{2}\\ (2\kappa-3)\sin\frac{\theta}{2} - \sin\frac{3\theta}{2}\end{bmatrix},$$

where, $K_{II}$ represents the *stress intensity factor* as before. The domain $\Omega$ is the same as for BVP (5.5). The BVP to be solved here is: Find $\mathbf{u}$, s.t.

$$\begin{aligned}\operatorname{div}\boldsymbol{\sigma}^t + \mathbf{b} = \mathbf{0}, \quad \boldsymbol{\sigma} = 2\mu\,\boldsymbol{\epsilon} + \lambda\,\operatorname{tr}\epsilon\,\boldsymbol{I} \quad \text{and } \boldsymbol{\epsilon} = \frac{1}{2}\left[\nabla\mathbf{u} + (\nabla\mathbf{u})^t\right] \qquad \text{in } \Omega,\\ \mathbf{u} = \tilde{\mathbf{s}}_{II} \qquad \text{on } \partial\Omega.\end{aligned} \tag{5.7}$$

with the material parameters

$$E = 2.1 \times 10^5 \quad \text{and} \quad \nu = 0.2$$

leading to

$$\lambda = 5.83 \times 10^4, \quad \mu = 87500, \quad \kappa = 2.20$$

and the stress intensity factor $K_{II} = 10^4$. Alike the Mode-I case, we solve this BVP on the family of meshes $\{\mathcal{T}_h\}_{h \le H}$ obtained from uniform refinement of the coarse mesh $\mathcal{T}_H$ shown in Figure 4.4a, so that the symmetry requirement is fulfilled.

Following the approach adopted for the Mode-I case, we first solve this test problem without any correction, so that we can develop an understanding of the nature of singularities for the two displacement components. At first glance, the plot of the function $u_1$ seems to be quite similar to that of the $u_2$ component for the Mode-I case (cf. Figure 5.11 and Figure 5.7), but the nature of the singularity is much different as is revealed by the error plot in Figure 5.12. The second displacement component $u_2$ depicts singular behaviour which is quite similar to that of the solution to the Poisson problem (cf. Figure 5.15 and Figure 4.9). This singular behaviour also exhibits itself in the form of sub-optimal convergence rates attained for the $L^2$-norm (cf. Table 5.2a).

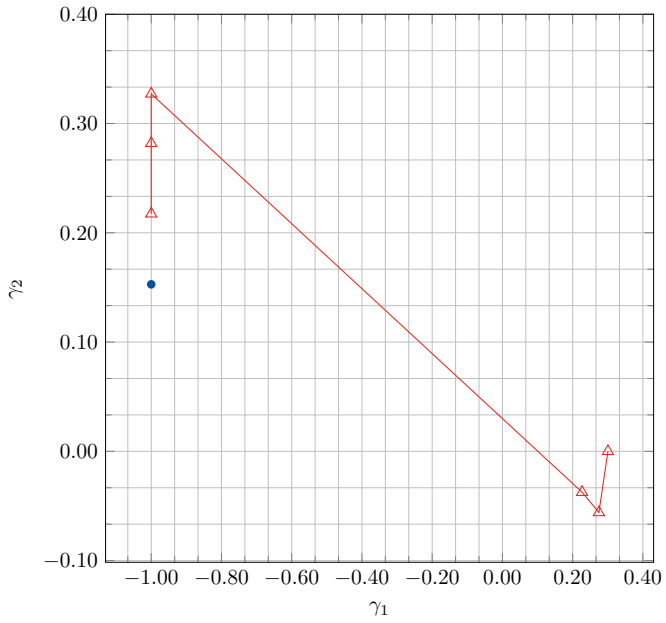


Figure 5.10: The level dependent correction parameters $(\gamma_1, \gamma_2)$ determined using the condition (5.6), for different mesh refinement levels for the BVP (5.7) with linear finite elements. The level independent optimal correction parameters $\left(\gamma_1^\infty, \gamma_2^\infty\right)$ obtained using extrapolation have been marked by the blue dot.

The optimal correction parameters are computed by minimising the target function of (5.6) as was done previously. The proposed approach however, does not seem work well for this model problem. A global minimum of the target function could not be achieved for some mesh refinement levels (cf. Figure 5.10), especially for the first optimization variable $\gamma_1$. The level independent optimal parameters obtained by the extrapolation procedure described in the previous numerical example yield the values

$$\left(\gamma_1^\infty, \gamma_2^\infty\right) = (-0.999999, 0.152822)$$

for the current model problem.

The BVP is then solved using the optimal correction parameters obtained above. The applied seems to work well to overcome the pollution effect for the $u_2$ component, as the spread of the

error decreases significantly (cf. Figure 5.15). The singularity of the $u_1$ component however, is not much affected by the correction (see Figure 5.13). Consequently, we only get limited improvement in the error norms when compared to the no-correction case (cf. Table 5.2).

These numerical experiments reveal that the proposed extension of the ECFEM for linear elasticity problems, seems to work well for the components which have singular behaviour of the form shown in Figure 5.5 (see also Figure 5.15). This correction scheme is however, not equally effective for components having different kind of singular behaviour, see Figure 5.12 for instance.

Table 5.2: Error norms using linear finite elements on non-uniform mesh, without and with optimal correction for the BVP (5.7) on non-uniform mesh.

(a) Results for $(\gamma_1, \gamma_2) = (0, 0)$: no correction applied

| $l$ | $h/\sqrt{2}$ | $\|\mathbf{u} - R_h^m \mathbf{u}\|_{0,1/2;\Omega}$ | eoc | $\|\mathbf{u} - R_h^m \mathbf{u}\|_{L^2(\Omega)}$ | eoc | $\|\mathbf{u} - R_h^m \mathbf{u}\|_{L^2(\Omega_s)}$ | eoc | $\|\mathbf{u} - R_h^m \mathbf{u}\|_{L^2(\Omega\setminus\Omega_s)}$ | eoc |
|---|---|---|---|---|---|---|---|---|---|
| 1 | 0.50000000 | 4.702355e-03 | - | 8.345392e-03 | - | - | - | 1.103175e-03 | - |
| 2 | 0.25000000 | 1.583975e-03 | 1.5698 | 3.349368e-03 | 1.3171 | - | - | 9.226623e-04 | 0.2578 |
| 3 | 0.12500000 | 5.582967e-04 | 1.5044 | 1.334766e-03 | 1.3273 | 1.039156e-03 | - | 3.051081e-04 | 1.5965 |
| 4 | 0.06250000 | 2.160386e-04 | 1.3697 | 5.401746e-04 | 1.3051 | 4.631722e-04 | 1.1658 | 1.191304e-04 | 1.3568 |
| 5 | 0.03125000 | 9.297442e-05 | 1.2164 | 2.262166e-04 | 1.2557 | 1.890674e-04 | 1.2926 | 6.090468e-05 | 0.9679 |
| 6 | 0.01562500 | 4.321425e-05 | 1.1053 | 9.906194e-05 | 1.1913 | 7.953710e-05 | 1.2492 | 3.117937e-05 | 0.9660 |
| 7 | 0.00781250 | 2.092988e-05 | 1.0459 | 4.532722e-05 | 1.1280 | 3.531145e-05 | 1.1715 | 1.537619e-05 | 1.0199 |
| 8 | 0.00390625 | 1.032880e-05 | 1.0189 | 2.147513e-05 | 1.0777 | 1.631407e-05 | 1.1140 | 7.670699e-06 | 1.0033 |

(b) Results for $(\gamma_1, \gamma_2) = (\gamma_1^\infty, \gamma_2^\infty) = (-0.999999, 0.152822)$: with optimal correction

| $l$ | $h/\sqrt{2}$ | $\|\mathbf{u} - R_h^m \mathbf{u}\|_{0,1/2;\Omega}$ | eoc | $\|\mathbf{u} - R_h^m \mathbf{u}\|_{L^2(\Omega)}$ | eoc | $\|\mathbf{u} - R_h^m \mathbf{u}\|_{L^2(\Omega_s)}$ | eoc | $\|\mathbf{u} - R_h^m \mathbf{u}\|_{L^2(\Omega\setminus\Omega_s)}$ | eoc |
|---|---|---|---|---|---|---|---|---|---|
| 1 | 0.50000000 | 7.836233e-03 | - | 1.168874e-02 | - | - | - | 3.389812e-03 | - |
| 2 | 0.25000000 | 2.670408e-03 | 1.5531 | 4.925062e-03 | 1.2469 | - | - | 2.019268e-03 | 0.7474 |
| 3 | 0.12500000 | 8.771676e-04 | 1.6061 | 1.951252e-03 | 1.3357 | 1.319468e-03 | - | 5.071089e-04 | 1.9935 |
| 4 | 0.06250000 | 2.912172e-04 | 1.5908 | 7.520964e-04 | 1.3754 | 6.696828e-04 | 0.9784 | 1.667889e-04 | 1.6043 |
| 5 | 0.03125000 | 1.007754e-04 | 1.5310 | 2.875581e-04 | 1.3871 | 2.606771e-04 | 1.3612 | 6.617762e-05 | 1.3336 |
| 6 | 0.01562500 | 3.714887e-05 | 1.4398 | 1.104416e-04 | 1.3806 | 1.001407e-04 | 1.3802 | 2.625793e-05 | 1.3336 |
| 7 | 0.00781250 | 1.482249e-05 | 1.3255 | 4.314864e-05 | 1.3559 | 3.875882e-05 | 1.3694 | 1.055929e-05 | 1.3142 |
| 8 | 0.00390625 | 6.405427e-06 | 1.2104 | 1.738689e-05 | 1.3113 | 1.523935e-05 | 1.3467 | 4.610085e-06 | 1.1956 |

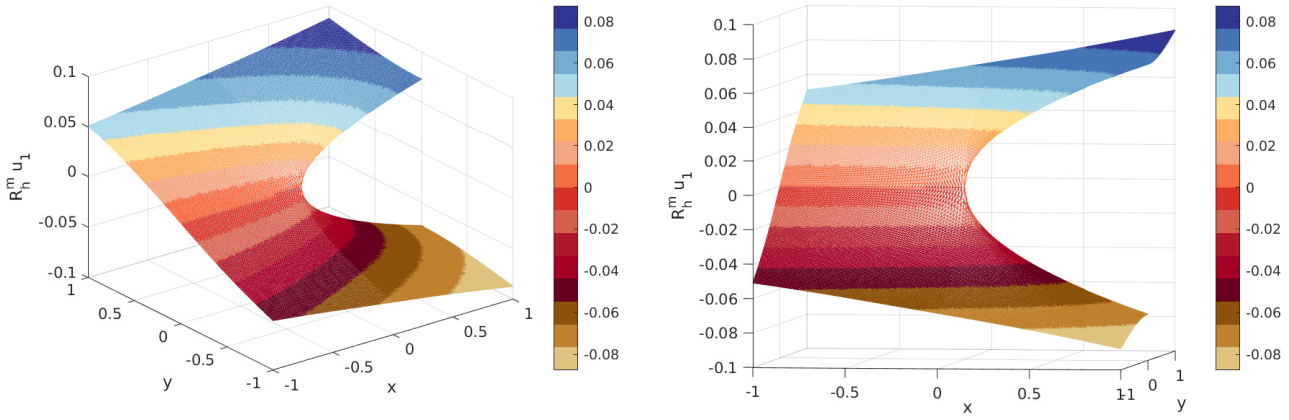


Figure 5.11: Plot of the finite element approximation for the displacement component $u_1$ obtained using linear finite elements for the BVP (5.7) for the $6^{th}$ mesh refinement level.

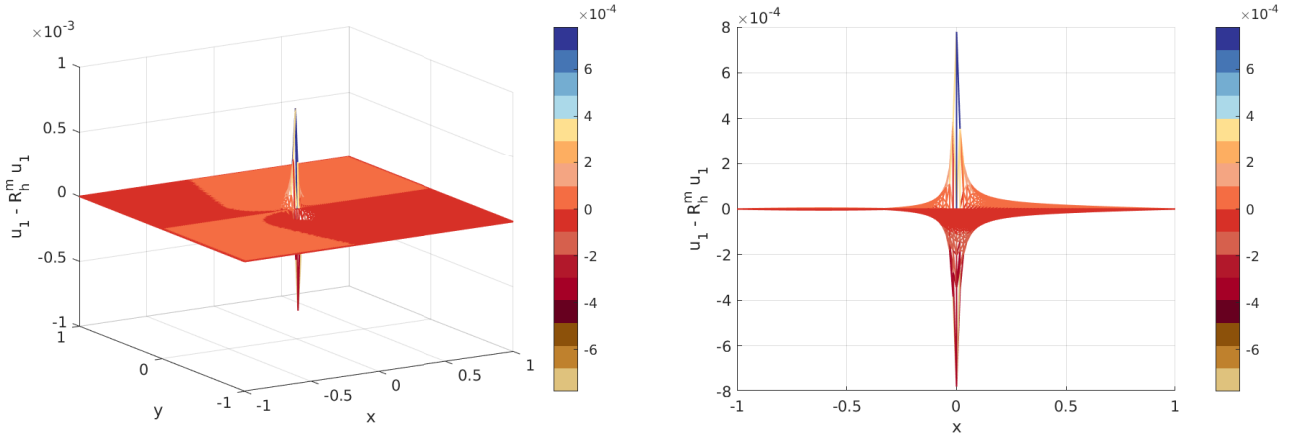


Figure 5.12: Plot of the finite element error for the displacement component $u_1$ obtained using linear finite elements with $(\gamma_1, \gamma_2) = (0, 0)$, i.e. no correction for the BVP (5.7) for the $6^{th}$ mesh refinement level.

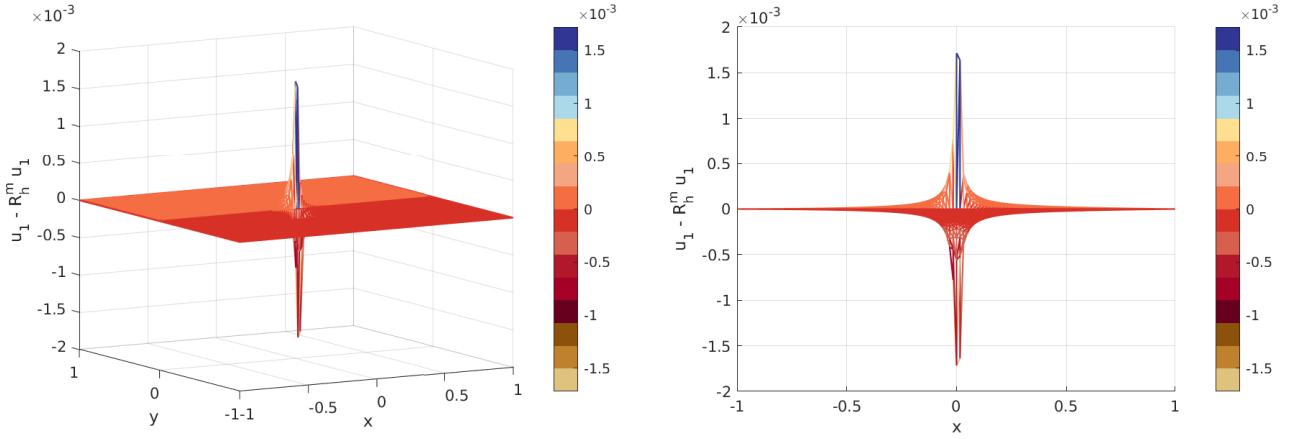


Figure 5.13: Plot of the finite element error for the displacement component $u_1$ obtained using linear finite elements with $(\gamma_1, \gamma_2) = (-0.999999, 0.152822)$, i.e. with optimal correction for the BVP (5.7) for the $6^{th}$ mesh refinement level.

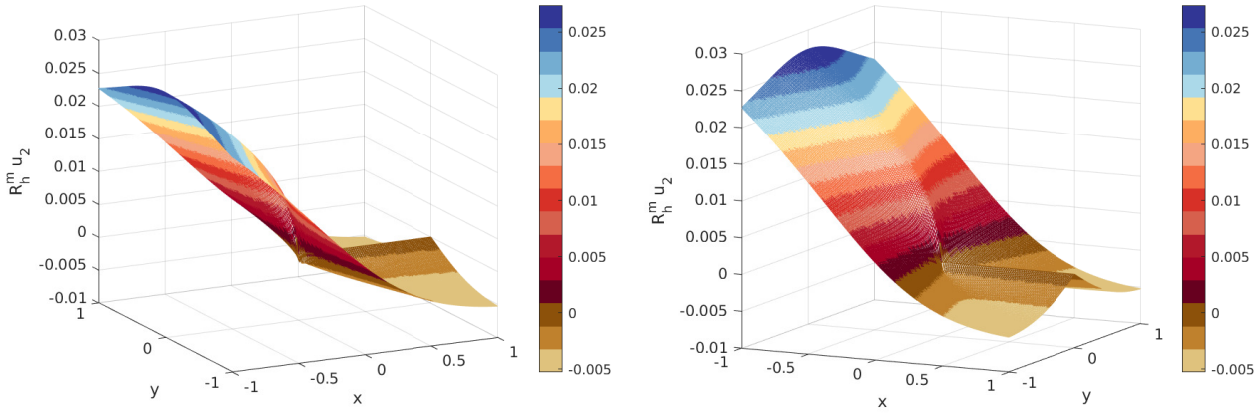


Figure 5.14: Plot of the finite element approximation for the displacement component $u_2$ obtained using linear finite elements for the BVP (5.7) for the $6^{th}$ mesh refinement level.

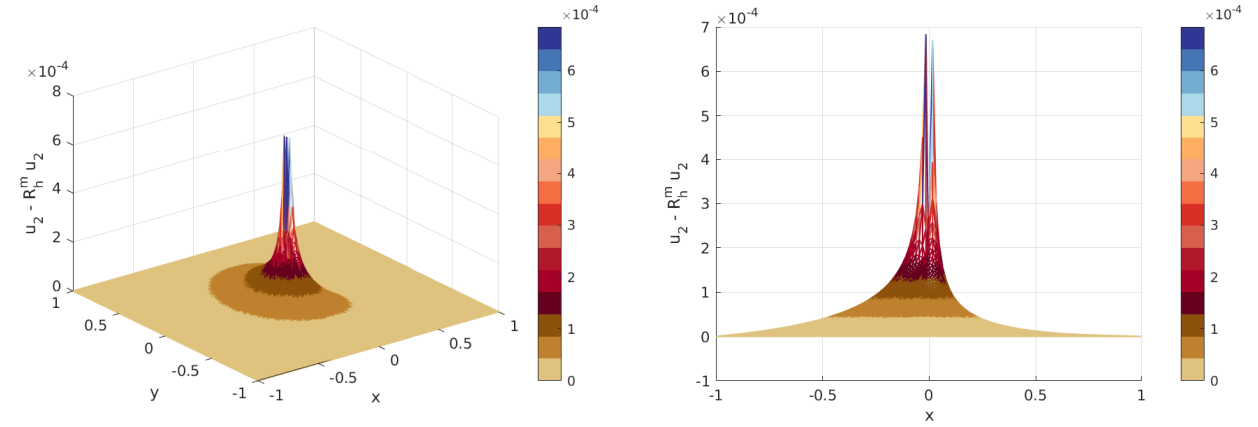


Figure 5.15: Plot of the finite element error for the displacement component $u_2$ obtained using linear finite elements with $(\gamma_1, \gamma_2) = (0, 0)$, i.e. no correction for the BVP (5.7) for the $6^{th}$ mesh refinement level.

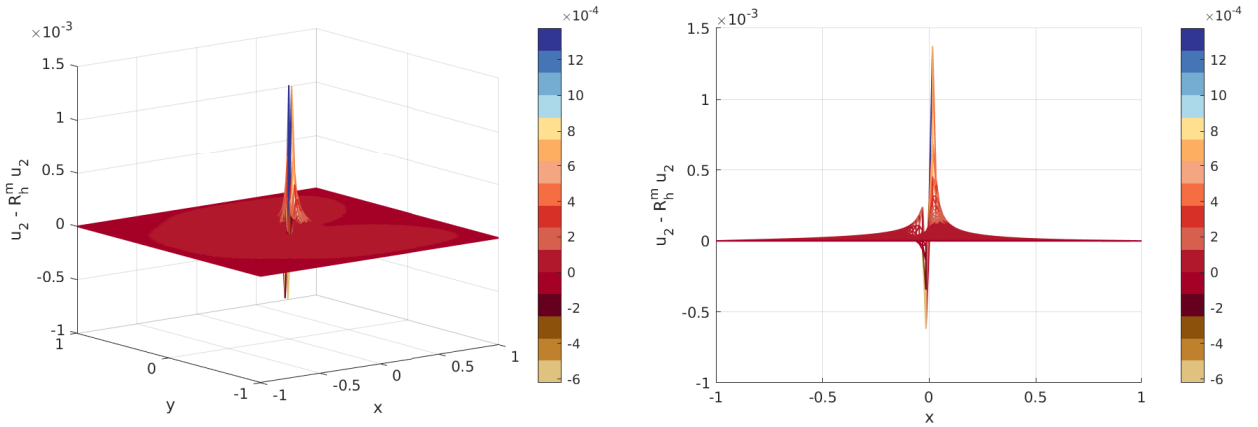


Figure 5.16: Plot of the finite element error for the displacement component $u_2$ obtained using linear finite elements with $(\gamma_1, \gamma_2) = (-0.999999, 0.152822)$, i.e. with optimal correction for the BVP (5.7) for the $6^{th}$ mesh refinement level.

# Chapter 6

# Conclusion

Systematic numerical experimentation has been carried out to analyse how the presence of a re-entrant corner *pollutes* the finite element approximation to the solution of an elliptic PDE, thereby culminating in sub-optimal convergence rates on *quasi-uniform meshes* irrespective of the order of polynomials used for the finite element basis functions. The error estimates in three different norms, namely $L^2$-norm, $H^1$-norm and the max norm, for the Poisson problem on domains with re-entrant corners have been reviewed exhaustively and compared with those attained in the case of a smooth domain boundary. These estimates have also been validated through numerical examples. The Energy Corrected Finite Element Method (ECFEM) which only entails a *local modification* of the weak form in the vicinity of the re-entrant corner in order to overcome this *pollution effect* has been studied comprehensively. An alternative strategy (which does not require any prior knowledge of the true solution) for determining the optimal correction parameter to be used in the modified Galerkin approximation has been explored. Numerical tests validating the applicability of this technique to scalar elliptic problems when using linear finite elements have been conducted. A minimal modification to this technique has been proposed such that *higher order* finite elements can be used. Optimal convergence rates have been achieved with quadratic finite elements. Furthermore, when using cubic and quartic finite elements, close to optimal convergence rates were observed during the numerical tests.

An extension of the ECFEM (involving the use of two correction parameters) for the planar linear elasticity problem has been proposed. This approach is primarily based on the extensive numerical experimentation done to understand the nature of singularities arising in each of the displacement components. The optimal correction parameters have been determined by solving a minimisation problem, for which the $L^2$-norm of the error in the region far away from the singular point has been considered as the *target function*. In order to validate the applicability of this approach, numerical tests considering the *Mode-I* and *Mode-II* problems of Linear Elastic Fracture Mechanics (LEFM) as model problems have been performed. The present technique performs quite well for the Mode-I problem, as the optimal correction parameters determined by the aforementioned approach yield optimal convergence rates for the error in the weighted $L^2$-norm globally and the $L^2$-norm in the outside region. Moreover, significant reduction in the magnitude of the error, as compared to the standard Galerkin approach has been observed. For the Mode-II problem however, this minimisation approach does not seem to converge, yielding correction parameters which are not fully optimal. Consequently, the convergence rates and the magnitude of the error norms do not show drastic improvement as was observed for the Mode-I problem. This could be probably due to the much different nature of the singularity observed for

the $u_1$ component. Numerical tests also reveal that the proposed technique is better capable of handling singular functions which have similar nature to that observed for the Poisson problem. It is hypothesised that an approach based on minimising the difference between the finite element solutions on consecutive mesh refinement levels could provide optimally performing correction parameters. Moreover, this approach would not require prior knowledge of the true solution. In order to have a robust technique which could work well for different problems, the special structure of the singularities arising in the case of the elasticity problem need to be taken into account. Asides, the present work and the relevant literature referenced only focus on planar problems. A fundamentally new idea would be required to deal with such singular problems on three-dimensional domains.

# Appendix A

# Norms: Definitions and Notations

## A.1 Standard Sobolev Norms

In this work, $\|\cdot\|_s$ represents the norm corresponding to the space $H^s(\Omega)$ for some $s \in \mathbb{N}_0$. This means,

$$\|\cdot\|_s \coloneqq \|\cdot\|_{H^s(\Omega)},$$

where, $H^s$ is the standard Sobolev space for $s \in \mathbb{N}$. For the special case $s = 0$, we have

$$\|\cdot\|_{H^0(\Omega)} \coloneqq \|\cdot\|_{L^2(\Omega)},$$

where, $L^2(\Omega)$ is the standard Lebesgue space. The space $H_0^1(\Omega)$ is defined as:

$$H_0^1(\Omega) \coloneqq \left\{u \in H^1(\Omega) : \ u\big|_{\partial\Omega} = 0\right\},$$

where, the term $u\big|_{\partial\Omega}$ is to be understood in the sense of the *trace* of a function. For a detailed discussion on Sobolev spaces, we refer the reader to [18, Chapter 7].

The *energy norm*, $\|\cdot\|_E$ corrsponding to a weak form $a(u, v)$ is defined as

$$\|u\|_E \coloneqq \left(a(u, u)\right)^{1/2}.$$

## A.2 Weighted Sobolev Norms

Consider a bounded polygonal domain $\Omega \in \mathbb{R}^2$, containing a single re-entrant corner with a interior angle $\pi < \omega \leq 2\pi$ and located at the origin (see Figure 3.1 for details). Let $r(x, y)$ denote the distance of the point $(x, y)$ from the re-entrant corner. For $\Omega_0 \subset \Omega$, $m \in \mathbb{N}_0$ and $\alpha \in \mathbb{R}$, the weighted Sobolev space is defined as

$$H_\alpha^m(\Omega_0) \coloneqq \left\{u\big|r^{\alpha+|\mu|-m} D^\mu u \in L^2(\Omega_0) : 0 \leq |\mu| \leq m\right\},$$

where, $\mu \in \mathbb{N}_0^2$ is a multi-index with $|\mu| = \mu_1 + \mu_2$. The corresponding weighted norm is

$$\|u\|_{m,\alpha;\Omega_0} \coloneqq \left(\sum_{|\mu|\leq m} \|r^{\alpha+|\mu|-m} D^\mu u\|_{L^2(\Omega_0)}^2\right)^{1/2}.$$

In this work, we will be primarily needing the weighted $L^2$-norm, which is obtained by inserting $m = 0$ in the above relation, yielding

$$\|u\|_{0,\alpha;\Omega_0} = \|r^\alpha\, u\|_{L^2(\Omega_0)}$$

The subscript $\Omega_0$ can be dropped for $\Omega = \Omega_0$. It should be noted that $H^m_\alpha$ is a *Hilbert space* when with its natural norm defined above. The above definition of weighted Sobolev space has been taken from [6]. A detailed explanation on various other kinds of weigthed Sobolev spaces and their applications can be found in [15].

# Appendix B

# Regularity of Singular Functions

Here, we estimate the regularity of the singular functions employed in describing the behaviour of the solution to an elliptic BVP in presence of a re-entrant corner. These regularity results are essential for the arguements presented in order to prove Theorem 3.2.

We consider functions of the form

$$u_n = r^{\nu_n} \sin \nu_n \theta, \tag{B.1}$$

with $\nu_n = \frac{n\pi}{\omega}$, on the domain

$$\Omega_0 = \{(r, \theta) \,:\, 0 < r < r_0, 0 \leq \theta \leq \omega\}, \tag{B.2}$$

which contains a single re-entrant corner located at the origin and having an interior angle $\pi < \omega \leq 2\pi$.

Depending on the values of $n$ and $\omega$, three different regimes need to considered for our purpose. It is clear that $\nu_1 < 1$ for all permissible values of $\omega$. Also, for $n \geq 2$, we have $\nu_n > 1$ for all permissible values of $\omega$ except $2\pi$. It is easy to see that $u_n \in H^2(\Omega_0)$ in this scenario. The third possibility occurs when $n = 2$ and $\omega = 2\pi$, and is special in the sense that it results in a function of the form $r \sin\theta$. We analyse the first and the third possibility in detail. It is evident that all of these functions are in $L^2$ space. Thus, we only have to focus on the semi-norms for the derivatives.

Before moving to the three cases explained above, we list the formulas for partial derivatives in polar coordinates, which will be required for our calculations. In order to simplify the notation, we drop the subscript $n$ as it is insignificant for the purpose of putting down these relations.

$$\frac{\partial u}{\partial x} = \frac{\partial u}{\partial r}\frac{\partial r}{\partial x} + \frac{\partial u}{\partial \theta}\frac{\partial \theta}{\partial x} = \frac{\partial u}{\partial r}\cos\theta - \frac{1}{r}\frac{\partial u}{\partial \theta}\sin\theta \tag{B.3}$$

$$\frac{\partial u}{\partial y} = \frac{\partial u}{\partial r}\frac{\partial r}{\partial y} + \frac{\partial u}{\partial \theta}\frac{\partial \theta}{\partial y} = \frac{\partial u}{\partial r}\sin\theta + \frac{1}{r}\frac{\partial u}{\partial \theta}\cos\theta \tag{B.4}$$

$$\|\nabla u\|^2 = \left(\frac{\partial u}{\partial x}\right)^2 + \left(\frac{\partial u}{\partial y}\right)^2 = \left(\frac{\partial u}{\partial r}\right)^2 + \frac{1}{r^2}\left(\frac{\partial u}{\partial \theta}\right)^2 \tag{B.5}$$

$$\frac{\partial^2 u}{\partial x^2} = \frac{\partial^2 u}{\partial r^2}\cos^2\theta + \frac{1}{r}\frac{\partial u}{\partial r}\sin^2\theta - \frac{2}{r}\frac{\partial^2 u}{\partial r\partial\theta}\sin\theta\cos\theta + \frac{2}{r^2}\frac{\partial u}{\partial\theta}\sin\theta\cos\theta + \frac{1}{r^2}\frac{\partial^2 u}{\partial\theta^2}\sin^2\theta \quad \text{(B.6)}$$

$$\frac{\partial^2 u}{\partial y^2} = \frac{\partial^2 u}{\partial r^2}\sin^2\theta + \frac{1}{r}\frac{\partial u}{\partial r}\cos^2\theta + \frac{2}{r}\frac{\partial^2 u}{\partial r\partial\theta}\sin\theta\cos\theta - \frac{2}{r^2}\frac{\partial u}{\partial\theta}\sin\theta\cos\theta + \frac{1}{r^2}\frac{\partial^2 u}{\partial\theta^2}\cos^2\theta \quad \text{(B.7)}$$

$$\frac{\partial^2 u}{\partial y\partial x} = \left[\frac{1}{2}\frac{\partial^2 u}{\partial r^2} - \frac{1}{2r}\frac{\partial u}{\partial r} - \frac{1}{2r^2}\frac{\partial^2 u}{\partial\theta^2}\right]\sin 2\theta + \left[\frac{1}{r}\frac{\partial^2 u}{\partial r\partial\theta} - \frac{1}{r^2}\frac{\partial u}{\partial\theta}\right]\cos 2\theta \quad \text{(B.8)}$$

**Case 1:** $n = 1$ **with** $\pi < \omega \leq 2\pi$

For this case we have,

$$u = r^{\frac{\pi}{\omega}}\,\sin\frac{\pi\,\theta}{\omega},$$

leading to

$$\frac{\partial u}{\partial r} = \frac{\pi}{\omega}\,r^{\frac{\pi}{\omega}-1}\,\sin\frac{\pi\,\theta}{\omega} \qquad \text{and} \qquad \frac{\partial u}{\partial\theta} = \frac{\pi}{\omega}\,r^{\frac{\pi}{\omega}}\,\cos\frac{\pi\,\theta}{\omega},$$

along with

$$\frac{\partial^2 u}{\partial r^2} = \frac{\pi}{\omega}\left(\frac{\pi}{\omega}-1\right)r^{\frac{\pi}{\omega}-2}\,\sin\frac{\pi\,\theta}{\omega}, \qquad \frac{\partial^2 u}{\partial\theta^2} = -\frac{\pi^2}{\omega^2}\,r^{\frac{\pi}{\omega}}\,\sin\frac{\pi\,\theta}{\omega} \quad \text{and} \quad \frac{\partial^2 u}{\partial r\partial\theta} = \frac{\pi^2}{\omega^2}\,r^{\frac{\pi}{\omega}-1}\,\cos\frac{\pi\,\theta}{\omega}.$$

The first derivatives computed using (B.3) and (B.4) then read

$$\frac{\partial u}{\partial x} = \frac{\partial u}{\partial r}\cos\theta - \frac{1}{r}\frac{\partial u}{\partial\theta}\sin\theta = \frac{\pi}{\omega}\,r^{\frac{\pi}{\omega}-1}\,\sin\frac{\pi\,\theta}{\omega}\,\cos\theta - \frac{\pi}{\omega}\,r^{\frac{\pi}{\omega}-1}\,\cos\frac{\pi\,\theta}{\omega}\,\sin\theta = \frac{\pi}{\omega}\,r^{\frac{\pi}{\omega}-1}\,\sin\left(\frac{\pi\,\theta}{\omega}-\theta\right),$$

$$\frac{\partial u}{\partial y} = \frac{\partial u}{\partial r}\sin\theta + \frac{1}{r}\frac{\partial u}{\partial\theta}\cos\theta = \frac{\pi}{\omega}\,r^{\frac{\pi}{\omega}-1}\,\sin\frac{\pi\,\theta}{\omega}\,\sin\theta + \frac{\pi}{\omega}\,r^{\frac{\pi}{\omega}-1}\,\cos\frac{\pi\,\theta}{\omega}\,\cos\theta = \frac{\pi}{\omega}\,r^{\frac{\pi}{\omega}-1}\,\cos\left(\frac{\pi\,\theta}{\omega}-\theta\right).$$

The second derivatives based on B.6, B.7 and B.8 are computed as

$$\begin{aligned}
\frac{\partial^2 u}{\partial x^2} &= \frac{\partial^2 u}{\partial r^2}\cos^2\theta + \frac{1}{r}\frac{\partial u}{\partial r}\sin^2\theta - \frac{2}{r}\frac{\partial^2 u}{\partial r\partial\theta}\sin\theta\cos\theta + \frac{2}{r^2}\frac{\partial u}{\partial\theta}\sin\theta\cos\theta + \frac{1}{r^2}\frac{\partial^2 u}{\partial\theta^2}\sin^2\theta \\
&= \frac{\pi}{\omega}\left(\frac{\pi}{\omega}-1\right)r^{\frac{\pi}{\omega}-2}\,\sin\frac{\pi\,\theta}{\omega}\,\cos^2\theta + \frac{\pi}{\omega}\,r^{\frac{\pi}{\omega}-2}\,\sin\frac{\pi\,\theta}{\omega}\,\sin^2\theta - 2\frac{\pi^2}{\omega^2}\,r^{\frac{\pi}{\omega}-2}\,\cos\frac{\pi\,\theta}{\omega}\,\sin\theta\,\cos\theta \\
&\quad + 2\frac{\pi}{\omega}\,r^{\frac{\pi}{\omega}-2}\,\cos\frac{\pi\,\theta}{\omega}\,\sin\theta\,\cos\theta - \frac{\pi^2}{\omega^2}\,r^{\frac{\pi}{\omega}-2}\,\sin\frac{\pi\,\theta}{\omega}\,\sin^2\theta \\
&= \frac{\pi}{\omega}\left(\frac{\pi}{\omega}-1\right)r^{\frac{\pi}{\omega}-2}\left[\sin\frac{\pi\,\theta}{\omega}\,\cos^2\theta - \sin\frac{\pi\,\theta}{\omega}\,\sin^2\theta - 2\cos\frac{\pi\,\theta}{\omega}\,\sin\theta\,\cos\theta\right] \\
\implies \frac{\partial^2 u}{\partial x^2} &= \frac{\pi}{\omega}\left(\frac{\pi}{\omega}-1\right)r^{\frac{\pi}{\omega}-2}\,\sin\left(\frac{\pi\,\theta}{\omega}-2\theta\right),
\end{aligned}$$

$$\frac{\partial^2 u}{\partial y^2} = \frac{\partial^2 u}{\partial r^2}\sin^2\theta + \frac{1}{r}\frac{\partial u}{\partial r}\cos^2\theta + \frac{2}{r}\frac{\partial^2 u}{\partial r\partial\theta}\sin\theta\cos\theta - \frac{2}{r^2}\frac{\partial u}{\partial\theta}\sin\theta\cos\theta + \frac{1}{r^2}\frac{\partial^2 u}{\partial\theta^2}\cos^2\theta$$

$$
\begin{aligned}
&= \frac{\pi}{\omega}\left(\frac{\pi}{\omega}-1\right) r^{\frac{\pi}{\omega}-2} \sin\frac{\pi\,\theta}{\omega}\, \sin^2\theta + \frac{\pi}{\omega}\, r^{\frac{\pi}{\omega}-2} \sin\frac{\pi\,\theta}{\omega}\, \cos^2\theta + 2\frac{\pi^2}{\omega^2}\, r^{\frac{\pi}{\omega}-2} \cos\frac{\pi\,\theta}{\omega}\, \sin\theta\, \cos\theta \\
&\quad - 2\frac{\pi}{\omega}\, r^{\frac{\pi}{\omega}-2} \cos\frac{\pi\,\theta}{\omega}\, \sin\theta\, \cos\theta - \frac{\pi^2}{\omega^2}\, r^{\frac{\pi}{\omega}-2} \sin\frac{\pi\,\theta}{\omega}\, \cos^2\theta \\
&= \frac{\pi}{\omega}\left(\frac{\pi}{\omega}-1\right) r^{\frac{\pi}{\omega}-2} \left[\sin\frac{\pi\,\theta}{\omega}\, \sin^2\theta - \sin\frac{\pi\,\theta}{\omega}\, \cos^2\theta + 2\cos\frac{\pi\,\theta}{\omega}\, \sin\theta\, \cos\theta\right] \\
\implies \frac{\partial^2 u}{\partial y^2} &= \frac{\pi}{\omega}\left(\frac{\pi}{\omega}-1\right) r^{\frac{\pi}{\omega}-2} \sin\left(2\theta - \frac{\pi\,\theta}{\omega}\right), \\
\frac{\partial^2 u}{\partial y \partial x} &= \frac{1}{2}\left[\frac{\partial^2 u}{\partial r^2} - \frac{1}{r}\frac{\partial u}{\partial r} - \frac{1}{r^2}\frac{\partial^2 u}{\partial \theta^2}\right] \sin 2\theta + \left[\frac{1}{r}\frac{\partial^2 u}{\partial r \partial \theta} - \frac{1}{r^2}\frac{\partial u}{\partial \theta}\right] \cos 2\theta \\
&= \frac{1}{2}\left[\frac{\pi}{\omega}\left(\frac{\pi}{\omega}-1\right)\, r^{\frac{\pi}{\omega}-2} \sin\frac{\pi\,\theta}{\omega} - \frac{\pi}{\omega}\, r^{\frac{\pi}{\omega}-2} \sin\frac{\pi\,\theta}{\omega} + \frac{\pi^2}{\omega^2}\, r^{\frac{\pi}{\omega}-2} \sin\frac{\pi\,\theta}{\omega}\right] \sin 2\theta \\
&\quad + \left[\frac{\pi^2}{\omega^2}\, r^{\frac{\pi}{\omega}-2} \cos\frac{\pi\,\theta}{\omega} - \frac{\pi}{\omega}\, r^{\frac{\pi}{\omega}-2} \cos\frac{\pi\,\theta}{\omega}\right] \cos 2\theta \\
\implies \frac{\partial^2 u}{\partial y \partial x} &= \frac{\pi}{\omega}\left(\frac{\pi}{\omega}-1\right) r^{\frac{\pi}{\omega}-2} \cos\left(\frac{\pi\,\theta}{\omega} - 2\theta\right).
\end{aligned}
$$

Using the above expressions, we compute the $H^1$ semi-norm as

$$
\begin{aligned}
|u|_{H^1(\Omega_0)} &= \int\limits_{\Omega_0} \left[\left(\frac{\partial u}{\partial x}\right)^2 + \left(\frac{\partial u}{\partial y}\right)^2\right] d\Omega = \int\limits_0^{r_0}\int\limits_0^{2\pi} r\, dr\, d\theta \\
&= \int\limits_{\Omega_0} \frac{\pi^2}{\omega^2}\, r^{\frac{2\pi}{\omega}-2} \left[\sin^2\left(\frac{\pi\,\theta}{\omega} - \theta\right) + \cos^2\left(\frac{\pi\,\theta}{\omega} - \theta\right)\right] r\, dr\, d\theta \\
&= \frac{\pi^2}{\omega^2}\left(\int\limits_0^{r_0} r^{\frac{2\pi}{\omega}-1}\, dr\right)\left(\int\limits_0^{\omega} d\theta\right) = \frac{\pi^2}{\omega^2}\left(r^{\frac{2\pi}{\omega}}\big|_0^{r_0}\right)\omega = \frac{\pi^2}{\omega} r_0^{\frac{2\pi}{\omega}} < \infty.
\end{aligned}
$$

This shows that $u_1 \in H^1(\Omega_0)$ for all permissible values of $\omega$. The computation for the $H^2$ semi-norm yields

$$
\begin{aligned}
|u|_{H^2(\Omega_0)} &= \int\limits_{\Omega_0} \left[\left(\frac{\partial^2 u}{\partial x^2}\right)^2 + \left(\frac{\partial^2 u}{\partial y^2}\right)^2 + \left(\frac{\partial^2 u}{\partial x \partial y}\right)^2\right] d\Omega \\
&= \int\limits_{\Omega_0} \frac{\pi^2}{\omega^2}\left(\frac{\pi}{\omega}-1\right)^2 r^{\frac{2\pi}{\omega}-4} \left[\sin^2\left(\frac{\pi\,\theta}{\omega} - 2\theta\right) + \sin^2\left(2\theta - \frac{\pi\,\theta}{\omega}\right) + \cos^2\left(\frac{\pi\,\theta}{\omega} - 2\theta\right)\right] r\, dr d\theta \\
&= \frac{\pi^2}{\omega^2}\left(\frac{\pi}{\omega}-1\right)^2 \left(\int\limits_0^{r_0} r^{\frac{2\pi}{\omega}-3}\, dr\right) \underbrace{\left(\int\limits_0^{\omega}\left[1 + \sin^2\left(2\theta - \frac{\pi\,\theta}{\omega}\right)\right] d\theta\right)}_{=:K<\infty}
\end{aligned}
$$

$$= \frac{\pi^2}{\omega^2}\left(\frac{\pi}{\omega}-1\right)^2\left(r^{\frac{2\pi}{\omega}-2}\Big|_0^{r_0}\right)K \not< \infty \quad \text{as } \frac{\pi}{\omega} < 1$$

which shows that $u_1 \notin H^2(\Omega_0)$ for all permissible values of $\omega$.

**Case 2:** $n = 2$ **with** $\omega = 2\pi$

For this scenario we have,

$$u = r\,sin\theta,$$

leading to

$$\frac{\partial u}{\partial r} = \sin\theta \qquad \text{and} \qquad \frac{\partial u}{\partial \theta} = r\cos\theta,$$

along with

$$\frac{\partial^2 u}{\partial r^2} = 0, \qquad \frac{\partial^2 u}{\partial \theta^2} = -r\,\sin\theta \quad \text{and} \qquad \frac{\partial^2 u}{\partial r \partial \theta} = \cos\theta.$$

The first derivatives in this case yield

$$\frac{\partial u}{\partial x} = \frac{\partial u}{\partial r}\cos\theta - \frac{1}{r}\frac{\partial u}{\partial \theta}\sin\theta = \sin\theta\cos\theta - \cos\theta\,\sin\theta = 0,$$
$$\frac{\partial u}{\partial y} = \frac{\partial u}{\partial r}\sin\theta + \frac{1}{r}\frac{\partial u}{\partial \theta}\cos\theta = \sin^2\theta + \cos^2\theta = 1.$$

The second derivatives are computed as

$$\begin{aligned}\frac{\partial^2 u}{\partial x^2} &= \frac{\partial^2 u}{\partial r^2}\cos^2\theta + \frac{1}{r}\frac{\partial u}{\partial r}\sin^2\theta - \frac{2}{r}\frac{\partial^2 u}{\partial r\partial\theta}\sin\theta\cos\theta + \frac{2}{r^2}\frac{\partial u}{\partial\theta}\sin\theta\cos\theta + \frac{1}{r^2}\frac{\partial^2 u}{\partial\theta^2}\sin^2\theta \\ &= \frac{1}{r}\,\sin^3\theta - \frac{2}{r}\,\sin\theta\,\cos^2\theta + \frac{2}{r}\,\sin\theta\,\cos^2\theta - \frac{1}{r}\,\sin^3\theta \\ \implies \frac{\partial^2 u}{\partial x^2} &= 0,\end{aligned}$$

$$\begin{aligned}\frac{\partial^2 u}{\partial y^2} &= \frac{\partial^2 u}{\partial r^2}\sin^2\theta + \frac{1}{r}\frac{\partial u}{\partial r}\cos^2\theta + \frac{2}{r}\frac{\partial^2 u}{\partial r\partial\theta}\sin\theta\cos\theta - \frac{2}{r^2}\frac{\partial u}{\partial\theta}\sin\theta\cos\theta + \frac{1}{r^2}\frac{\partial^2 u}{\partial\theta^2}\cos^2\theta \\ &= \frac{1}{r}\sin\theta\,\cos^2\theta + \frac{2}{r}\sin\theta\,\cos^2\theta - \frac{2}{r}\sin\theta\,\cos^2\theta - \frac{1}{r}\sin\theta\,\cos^2\theta \\ \implies \frac{\partial^2 u}{\partial y^2} &= 0,\end{aligned}$$

$$\begin{aligned}\frac{\partial^2 u}{\partial y\partial x} &= \left[\frac{1}{2}\frac{\partial^2 u}{\partial r^2} - \frac{1}{2r}\frac{\partial u}{\partial r} - \frac{1}{2r^2}\frac{\partial^2 u}{\partial\theta^2}\right]\sin 2\theta + \left[\frac{1}{r}\frac{\partial^2 u}{\partial r\partial\theta} - \frac{1}{r^2}\frac{\partial u}{\partial\theta}\right]\cos 2\theta \\ &= \frac{1}{2}\left[-\frac{1}{r}\sin\theta + \frac{1}{r}\sin\theta\right]\sin 2\theta + \left[\frac{1}{r}\cos\theta - \frac{1}{r}\cos\theta\right]\cos 2\theta\end{aligned}$$

$$\implies \frac{\partial^2 u}{\partial y \partial x} = 0.$$

Computing the $H^1$-norm for this function, we obtain,

$$|u|_{H^1(\Omega_0)} = \int_{\Omega_0} \left[ \left( \frac{\partial u}{\partial x} \right)^2 + \left( \frac{\partial u}{\partial y} \right)^2 \right] d\Omega = \int_0^{r_0} \int_0^{2\pi} r \, dr \, d\theta = r_0^2 \, \pi < \infty$$

which shows that $u_2 \in H^1(\Omega_0)$ for $\omega = 2\pi$. The computation for the $H^2$ semi-norm yields

$$|u|_{H^2(\Omega_0)} = \int_{\Omega_0} \left[ \left( \frac{\partial^2 u}{\partial x^2} \right)^2 + \left( \frac{\partial^2 u}{\partial y^2} \right)^2 + \left( \frac{\partial^2 u}{\partial x \partial y} \right)^2 \right] d\Omega = 0 < \infty$$

Thus, it is proven that $u_2 \in H^2(\Omega_0)$ for $\omega = 2\pi$.

# Appendix C

# Tensor Notation

In order to deal with the vector and tensor quantities considered in Chapter 5, we follow the *Einstein summation convention*, which is quite common in *Continuum Mechanics*. The relevant point for the current work is that a repeated index implies summation as is explained below. A detailed explanation of these notations can be found in many books on Continuum Mechanics, see for e.g. [10].

Let $\mathbf{u} \in \mathbb{R}^2$ be a vector (which is essentially a first order tensor) and $\mathbf{A} \in \mathbb{R}^{2\times 2}$, a second order tensor. Then, in the *index notation*, we have

$$\begin{aligned} & \mathbf{u} = u_i\, \mathbf{e}_i, \quad i \in \{1,2\}\,, \\ \text{and,} \qquad & \boldsymbol{A} = A_{ij}\, \mathbf{e}_i \otimes \mathbf{e}_j, \quad i \in \{1,2\}\,,\ j \in \{1,2\}\,, \end{aligned}$$

where, $\mathbf{e}_j$ represents the unit vector along the coordinate axis and the symbol $\otimes$ represents the *dyadic product* of two tensors.

The *transpose* of a second order tensor $\boldsymbol{A}$, denoted by $\boldsymbol{A}^t$, is defined as

$$\boldsymbol{A}^t = A_{ji}\, \mathbf{e}_i \otimes \mathbf{e}_j.$$

Moreover, a second order tensor is said to be *symmetric* if $\boldsymbol{A} = \boldsymbol{A}^t$. The strain tensor $\boldsymbol{\epsilon}$ and the stress tensor $\boldsymbol{\sigma}$ considered in this work are symmetric.

The *single contraction* or dot product of a second order tensor and a vector is defined as

$$\begin{aligned} \boldsymbol{A} \cdot \mathbf{u} &= A_{ij}\, \mathbf{e}_i \otimes \mathbf{e}_j \cdot u_k\, \mathbf{e}_k \\ &= A_{ij}\, u_k\, \delta_{jk}\, \mathbf{e}_i \\ \implies \boldsymbol{A} \cdot \mathbf{u} &= A_{ij}\, u_j\, \mathbf{e}_i, \end{aligned}$$

where, $\delta_{ij}$ is *Kronecker's delta* and is defined as

$$\delta_{ij} = \begin{cases} 1 & \text{if, } i = j \\ 0 & \text{if, } i \neq j \end{cases}.$$

The *double contraction* or the scalar product of two second order tensors $\boldsymbol{A}$ and $\boldsymbol{B}$ is defined as

$$\begin{aligned} \boldsymbol{A} : \boldsymbol{B} &= A_{ij}\, \mathbf{e}_i \otimes \mathbf{e}_j : B_{kl}\, \mathbf{e}_k \otimes \mathbf{e}_l \\ &= A_{ij}\, B_{kl}\, \delta_{ik}\, \delta_{jl} \\ &= A_{ij}\, B_{kj}\, \delta_{ik} \\ \implies \boldsymbol{A} : \boldsymbol{B} &= A_{ij}\, B_{ij}. \end{aligned}$$

The *trace* of a second order tensor, denoted by $\operatorname{tr} \boldsymbol{A}$ is defined as its double contraction with the *second order unit tensor* $\boldsymbol{I} = \delta_{ij} \mathbf{e}_i \otimes \mathbf{e}_j$, and is computed as

$$\begin{aligned} \operatorname{tr} \boldsymbol{A} &= \boldsymbol{A} : \boldsymbol{I} \\ &= A_{ij}\, \mathbf{e}_i \otimes \mathbf{e}_j : \delta_{kl}\, \mathbf{e}_k \otimes \mathbf{e}_l \\ &= A_{ij}\, \delta_{kl}\, \delta_{ik}\, \delta_{jl} \\ &= A_{ij}\, \delta_{kj}\, \delta_{ik} \\ &= A_{ij}\, \delta_{ij} \\ \implies \operatorname{tr} \boldsymbol{A} &= A_{ii}, \end{aligned}$$

which is basically the sum of diagonal entries of the matrix $\{A_{ij}\}_{i,j \in \{1,2\}}$ containing the entries of the tensor.

The *divergence* of a second order tensor $\boldsymbol{A} = \boldsymbol{A}(x_1, x_2)$, denoted by $\operatorname{div} \boldsymbol{A}$ is a vector and is defined as

$$\operatorname{div} \boldsymbol{A} = A_{ij,j}\, \mathbf{e}_i \qquad \text{with} \quad A_{ij,j} = \frac{\partial A_{ij}}{\partial x_j}.$$

Similarly, the divergence of a vector $\mathbf{u} = \mathbf{u}(x_1, x_2)$, which is a scalar, is given as

$$\operatorname{div} \mathbf{u} = u_{i,i} \qquad \text{with} \quad u_{i,i} = \frac{\partial u_i}{\partial x_i}.$$

The *gradient* of a vector $\mathbf{u} = \mathbf{u}(x_1, x_2)$ , denoted by $\operatorname{grad} \mathbf{u}$ is a second order tensor and is defined as

$$\operatorname{grad} \mathbf{u} = u_{i,j}\, \mathbf{e}_i \otimes \mathbf{e}_j \qquad \text{with} \quad u_{i,j} = \frac{\partial u_i}{\partial x_j}.$$

# References


[1] Babuška, I. Finite element method for domains with corners. *Computing 6*, 3-4 (1970), 264–273.

[2] Babuška, I., and Suri, M. The *hp* version of the finite element method with quasiuniform meshes. *ESAIM: Mathematical Modelling and Numerical Analysis 21*, 2 (1987), 199–238.

[3] Behairy, A. *Corrected finite element and finite difference methods for elliptic problems with singularities.* Doctoralthesis, Friedrich-Alexander-Universität Erlangen-Nürnberg (FAU), 2018.

[4] Blum, H., and Dobrowolski, M. On finite element methods for elliptic equations on domains with corners. *Computing 28*, 1 (1982), 53–63.

[5] Blum, H., and Rannacher, R. Extrapolation techniques for reducing the pollution effect or reentrant corners in the finite element method. *Numerische Mathematik 52*, 5 (1987), 539–564.

[6] Egger, H., Rüde, U., and Wohlmuth, B. Energy-corrected finite element methods for corner singularities. *SIAM Journal on Numerical Analysis 52*, 1 (2014), 171–193.

[7] Ern, A., and Guermond, J. *Theory and Practice of Finite Elements*, vol. 159 of *Applied Mathematical Sciences.* Springer New York, 2004.

[8] Gockenbach, M. S. *Understanding and implementing the finite element method.* Society for Industrial and Applied Mathematics, 2006.

[9] Grisvard, P. *Elliptic Problems in Nonsmooth Domains.* Society for Industrial and Applied Mathematics, 2011.

[10] Holzapfel, G. *Nonlinear Solid Mechanics: A Continuum Approach for Engineering.* Wiley, 2000.

[11] Horger, T., Pustejovska, P., and Wohlmuth, B. Higher order energy-corrected finite element methods. *arXiv preprint arXiv:1704.05638* (2017).

[12] John, L., Pustejovska, P., Wohlmuth, B., and Rüde, U. Energy-corrected finite element methods for the stokes system. *IMA Journal of Numerical Analysis 37*, 2 (2017), 687–729.

[13] Knabner, P., and Angermann, L. *Numerical Methods for Elliptic and Parabolic Partial Differential Equations*, vol. 44 of *Texts in Applied Mathematics.* Springer-Verlag, New York, 2003.

[14] Kondrat'ev, V. A. Boundary value problems for elliptic equations in domains with conical or angular points. *Trudy Moskovskogo Matematicheskogo Obshchestva 16* (1967), 209–292.

[15] Kufner, A. *Weighted sobolev spaces*, vol. 31 of *Teubner-Texte zur Mathematik*. B.G. Teubner, 1985.

[16] Kuna, M. *Finite elements in fracture mechanics*, vol. 201 of *Solid Mechanics and Its Applications*. Springer, 2013.

[17] Li, Z.-C., and Lu, T.-T. Singularities and treatments of elliptic boundary value problems. *Mathematical and Computer Modelling 31*, 8-9 (2000), 97–145.

[18] Reddy, B. *Introductory Functional Analysis: With Applications to Boundary Value Problems and Finite Elements*, vol. 27 of *Texts in Applied Mathematics*. Springer-Verlag New York, 1998.

[19] Rüde, U., and Zenger, C. On the treatment of singularities in the finite element method. Technical Report I9220, Institut für Informatik, Technische Universität München, 1992.

[20] Rüde, U. Local corrections for eliminating the pollution effect of reentrant corners. Technical Report I8901, Institut für Informatik, Technische Universität München, 1989.

[21] Rüde, U., Waluga, C., and Wohlmuth, B. Nested newton strategies for energy-corrected finite element methods. *SIAM Journal on Scientific Computing 36*, 4 (2014), A1359–A1383.

[22] Sadd, M. H. *Elasticity: Theory, Applications, and Numerics*. Academic Press, 2009.

[23] Schatz, A., and Wahlbin, L. Maximum norm estimates in the finite element method on plane polygonal domains. i. *Mathematics of Computation 32*, 141 (1978), 73–109.

[24] Scott, R. Optimal $L^\infty$ estimates for the finite element method on irregular meshes. *Mathematics of Computation 30*, 136 (1976), 681–697.

[25] Strang, G., and Fix, G. J. *An Analysis of the Finite Element Method*. Wellesley-Cambridge Press, 2008.

[26] Yosibash, Z. *Singularities in elliptic boundary value problems and elasticity and their connection with failure initiation*, vol. 37 of *finite elements in fracture mechanics*. Springer Science & Business Media, 2011.

[27] Zenger, C., and Gietl, H. Improved difference schemes for the dirichlet problem of poisson's equation in the neighbourhood of corners. *Numerische Mathematik 30*, 3 (1978), 315–332.